AD-A267 947 PAGE

Form Approved
OMB No 0704-0188

1. AGENCY USE ONLY (Leave blank)	2. REPORT DATE	3. REPORT TYPE AND DATES COVERED
	Mar 1993	THESIS/DISSERTATION

4. TITLE AND SUBTITLE
Spatial and Temporal Variations of Satellite Microwave Measurements of Latent Heat Release in Tropic Cyclones Due to Environmental Forcing Obtained From A Numerical Model

5. FUNDING NUMBERS

6. AUTHOR(S)
Lt Derek Allen West

7. PERFORMING ORGANIZATION NAME(S) AND ADDRESS(ES)
AFIT Student Attending: Ohio State University

8. PERFORMING ORGANIZATION REPORT NUMBER
AFIT/CI/CIA- 93-053

9. SPONSORING/MONITORING AGENCY NAME(S) AND ADDRESS(ES)
DEPARTMENT OF THE AIR FORCE
AFIT/CI
2950 P STREET
WRIGHT-PATTERSON AFB OH 45433-7765

10. SPONSORING/MONITORING AGENCY REPORT NUMBER

11. SUPPLEMENTARY NOTES

12a. DISTRIBUTION/AVAILABILITY STATEMENT
Approved for Public Release IAW 190-1
Distribution Unlimited
MICHAEL M. BRICKER, SMSgt, USAF
Chief Administration

12b. DISTRIBUTION CODE

13. ABSTRACT (Maximum 200 words)

14. SUBJECT TERMS	15. NUMBER OF PAGES 115
	16. PRICE CODE

17. SECURITY CLASSIFICATION OF REPORT	18. SECURITY CLASSIFICATION OF THIS PAGE	19. SECURITY CLASSIFICATION OF ABSTRACT	20. LIMITATION OF ABSTRACT

SPATIAL AND TEMPORAL VARIATIONS OF SATELLITE MICROWAVE MEASUREMENTS OF LATENT HEAT RELEASE IN TROPICAL CYCLONES DUE TO ENVIRONMENTAL FORCING OBTAINED FROM A NUMERICAL MODEL

A Thesis

Presented in Partial Fulfillment of the Requirements for the degree Master of Science in the Graduate School of The Ohio State University

by

Derek Allen West, B.S.

* * * * *

The Ohio State University

1993

Master's Examination Committee:

Dr. John N. Rayner

Dr. Jeffery C. Rogers

Dr. Jay S. Hobgood

Approved by

Jay S. Hobgood

Advisor

Atmospheric Sciences Program

To Mom, Dad, Andy, and Phil

ACKNOWLEDGMENTS

There are a multitude of people to thank for helping make this research possible. First, I would like to thank Dr. Edward B. Rodgers of the NASA Goddard Space Flight Center's Severe Storms Branch for taking time out of his busy research schedule to teach me and patiently guide me towards the completion of this research project. Second, I would like to thank Mrs. Antoinette Cheek, a fellow summer intern at Greenbelt, Maryland who assisted Dr. Rodgers and myself with weeks of data manipulation and calculations. Without her help, this project could not have been completed in as much detail as it was and in such a limited amount of time. Third, I would like to thank Mr. Hal Pierce of Science Systems Applications, Inc. (SSAI) for the tremendous amount of time and effort he put into manipulating the SSM/I images and sampling the data. Next, I would like to thank all the people in Code 912 Severe Storms Branch for their help and thoughtful insights; especially, Dr. Mike McCumber, Dr. Jong-Jin Baik, Dr. Dean Duffy, Dr. Chris Kummerow, Mr. Lafayette Long (The King of Macintosh Computers) from SSAI, Mr. Bill Skillman, Dr. George Huffman, Dr. Bob Adler, and Dr. John Manobianco.

Thanks also go to the people at the USRA/NASA Graduate Student Summer Program office (Ms. Paula Webber) who made it happen by providing me with excellent support and an incredible research opportunity. The Ohio State University, Atmospheric Sciences Program (ASP), gave me their total support in my efforts to attend this program and prepared me for it with the proper academic background (Dr. John Rayner, Dr. Jay Hobgood, Dr. Jeff Rogers, and Dr. John Arnfield). I would like to especially thank Dr. Hobgood, my advisor, for taking an active interest in both my academic performance and preparation of this thesis.

My fellow ASP students and friends Ms. Sabrina Taijeron, Ms. Margo Willoughby, and Mr. Ken Yetzer were invaluable and very supportive. Lastly, I would like to thank the U.S. Air Force for giving me the opportunity to pursue an advanced degree through the AFIT program (Major Mary Smith).

VITA

January 3, 1969 . . . . . Born - Macon, Georgia

1991 . . . . . B.S., United States Air Force Academy, Colorado Springs, Colorado

PUBLICATION

West, D. A. and B. L. Dilla, 1992: Cadets' perceptions of leadership development activities at the United States Air Force Academy. *Proceedings of the Thirteenth Symposium, Psychology in the Department of Defense 15-17 April 1992*, Colorado Springs, United States Air Force Academy, 36-40.

FIELDS OF STUDY

Major Field: Atmospheric Sciences

Studies in tropical and satellite meteorology

TABLE OF CONTENTS

LIST OF TABLES

LIST OF FIGURES

LIST OF ACRONYMS

AOIPS: Atmospheric and Oceanographic Information Processing System

CDO: Central Dense Overcast

DMSP: Defense Meteorological Satellite Program

ECMWF: European Centre for Medium-range Weather Forecasts

EFC: Eddy Flux Convergence

ERFC: Eddy RAM Flux Convergence

GEMPAK: GEneral Meteorological software PAcKage

ITCZ: Inter Tropical Convergence Zone

JTWC: Joint Typhoon Warning Center

LHR: Latent Heat Release

MFC: Moisture Flux Convergence

MSLP: Minimum Sea Level Pressure

OFCM: Office of the Federal Coordinator for Meteorology

PIP: Precipitation Index Parameter

RAM: Relative Angular Momentum

SSM/I: Special Sensor Microwave/Imager

SST: Sea Surface Temperature

TC: Tropical Cyclone

TUTT: Tropical Upper Tropospheric Trough

UTC: Uniform Time Coordinate

ABSTRACT

Understanding tropical cyclone (TC) intensification is a problem that continues to intrigue researchers and forecasters. The objective of this case study was to investigate, by examination of the fields from a numerical model and satellite rain rate observations, the following: 1) the relationship between TC precipitation and intensity changes and 2) the relationship between spatial and temporal changes in a TC's precipitation and large scale environmental tropospheric forcing.

Numerous studies have shown that increased latent heat release (LHR) often precedes TC intensification. Using Defense Meteorological Satellite Program (DMSP) Special Sensor Microwave/Imager (SSM/I) observed brightness temperatures and a rain rate algorithm (Adler *et al.* 1992), the fluctuations in diabatic heating accompanying spatial and temporal changes in rain rates were obtained for a Northwestern Pacific TC named Freda. This TC occurred during September of 1987 and did not make landfall.

The environmental forcing parameters (e.g., vertical shear of the horizontal wind, tropospheric water vapor flux, upper tropospheric eddy relative angular momentum [RAM] flux

convergence [ERFC]) derived from European Center for Medium-range Weather Forecasting (ECMWF) model initialization fields and climatological sea surface temperature (SST) were used to examine the environmental influences on Freda's precipitation.

The relationship between LHR and intensification in this case study was consistent with previous research. Also, the convective ring cycle (Willoughby *et al.* 1982) was observed with one major exception. As the outer rings contracted radially inward, the expected reintensification did not take place. Large scale environmental forcing may explain this deviation.

Specifically, environmental forcing was examined to understand the relationship between core (i.e., within 222 km radius) LHR and the TC's environment. SST's were not a factor in this case study as Freda stayed over warm ocean water (>26° C) during the period of study. Moisture flux appeared to affect the outer core (i.e., the annulus 111 to 222 km from the center) LHR, but not inner core (i.e., within 111 km radius) LHR. ERFC, a measure of the asymmetry of the TC's outflow, played a major role in influencing both outer and inner core LHR until the storm moved into the Westerlies and experienced extreme vertical shear.

This case study illustrates the importance that the upper tropospheric adjustment between the TC and its large scale environment (e.g., ridges and troughs) can have on LHR

and subsequent TC intensification and evolution of the convective ring cycle. Limitations of SSM/I coverage and ECMWF model resolution are factors that should be addressed when comparing this case study to others.

CHAPTER I

INTRODUCTION

1. Overview

Tropical cyclones are one of nature's deadliest phenomena. They can cause massive destruction and bring a major metropolitan area to its knees (e.g., the loss of life and property that occurred in South Florida due to Hurricane Andrew in 1992). Therefore, an understanding of their characteristics is a very important endeavor. The purpose of this chapter is to provide the reader with a general description of tropical cyclones in order to build a framework for the specific research problem addressed by this thesis.

Prediction of tropical cyclone intensification is a problem that continues to intrigue researchers and forecasters. The *specific research problem* of this thesis was to investigate, by examination of the data fields from a numerical model and satellite rain rate observations, the following: 1) the relationship between tropical cyclone precipitation and intensity changes and 2) the relationship between spatial and temporal changes in a tropical cyclone's precipitation and large scale environmental tropospheric forcing.

Numerous studies have shown that increased latent heat release (LHR) often precedes intensification of tropical cyclones. Defense Meteorological Satellite Program (DMSP) Special Sensor Microwave/Imager (SSM/I) observed brightness temperatures and a rain rate algorithm (Adler *et al.* 1992), were used to obtain the fluctuations in diabatic heating accompanying spatial and temporal changes in rain rates for a Northwestern Pacific tropical cyclone named Freda. This tropical cyclone occurred during September of 1987.

Environmental forcing parameters (e.g., vertical shear of the horizontal wind, lower tropospheric water vapor flux, upper tropospheric eddy relative angular momentum [RAM] flux convergence [ERFC]) derived from European Center for Medium-range Weather Forecasting (ECMWF) model initialization fields, and climatological sea surface temperature (SST) were used to examine the environmental influences on Freda's precipitation. Specifically, environmental forcing was examined to understand the relationship between core (i.e., within 222 km radius) LHR and Freda's environment.

The second chapter contains a review of literature relevant to this research. The methodology that was used to obtain and analyze the data for this thesis will be detailed in the third chapter. Presentation of the results obtained and discussion of how they compare to previous research is contained in the fourth chapter. The fifth chapter

summarizes the research that was done and suggests future areas of study.

2. To Name a Beast

These "meteorological monsters from the sea" are those potentially devastating storms which originate over the tropics. Tropical cyclones have special names according to the areas of the world in which they occur. These names include: hurricane (North America), cyclone (India and Australia), typhoon (eastern Asia), and baguio (China Sea). Of these names, the most commonly used term is hurricane (Miller and Anthes 1980). However, to avoid any misunderstanding, the term tropical cyclone will be used to describe this meteorological phenomena throughout its life cycle.

3. Life Cycle

Tropical cyclones generally form in distinct stages. Simpson and Riehl (1981) explain that such a system undergoes four stages during its life cycle (formative, immature, mature, and dissipation). Each stage is characterized by certain dynamic properties. The following discussion is for the Northern hemisphere only.

a. Formative Stage

The formative stage may be identified by monitoring vorticity centers usually within 500 km of the equatorial trough. These areas may experience unusual pressure falls of 2-3 mb during a 24 hour period. The wind field changes

to include asymmetric strengthening of the wind and, in the northeast trades, southeast winds strengthen and winds with westerly components develop in the usually easterly wind pattern. In this area, large elliptical wind envelopes form and may begin to contract. This stage of development is characterized by wind speeds of less than 17 m s^{-1} and the system is termed a tropical depression. On satellite photographs, this situation is indicated by the appearance of an isolated ring or arc of convective clouds which may have associated spiral bands. If the system continues to develop, it becomes a tropical storm and has wind speeds between 17 and 32 m s^{-1}.

Where and under what conditions do these systems form? They normally form at latitudes between 5°-30° in the intertropical convergence zone (ITCZ), have an average lifetime of about nine days (Eagleman 1983), and they occur mostly from August to October when the sea surface temperature is highest (U.S. Air Force 1982). This situation is because of two main factors. First, only poleward of 5° latitude is the Coriolis force strong enough to initiate rotation. Second, the sea surface temperature required for formation is above 26 °C, which generally occurs equatorward of 30° latitude due to heating of the ocean by the sun (Eagleman 1983).

Water temperatures above 26 °C are necessary because this temperature ensures that enough evaporation will take

place. It is the evaporated water which is the "fuel" for a tropical cyclone. The release of tremendous amounts of latent energy by condensation into large cloud bands causes rising air, which causes even more condensation and precipitation. In effect, this cycle of evaporation, condensation, and then precipitation results in a "heat engine"--to use thermodynamic terms (Emanuel 1986). Because this system creates a "warm-cored" low pressure system converging at the surface, a high pressure ridge will be set up aloft over the tropical cyclone and allow it to keep growing. The upper level divergence thus created is called outflow, which is normally carried east by the upper level prevailing westerlies.

b. Immature Stage

If conditions are favorable, the tropical cyclone may now enter the immature stage where winds intensify to hurricane or typhoon strength ($\geq$ 33 m s^{-1}) at about 50 km from a clearly identifiable cyclone center (Simpson and Riehl 1981). Pressure falls intensify, sometimes very rapidly in the span of a few hours. Satellite images of such a system will show a small solid core with surrounding puffy clouds.

c. Mature Stage

The tropical cyclone now progresses to its fully mature stage. The progression to this stage may take from hours to a month to complete (Simpson and Riehl 1981). This stage

typically lasts for several days. Central pressure and wind speeds may remain the same as the immature stage but the circulation widens out. In a moving tropical cyclone, winds greater than 33 m s^{-1} may extend out several hundred kilometers to the right of the direction of motion of the center. An inner ring of maximum winds encloses the eye at an average radius of 50 km. At this stage, the release of latent heat from convective clouds continues to provide the potential energy necessary for the maintenance of this "warm-cored" cyclone. The tropical cyclone can at this stage reasonably be approximated as a stable vortex.

Tropical cyclones are characterized by strong cyclonic circular flow around a very strong low pressure center, with surface pressures as low as 880 mb (Henderson-Sellers and Robinson 1986). In the center there typically exists an eye which is a region of calm air, usually a 10-50 km radius (Critchfield 1983). As one proceeds outward from the eye, a continuous mass of cumulonimbus clouds with upwardly spiraling motion called the eye wall is encountered. Further outward from the eye additional convective, spirally-configured, cloud bands are encountered. As air rises and reaches the tropopause, it moves outward and creates a spiraling cirrus cloud top over the tropical cyclone called the central dense overcast (CDO) region, which shows up very nicely on infrared and visible satellite pictures. For a diagram of the structure of a mature

tropical cyclone see Fig. 1. The overall diameter of a typical tropical cyclone is quite variable between 150-1000 km. In general, the diameter tends to increase with latitude (Critchfield 1983).

1) Winds

An obvious feature of a tropical cyclone's structure is the wind field. The extreme wind speeds of a mature tropical cyclone are caused by the very large concentric pressure gradient associated with the system. The winds increase in speed as one moves closer to the center or eye. This is due to the principle of conservation of angular momentum. As the radius of curvature decreases, the speed increases to a maximum at the eye wall, sometimes as much as 65 m s^{-1} with gusts up to 110 m s^{-1} (Critchfield 1983). This also accounts for the fact that tropical cyclones with smaller eyes tend to have higher wind speeds. Also, the wind speeds tend to be greater on the right side of the path of the tropical cyclone because of the addition of the speed of motion for the system. As a tropical cyclone moves in the same direction as the overall easterly steering current, the speed of the current in which it is embedded acts to increase the wind speeds on the right side with respect to the direction of motion and decrease them on the left. This explains why the right side of such systems are associated with the greatest amount of danger and destruction.

2) Precipitation

Precipitation that results from the initial formation of the tropical cyclone later becomes the driving force or engine of the cyclone through the release of latent energy. The largest amounts of rain are associated with the area of highest winds (Simpson and Riehl 1981). Measurement of precipitation over the ocean is extremely complicated and difficult to perform. The best known procedure is to use Doppler radar-equipped reconnaissance aircraft flying at various levels to measure the precipitation occurring in concentric rings around the center. Also, the heaviest amounts of precipitation are generally found on the right side of the system (U.S. Air Force 1982). Further, the amount of precipitation is a function of the progression of the tropical cyclone through its life cycle. More mature and intense storms have greater precipitation, as might be expected.

3) Eye

One of the most fascinating phenomena in nature that exists is the "eye of the storm." This area of relative calm within the tempest is usually about 5-60 km in diameter and is characterized by a general sinking motion--subsidence, warming, and slight winds (Simpson and Riehl 1981). An unusual feature is that, inside the eye, air is descending. This is not what one would expect in the middle of a low pressure system. However, because of the high rate

of rotation of the vortex, air is forced outward away from the eye. As a result, air from above sinks downward to replace it. The descending air is relatively warm due to adiabatic compression and causes the eye to be clear or contain only a few low level stratiform clouds (Eagleman 1983).

4) Motion

The above discussion has explained many of the traits of mature tropical cyclones. Another interesting aspect is the motion of these systems. Generally, they have a translation speed of about 6 m s^{-1} in the tropics and travel in a westerly or northwesterly direction. As they reach 25° latitude, they tend to "recurve" towards the north or northeast and speed up--in some extreme cases with translation speeds equal to 25 m s^{-1} (U.S. Air Force 1982). The "steering" of the system is the result of three main factors: 1) lower level winds (surface trade winds), 2) upper level winds (prevailing westerlies), and 3) the "β-effect" (an apparent force caused by the variation of the Coriolis parameter, **f**, with latitude which acts to the right of the path of motion [Anthes 1982]). Added to this is a tendency for tropical cyclones to be steered around subtropical high pressure systems (Eagleman 1983). The interaction of these variables makes predicting if, when, and where the "beast" will hit land a tricky task, indeed.

5) Latent Heat Release

A couple of statistics illustrate the enormity of these storms. The average tropical cyclone energy output is about 1.82×10^{13} watts (200 times the total electrical power produced in the United States). It also produces 9-18 trillion kilograms of precipitated water day^{-1} (Miller and Anthes 1980).

d. Dissipation

If the path of the tropical cyclone crosses the coast, thus making landfall, a great amount of damage can result. For example, the preliminary damage estimates for Hurricane Andrew (1992) exceed $30 billion dollars (Sheets 1992). The high winds discussed earlier may create much destruction. However, it is the storm surge which results from the uplift of the ocean surface (10 m in some cases) due to the low pressure center which can cause even greater damage (Miller and Anthes 1980). Also, the winds, due to the frictional effects with the water surface, produce large waves called swells which precede landfall (Critchfield 1983). As the warm, humid air of the tropical cyclone approaches land, a warm front is set up which causes precipitation to occur in advance of its arrival. All of these factors (high winds, surges, swells, frontal rain, and torrential rain from the rain bands) combine to produce devastating effects along great stretches of coastline and inland, as well.

After landfall, the tropical cyclone begins to

dissipate because it becomes deprived of its "fuel"--warm, moist air disappears and surface temperatures drop. Also, frictional effects can cause strong vertical wind shear. As the air speed is slowed, air starts to blow directly into the center and in effect fills the core of the system (Miller and Anthes 1980).

Often, as the tropical cyclone moves poleward it draws in cool polar air, becomes baroclinic, and turns into an extratropical cyclone. In some cases, such as in mountainous areas, this decay occurs very rapidly. However, on some occasions when the tropical cyclone makes landfall or leaves the tropics at the same time a midlatitude cyclone is forming, the tropical cyclone will provide the nucleus for strong, rapid development. This situation before landfall gives rise to an increased forward speed of the tropical cyclone and results in early landfall with devastating winds and torrential rains over land.

Upon first glance, it might seem that a tropical cyclone has no positive attributes. But, if one considers their function--poleward transport of latent and sensible heat--tropical cyclones play an important role in balancing the earth's energy budget.

4. Thermodynamics and Dynamics of Tropical Cyclones

a. Vertical Structure

The vertical dynamical structure of a tropical cyclone is, in general terms, characterized by inflow below the 800

mb level and upper level outflow up to the 100 mb level--top of the stratosphere (Simpson and Riehl 1981). The low level inflow rotational wind speed, **u**, is greater than the upper level outflow. Since rotational wind speed decreases upward, the core of the storm will be warmer than its environment. This leads to what Simpson and Riehl (1981) call the most fundamental statement about tropical cyclones, "A balanced, nondispersing temperature field can be maintained in steady state to the degree that surface friction extracts absolute angular momentum from the hurricane." Angular momentum per unit mass can be given by the following equation:

$$\Omega = ur + \frac{fr^2}{2}. \qquad (1)$$

The left hand side term, Ω, is absolute angular momentum, the first right hand side term is the relative angular momentum (**r** is radius from center of circulation), and the second right hand side term is the angular momentum of the earth's rotation at a given latitude (**f** is the Coriolis parameter).

b. Basic Equations for a Tropical Cyclone

A more erudite explanation of the tropical cyclone's thermodynamic and dynamic structure can be given by a basic set of equations discussed in Anthes (1982). In order to facilitate the study of the tropical cyclone as a vortex, the equations of motion, horizontal (Eqs. 2-3) and vertical

(Eqs. 4-5), are given below in the cylindrical coordinate system (r, λ, z):

$$\frac{\partial v}{\partial t}+u\frac{\partial v}{\partial r}+\frac{v}{r}\frac{\partial v}{\partial \lambda}+w\frac{\partial v}{\partial z}+fu+\frac{uv}{r}=-\frac{1}{\rho r}\frac{\partial p}{\partial \lambda}+\frac{1}{\rho}\frac{\partial \tau_{z\lambda}}{\partial z}+F_{H\lambda} \qquad (2)$$

$$\frac{\partial u}{\partial t}+u\frac{\partial u}{\partial r}+\frac{v}{r}\frac{\partial u}{\partial \lambda}+w\frac{\partial u}{\partial z}-fv-\frac{v^2}{r}=-\frac{1}{\rho}\frac{\partial p}{\partial r}+\frac{1}{\rho}\frac{\partial \tau_{zr}}{\partial z}+F_{Hr} \qquad (3)$$

$$\frac{dw}{dt}=-\frac{1}{\rho}\frac{\partial p}{\partial z}-g+F_z \qquad (4)$$

$$\frac{\partial p}{\partial z}=-\rho g \qquad (5)$$

where **u**, **v**, and **w** are the radial, tangential, and vertical velocities, respectively. Pressure is **p** and the acceleration due to gravity is **g**. Density of the air is given by ρ. In Eq. 2, the τ term represents tangential stress due to small-scale vertical mixing. Similarly in Eq. 3, the τ term represents radial stress due to small-scale vertical mixing. Eq. 5 represents the hydrostatic approximation and results from a tropical cyclone scale analysis of Eq. 4. The **F** terms in the Eqs. 2-4 represent frictional forces, such as turbulent mixing due to drag.

Changes in density with respect to horizontal and vertical divergence can be given by the following continuity equation:

$$\frac{\partial \rho}{\partial t}+\frac{\partial \rho r u}{r\partial r}+\frac{\partial \rho v}{r\partial \lambda}+\frac{\partial \rho w}{\partial z}=0. \qquad (6)$$

The first law of thermodynamics in terms of potential temperature, θ, changes with respect to time at a grid point

are determined by:

$$\frac{\partial \theta}{\partial t} = -u\frac{\partial \theta}{\partial r} - \frac{v}{r}\frac{\partial \theta}{\partial \lambda} - w\frac{\partial \theta}{\partial z} + \frac{\theta}{c_p T}\left(Q - \frac{1}{\rho}\frac{\partial H_s}{\partial z}\right) + F_{H\theta}. \qquad (7)$$

The first two right hand side terms represent radial and tangential advection, respectively, of potential temperature and the third term is the vertical transfer of potential temperature. The next term describes diabatic heating (**Q** is diabatic heating rate per unit mass, c_p is specific heat at constant pressure, **T** is temperature, and the **H** term is the vertical heat flux due to small-scale turbulent eddies). The **F** term depicts sub-grid scale horizontal mixing by turbulence--friction.

There are three important diabatic heating mechanisms relevant to tropical cyclones (in order of importance): latent heating due to condensation, sensible heat transfer, and radiation (Anthes 1982). The first and most important mechanism, the driving force behind tropical cyclone intensification, can be related by:

$$\frac{\partial T}{\partial t_{cond}} = \frac{L}{c_p} C \qquad (8)$$

where **L** is the latent heat of condensation and **C** is the local condensation rate.

The above equations along with the Equation of State and the following continuity equation for water vapor

provide a basic, comprehensive, and quantitative analysis of the dynamic and thermodynamic structure of a tropical cyclone.

$$\frac{\partial \bar{q}}{\partial t} = -u\frac{\partial \bar{q}}{\partial r} - \frac{v}{r}\frac{\partial \bar{q}}{\partial \lambda} - w\frac{\partial \bar{q}}{\partial z} - C - \frac{1}{\rho}\frac{\partial H_{\bar{q}}}{\partial z} + F_{H\bar{q}}. \qquad (9)$$

The **H** term in this equation is the vertical flux of water vapor, **q** is the specific humidity, and the **F** term is the effect of horizontal mixing.

The above discussion of the dynamics of tropical cyclones provides an essential foundation for the integration of the following discussion of recent research.

5. Observations of Tropical Cyclones

The two most important observing platforms for tropical cyclone research are aircraft and satellites. With budget dollars becoming increasingly scarce, agencies which play an active role in the study of tropical cyclones, such as NOAA and the U.S. Air Force, have been asked to curtail their use of aerial reconnaissance aircraft. It has been argued by budget-cutters that the use of aircraft is no longer a cost effective method for the study of tropical cyclones because of the increased ability of weather satellites to assume this task.

A very recent assessment of aerial reconnaissance of tropical cyclones was performed by William Gray, Charles Neumann, and Ted Tsui (1991). They found that satellite assessments of tropical cyclone position, intensity, outer

wind distribution, and ambient steering current are inferior to that provided by aircraft measurements. Further, they conclude that the degradation of these measurements by the loss of aerial reconnaissance assets will be operationally significant, since accurate forecasts are extremely dependent upon these parameters.

NOAA WP-3D aircraft are--through the use of Omega dropwindsondes, flight-level temperature, humidity, Doppler radial velocities and radar reflectivity, and onboard computer workstations--able to provide thorough descriptions of eye wall and rainband structure (Griffin *et al.* 1991).

A few recent and significant studies illustrate the role that aircraft have played in tropical cyclone research. In order for progress in tropical cyclone research to occur, it is necessary that satellites be eventually able to gather data in such a matter as to complement previous aircraft studies. William M. Frank (1984) used data obtained from aircraft research in conjunction with surface observations from another author to develop a composite analysis of the core of a mature tropical cyclone (Hurricane Fredric [1979]). He analyzed vertical fluxes, sensible heat budgets, and angular momentum budgets. He found that the two data sets combined allowed for accurate analysis of divergence and vertical motion.

Mark D. Powell (1985) was able to analyze the horizontal wind field at the mesoscale level from Doppler

radar data gathered aboard a NOAA research aircraft. This analysis was done on two hurricanes (Debby [1982] and Tico [1983]).

Weatherford and Gray (1987 a and b) used data obtained from US Air Force WC-130 aircraft to describe the structure of Northwestern Pacific tropical cyclones. They were able to analyze 700 mb data from flights through 66 cyclones over a period from 1980-82. Their analysis relates inner and outer core intensity to climatological variables and structural variability. The unique role and importance of aircraft research was emphasized by these researchers.

Mark D. Powell (1989 a and b) used data obtained from NOAA aircraft to show that boundary layer structure and dynamics of outer rainbands of three hurricanes (Josephine [1984], Earl [1986], and Floyd [1981]) have similar mesoscale and convective scale features. He found that convective downdrafts were capable of transporting cool, dry, low equivalent potential temperature to the surface of the ocean in the outer convective rainbands.

6. The Necessity of this Research

Satellites currently cannot provide researchers with data and techniques that equal aircraft-based research. It will be another ten years until they are able to do so according to Dr. Robert Sheets, Director of the National Hurricane Center (1992). The purpose of this research is, given cuts in funding for aircraft research, to develop

techniques that allow forecasters to use satellite data and numerical models--two of the remaining research alternatives--to understand and predict tropical cyclone intensity changes.

Study in this area is so important that an ad-hoc committee of federal agencies tasked with identifying areas that deserve attention in tropical cyclone research has stated specific requirements for research involving the use of SSM/I (OFCM 1992). The committee cites a "pressing" need for research aimed at using SSM/I data to provide forecasters with accurate satellite positioning, motion, and rainfall estimates. Also, listed in the *National Plan for Tropical Cyclone Research* (OFCM 1992) is a critical need to understand processes that cause different precipitation distributions and how these distributions affect intensity changes. This thesis is based upon specific research activities currently being conducted by Dr. Edward Rodgers at the NASA/Goddard Space Flight Center. The committee has tasked Dr. Rodgers with research of the following three topics: 1) Remote sensing of precipitation in tropical cyclones, 2) Upper tropospheric processes affecting tropical cyclone intensity change, and 3) Tropical cyclone precipitation response to intensity and motion change and environmental influence. It is these three topics that provide the focus for this thesis.

CHAPTER II

RELEVANT LITERATURE REVIEW

A major problem in forecasting tropical cyclones is the lack of ability to understand how they will intensify (Mayfield 1992). One approach advocated by Samsury and Rappaport (1991) is to use aircraft derived tropical cyclone dynamic and structural observations to predict intensification. This method involves comparison of a tropical cyclone's wind profile and convective ring pattern with previous aircraft obtained data on these parameters and associated intensification of similar past cyclones to produce a forecasted intensification. This is simply a regression technique that does not address the physical relationships. Therefore, understanding the mechanisms that affect intensification is an important research objective.

A very important element of tropical cyclone structure is the core intensity defined as the maximum surface winds or minimum sea level pressure (MSLP) of the tropical cyclone (Elsberry *et al.* 1987). The intensification is strongly related to the distribution of rain within the inner core (i.e., within 1° or 111 km from the center of the circulation [Weatherford 1985]). The diabatic heating that

results from the release of latent heat by inner core convection has been shown to precede tropical cyclone intensification in many previous studies.

1. Importance of Latent Heating

Numerical model studies by Kurihara and Tuleya (1974) and Rosenthal (1978) found that the maximum intensity occurred 24-72 hours after the maximum amount of latent heat release (LHR). Satellite studies have also found the same relationship. Latent heat measurements obtained from the Nimbus-5 Electrically Scanning Microwave Radiometer (EMSR) of North Pacific tropical cyclones (Adler and Rodgers 1977; Rodgers and Adler 1981) revealed a lag time between maximum LHR and intensification of approximately one to two days. Using data from the *Defense Meteorological Satellite Program* (DMSP) Special Sensor Microwave/Imager (SSM/I), MacArthur (1991) found that LHR or volumetric rain rates could be used to predict intensification events (i.e., rapid drops in MSLP or increases in surface winds) for Northwestern Pacific tropical cyclones. Alliss and Raman (1992) found similar results for the Atlantic tropical cyclone Hurricane Hugo (1989) by analyzing DMSP SSM/I data. In a later study by Alliss *et al.* (1992) involving the Atlantic Hurricane Florence (1988), it was observed that intensification was preceded by an increase in LHR indicated by SSM/I derived rainfall rates.

The method for calculating LHR over an area is given by

the following equation:

$$LHR = L\rho\int_A R\, da \qquad (10)$$

where ρ is the density of water (1.0×10^3 kg m^{-3}), **L** is the latent heat of condensation (2.5×10^6 J kg^{-1}), **da** is the incremental area, **A** is the area of integration, and **R** is the rain rate in mm h^{-1} (Rodgers and Adler 1981). Palmen and Newton (1969) were among the first to state that LHR within tropical cyclones could be obtained from such an equation, given a suitable rain rate measurement. However, it was not until the advent of airborne radar and satellites that adequate rain rate measurements were available for such calculations.

In addition, it has been found through numerical modelling and observational research that as a tropical cyclone becomes more intense the lower and middle tropospheric inertial stability increases (Baik *et al.* 1991; Rodgers 1992). This increase in inertial stability (an air parcel's resistance to horizontal displacement) enhances the efficiency of the inner core diabatic heating and results in a hydrostatically lower surface pressure. The lowering of the surface pressure increases lower tropospheric tangential winds which act to increase further inertial stability in the middle to lower troposphere. Therefore, as the storm becomes more intense, the effects of changes in latent heating, especially within the core, have a more pronounced

impact (Hack and Schubert 1986). This translates into less lag time between LHR and intensification as the storm becomes more intense; setting up a positive feedback system.

2. Environmental Factors

The challenge now becomes one of determining how precipitation and its associated LHR is affected by environmental parameters such as mean sea surface temperature (SST), tropospheric moisture flux convergence, vertical shear of the horizontal wind, and upper tropospheric eddy flux convergence of relative angular momentum (RAM). These parameters have been shown to be useful as statistical predictors of intensity change in studies by DeMaria and Kaplan (1991). An examination of each of these parameters illustrates their importance to the intensity of tropical cyclones. They are defined below from bottom to top according to where in the overall environment the parameter influences tropical cyclone intensification. Fig. 2 illustrates the environmental parameters that influence tropical cyclones. It should be understood that these parameters may have complex interactions. Therefore, all must be considered together in determining how a tropical cyclone is impacted by its large scale environment.

a. Sea Surface Temperature

The potential intensity that a tropical cyclone may attain is dependent upon the surface energy flux which increases with SST (Miller 1958; Malkus and Riehl 1960;

Emanuel 1986; Merrill 1988). Gray (1979) found that a SST greater than 26 °C is required for intensification of tropical cyclones. Thus, SST can have a limiting effect on the intensity that a tropical cyclone may attain. An equation developed by Merrill (1988) illustrates this concept:

$$V_{max} = 74e^{[0.2(SST-25.0)]} \quad (11)$$

where V_{max} is in knots and **SST** is in °C. For example, a SST value of 26 °C would yield a V_{max} of 90 knots (45 m s^{-1}) using the above equation.

b. Tropospheric Moisture Flux Convergence

A moist, unstable environment is necessary for intense convection to occur in a tropical cyclone. Growth of convection in tropical cyclones can be influenced by inward surges of moisture or water vapor (Lee 1986; Molinari and Skubis 1985). Through numerical modelling, moisture flux convergence has been shown to create a favorable environment for tropical cyclone convection (Frank 1977; Reuter and Yau 1986). The moisture convergence contributes to the moist, unstable environment necessary to support convection by providing the requisite potential energy for intensification through the release of latent heat. Areal mean moisture flux convergence (MFC) is given by the following equation:

$$MFC = -\frac{2\pi r}{g}\int_{1000mb}^{300mb} q\, u_L\, dp \quad (12)$$

where **r** is the radius of interest (222 km), **q** is the mixing

ratio, u_L is the Lagrangian (with the storm) radial wind, and **dp** is the incremental pressure layer.

c. Vertical Shear of the Horizontal Wind

Vertical shear is simply the vector difference between the horizontal upper and lower tropospheric winds given by the following equation:

$$Vertical\ Shear = |U_{200mb} - U_{850mb}| \qquad (13)$$

where **U** is the horizontal wind (vector sum of the radial and tangential wind at each level). Weak vertical shear is important for intensification because it allows deep convection to develop in the inner core of a tropical cyclone. Gray (1979) emphasizes that strong vertical shear prevents the necessary coupling of the lower and upper troposphere required for intensification. The system, in effect, topples over under conditions of extreme vertical shear.

d. Upper Level Eddy Flux Convergence of RAM

The equation for the change of the tangential wind in a Lagrangian or storm-relative cylindrical coordinate system (see Eq. 6 from Molinari and Vollaro 1990) contains a term that represents the eddy flux convergence (EFC) of RAM which is:

$$EFC = r^{-2} \frac{\delta (r^2 \overline{u'v'})}{\delta r} \qquad (14)$$

where **r** is the radius from the storm center, **u** is the Lagrangian radial wind, **v** is the Lagrangian tangential wind,

the over-bar represents an azimuthal average, and the prime denotes the deviation from the azimuthal average or the eddy term (Baik *et al.* 1991; DeMaria *et al.* 1991). Positive EFC values have the effect of making the mean tangential wind more cyclonic and, therefore, act to increase the intensity of a tropical cyclone. Negative EFC values have an opposite, inhibiting effect on intensification.

EFC or ERFC, as it will be referred to in this paper, is a measure of environmental forcing that can be associated with upper tropospheric interactions between a tropical cyclone and the upper tropospheric environment. ERFC is able to interact with a tropical cyclone in the upper troposphere, because even though the inertial stability in the middle and lower troposphere increases with intensity, upper tropospheric inertial stability remains susceptible to environmental forcing (Holland and Merrill 1984; Rodgers 1992). Molinari and Vollaro (1989 and 1990) found that intensification of Hurricane Elena (1985) was influenced by an approaching midlatitudinal trough. In a composite of intensifying storms, McBride (1981) found that high amounts of inward directed positive ERFC existed in the outflow layer above 200 mb. Modelling studies have also shown the same effect in two-dimensional balanced axisymmetric tropical cyclone models (Pfeffer and Challa 1981; McBride and Zehr 1981) and in three-dimensional simulations by Challa and Pfeffer (1990).

Observational studies using satellites have also shown the important impact that ERFC can have upon the intensification of tropical cyclones. Several studies have found that the mutual adjustment between tropical cyclones and upper tropospheric troughs results in more asymmetric outflow (Stout and Rodgers 1992; Rodgers *et al.* 1990 and 1991; Rodgers 1992). Positive ERFC values are associated with the resulting asymmetric outflow (Pfeffer 1958; Palmen and Riehl 1957; Black and Anthes 1971; Holland 1983; Molinari and Vollaro 1989; Challa and Pfeffer 1980). Sadler (1976 and 1978) showed that enhancement and asymmetry of the outflow channels was related to the tropical cyclone's relative position with respect to midlatitudinal upper tropospheric troughs and tropical upper tropospheric troughs (TUTTs). The approach of a trough can act to channel the outflow, thus producing an anticyclonic jet.

Two theories exist for the observation that positive ERFC values are responsible for increased convection and resulting intensification. One explanation is provided by Chen and Gray (1985). They argue that the import of ERFC increases cyclonic spin-up in the upper troposphere which provides the necessary upper level divergence for convection to increase by a geostrophic adjustment process. A second theory is that the convection could be caused by an outflow channel-induced, thermally-direct secondary circulation located in the outflow jet entrance region (Merrill 1984;

Shi *et al.* 1990). This explanation is similar to the effect found in subtropical (Uccellini *et al.* 1984) and polar (Palmen and Newton 1969) jets. It is evident that ERFC is a very important parameter that indicates how the upper troposphere can influence inner core precipitation and subsequent intensification of tropical cyclones. This is true because even at the most intense stage of a tropical cyclone the upper level inertial stability is still relatively weak allowing upper level features to interact with it.

3. Precipitation Structure

Several studies have addressed the temporal and spatial distribution of precipitation near the core of tropical cyclones. These studies indicate the importance of rainfall and its associated release of latent energy to the evolution of a tropical cyclone. Willoughby *et al.* (1982) used research aircraft radar data in conjunction with numerical models to identify a convective ring cycle. The latent heating caused by convection in a ring around the center of a cyclone speeds up the tangential winds within the ring. Often in strong tropical cyclones, secondary outer convective rings form, intensify, and contract. This cycle occurs at the expense of the inner ring, which weakens and then disappears, delineating the end of a period of tropical cyclone intensification and, in some cases, marking the beginning of a period of weakening. The outer convective

ring then begins to constrict and the tropical cyclone reintensifies (Willoughby 1988).

In a study using airborne radar Marks (1980) showed that Hurricane Allen (1980) underwent the same vortex evolution described by Willoughby *et al.* (1982). Marks suggests the reason that the outer convective ring supplants the inner ring is because it blocks the transport of moist air into the eyewall region (i.e., a barrier effect). He also found that, as the eyewall contracted, the rainfall in the inner core increased until an outside convective ring formed. Average rain rate in the inner core of the hurricane was larger than outside the core by a factor of six.

A more recent airborne radar study by Burpee and Black (1989) examined the variation of precipitation within Hurricanes Alicia (1983) and Elena (1985). They found that the outer core (1-2° or 111-222 km [Weatherford 1985]) rain rates were less variable than inner core rain rates. Also, they confirmed that inner core rain rates were much higher than those further away from the center of the circulation.

Willoughby (1988) suggests that the upper level tropospheric eddy momentum fluxes (e.g., ERFC) may control convection in the inner core and, therefore, intensification. This process is controlled by forced ascent and causes adiabatic upper tropospheric cooling which acts to create instability (Merrill 1984). Large scale

environmental influences (i.e., tropospheric moisture flux convergence) may cause the formation of convective rings, but the maintenance and evolution of convective rings appears to be driven by internal dynamics (i.e., upper level ERFC and vertical shear) (Willoughby 1988 and 1990; Molinari and Skubis 1985; Molinari and Vollaro 1989).

4. Summary

The intensification of tropical cyclones is related to latent heating. This latent heating can be influenced by a variety of environmental factors (i.e., SST, vertical shear, moisture flux convergence, and upper level ERFC) which can themselves interact to influence the spatial and temporal distribution of precipitation in tropical cyclones via the convective ring cycle.

CHAPTER III

METHODOLOGY

This thesis describes a case study that evaluated a Northwestern Pacific tropical cyclone named Freda (1987). Specifically, the relationship of the aforementioned environmental factors to its spatial and temporal precipitation, the associated latent heat release, and intensification were examined. Precipitation measurements were obtained from Defense Meteorological Satellite Program (DMSP) Special Sensor Microwave/Imager (SSM/I) data and environmental parameters, except for SST, from European Centre for Medium-range Weather Forecasts (ECMWF) model fields. SST values were obtained from a data set used in global climate change research at the NASA/Goddard Space Flight Center (Kummerow and Duffy 1992).

1. Tropical Cyclone Freda

The *1987 Annual Joint Typhoon Warning Center Report* indicates that Tropical Cyclone Freda became a tropical disturbance at about 2000 UTC on September 3, 1987; forming from a persistent cluster of convection associated with an active monsoon trough. Freda was the second of a series of three tropical cyclones that were active in the Northwestern

Pacific at one time. However, it never came any closer to the other systems than 1700 km. Therefore, the Fujiwhara effect (a phenomenon in which tropical cyclones within 1300 km of each other begin to rotate around about one another [U.S. Fleet Weather Center/JTWC 1987]) was not encountered. Decreased vertical shear allowed it to develop through the depression stage to the tropical storm stage by September 5. At approximately 0000 UTC on September 6, Freda became quasi-stationary about 470 km from Guam, while performing a tight cyclonic loop in its track. The tropical cyclone reached typhoon stage on September 6 and had a maximum intensity of 125 knots and a mean sea level pressure (MSLP) of 916 mb by 0000 UTC on September 10. Typhoon Freda (JTWC number 13W) had the longest life span of any named storm in the 1987 Northwestern Pacific tropical cyclone season. It traversed 10° of longitude and 25° of latitude and did not make landfall throughout its existence. Freda was caught in the Westerlies on September 15 and dissipated until becoming extratropical on September 17 (U.S. Fleet Weather Center/JTWC 1987). See Fig. 3 for the Best Track data. Intensity estimates are from satellite imagery using the Dvorak (1975) method and MSLP is obtained using the empirical relationship between intensity (V_{max}) and MSLP (P_{min}) derived for Northwestern Pacific tropical cyclones by Atkinson and Holliday (1977):

$$P_{min} = 1010 - \left(\frac{V_{max}}{6.7}\right)^{1.553} \quad (15)$$

where P_{min} is the MSLP (mb) and V_{max} is the maximum sustained surface wind speed (knots).

2. DMSP SSM/I

a. The Satellite

The DMSP flight eight (F8) satellite carrying the SSM/I that collected the data used in this research was launched by the Department of Defense in June of 1987. This occurred just before U.S. Air Force WC-130 aerial reconnaissance flights into tropical cyclones were halted in the Pacific on October 1, 1987. The F8 is a polar orbiting satellite that has an orbital inclination to the equator of 98.8° and a period of 102 minutes which allows for 14.1 sun-synchronous orbits a day (MacArthur 1991). Its altitude is 833 km which allows the SSM/I a 1400 km wide field of view near the earth's surface (Rappaport 1991). See Figs. 4-6 for illustrations of SSM/I orbital and scan parameters.

b. The SSM/I

This sensor is a passive radiometer that has seven channels. It measures upwelling reflected and emitted microwave radiation in frequencies of 19.4, 22.2, 37.0, and 85.5 GHz. All but the 22.2 GHz frequency are dual-polarized into vertical and horizontal channels. The 22.2 GHz has only a vertical polarization. Table 1 contains information on the characteristics of the SSM/I channels.

The sensor scans conically at 45° from nadir (Negri *et al.* 1989) and converts the radiometer power it receives into a brightness temperature (the accuracy of which is ± 0.6 K [Hollinger *et al.* 1987]). The brightness temperature (T_B) measured by each of the above channels is a function of the radiation from the earth's surface and the intervening atmosphere which has an attenuating effect. T_B, measured in K, is almost directly related to "black body" temperature (T_{BB}) in the microwave region of the electromagnetic spectrum and is dependent upon the emissivity (ϵ) and thermodynamic temperature of the emitting surface. This results in the following expression for a "grey" body (Negri *et al.* 1989):

$$T_B = \epsilon\, T_{BB}. \qquad (16)$$

The dielectric characteristic of the emitting surface determines the ϵ (where, $0<\epsilon<1$). For instance, a calm ocean surface has a high dielectric constant and, therefore, a low ϵ (≈ 0.61) and low T_B. Rough ocean surface (due to winds) has a lower dielectric constant, higher ϵ (≈ 0.65) and, consequently, a higher T_B. Land surface has a far lower dielectric constant, $\epsilon \approx 1.0$, and therefore, a very high T_B.

Additionally, the SSM/I measured T_B values are affected by the intervening atmospheric constituents. Atmospheric water vapor, liquid water droplets, and ice particles in clouds emit at equilibrium temperatures greater than the relatively "cold" water surface (i.e., low T_B) but less than

the land surface. As a result, these "warm" constituents can be easily resolved over the ocean, but not land. Extremely large hydrometeors (e.g., large raindrops, hail, and graupel) scatter microwave radiation in the higher SSM/I frequencies since these particles are approximately the same size as the wavelength. This results in a greatly reduced T_B which can be resolved over both the ocean and land, an effect first discovered in aircraft microwave studies by Wilheit *et al.* (1982). Cirrus clouds, comprised mainly of very tiny ice crystals, are transparent to the SSM/I channels and this allows for observations below these overlying clouds, which would otherwise have an obscuring effect on visible and infrared radiometers. Further information on the instrumentation, calibration, and validation of the SSM/I can be obtained from Hollinger (1989).

Previous research with SSM/I at the Air Force Geophysics Laboratory has found that T_B data can be used to delineate intense convection within cloud bands and locate storm centers (Glass and Felde 1989 and 1990). Also, channels on the SSM/I have been used to define tropical cyclone dimensions (the area with vertically polarized 19.4 GHz T_Bs > 230 K is considered to define the tropical cyclone's extent [Glass and Felde 1990; Felde and Glass 1991]). Additionally, the 19.4 GHz and 85.5 GHz channels have been found to be useful in estimates of tropical

cyclone intensity (Felde and Glass 1991; Glass and Felde 1992).

c. Rain Rate Algorithm

Passive microwave rain rate algorithms using SSM/I have a strong physical relationship between precipitation and satellite measurements (Spencer *et al.* 1989; Manobianco *et al.* 1991; Adler *et al.* 1992). Though the polar orbiting SSM/I does not provide continuous coverage of an area, the data it provides permits better precipitation estimation and resolution of active precipitation regions in storm systems than does techniques utilizing infrared and visible wavelengths (Parmenter-Holt 1992).

An algorithm developed by Adler *et al.* (1991) was used to estimate rain rates using SSM/I brightness temperatures. The algorithm uses only the 85.5 and 37.0 GHz horizontally polarized channels. Both channels are used to define raining areas over the ocean only (this algorithm does not work over land). Non-raining areas over the ocean are defined where the 37.0 GHz $\mathbf{T_B}$ is less than 185 K and the 85.5 GHz $\mathbf{T_B}$ minus the 37.0 GHz $\mathbf{T_B}$ is greater than zero. Once non-raining areas have been identified, their 85.5 GHz $\mathbf{T_B}$s (which could be low) are adjusted to be greater than 247 K. The adjusted 85.5 GHz $\mathbf{T_B}$ is then used to calculate rain rate with the following equation based upon ice scattering patterns:

$$R = -\left(\frac{T_B - 251}{4}\right) \qquad (17)$$

where **R** is the rain rate in mm h^{-1} and $\mathbf{T_B}$ is the adjusted 85.5 GHz $\mathbf{T_B}$ in K. Therefore, the minimum rain rate calculated by this algorithm is 1 mm h^{-1} given by a 85.5 GHz $\mathbf{T_B}$ of 247 K (i.e., values below the 247 K cut-off yield higher rain rates). The relationship for defining non-raining areas over the ocean and the equation for determining the rain rates were developed by using a cloud model and microwave calculations (Adler *et al.* 1991).

Validation of this algorithm was done by comparing SSM/I derived rain rates with rain rates derived by "ground truth" high quality, land-based radars at Darwin, Australia. The results of the validation indicate that the algorithm does extremely well at identifying areas where it is raining over the ocean, but tends to underestimate small rain systems and overestimate large rain systems (Adler *et al.* 1992). SSM/I-based results underestimated radar depiction of area with rain by 6% and were found to have an overall bias of zero in estimates of rain rate. Further algorithm validation efforts by Adler *et al.* (1992) were conducted involving land-based radars in Japan. They found that the SSM/I derived rain rates tended to underestimate (negative bias) radar-based measurements by 0.03 mm h^{-1}. This is 12% of the average rain rate determined by the radars. From the above validation efforts, if any error is introduced by the

algorithm it will be a slight systematic tendency to underestimate rain rate. Another source of error, the precision of the SSM/I measured $\mathbf{T_B}$ (± 0.6 K), affects the accuracy of the algorithm output by ± 0.15 mm h^{-1}.

d. Sampling the Data

Using the second generation Atmospheric and Oceanographic Information Processing System (AOIPS-2) at the NASA Goddard Space Flight Center, images using the 85.5 GHz SSM/I were generated for all orbits that had any pixels between 5° N and 40° N latitudes and 140° E and 165° E longitudes for the period between September 3-17, 1987. Center fixes using these images can be very accurate due to the 12.5 km resolution of the 85.5 GHz channel (Velden *et al.* 1989; Alliss *et al.* 1992). These images along with the Best Track data from the *1987 Annual Joint Typhoon Warning Center Report* were used to locate orbits with coverage of at least 0.5° (55.5 km) of radius around the center of Tropical Cyclone Freda's circulation. This process resulted in selecting 17 orbits which had sufficient coverage. At least one orbit a day was selected except for September 8 and September 15-17. These periods lacked adequate coverage and represent data gaps. On the average, a descending orbit would pass over the area of interest at about 0900 UTC and an ascending orbit would pass overhead near 2100 UTC. The resulting lack of continuous coverage is a limitation of the SSM/I because of its orbital nature and a problem

encountered in operational forecasting applications where continuity is important (Rappaport 1991). However, over a normally data sparse region, this coverage is a welcome addition and when compared to other SSM/I studies (MacArthur 1991; Alliss *et al.* 1992) is very good. In fact, during the search for a case study, ten other Northwestern Pacific tropical cyclones from the 1987 to 1989 seasons were analyzed in the aforementioned manner. The coverage was found to be insufficient, because data gaps of over two days existed in those cases.

The Best Track indicating the time of SSM/I orbits that were used in this study is contained in Fig. 3 and Table 2. Once the centers were identified and images selected, rain rates for each pixel (the resolution of which is 25 km dictated by the 37.0 GHz channel resolution) were developed for each of the observations by creating a new channel, "channel eight." The SSM/I channel eight image was then sampled using the boundaries of a stereographic horizon map grid (Shenk *et al.* 1971) projected onto the SSM/I image to delineate 64 areas defined by eight equally spaced rings (maximum radius is 444 km) and eight equally spaced azimuths centered on the tropical cyclone's center. Each ring therefore represented 0.5° or 55.5 km of radius and each azimuth was separated by 45°. Area averaged rain rates were then calculated for two grid rotations. One was a rotation in which the zero azimuth pointed to the North, in order to

examine distribution with respect to earth coordinates. The second orientation was so that the zero azimuth was pointed in the direction of tropical cyclone's motion (direction-of-motion grid), derived using Best Track data. The results of this process are illustrated by the rain rate images with the grid superimposed and oriented towards the North contained in Figs. 7-23. These figures show Tropical Cyclone Freda from September 3-14, 1987. The thick bold grey line indicates the edge of the scan. Data outside of the scan swath were not used. Statistics for each of the 64 areas were calculated and tabulated into a histogram which was printed and used for further calculations.

LHR was calculated using Eq. 10. Appendix C contains an example calculation of LHR. Two other SSM/I parameters were calculated, to include: 1) Precipitation Index Parameter (PIP), this is the ratio of rain rate pixels greater than or equal to 5 mm h^{-1} to rain rate pixels greater than or equal to 1 mm h^{-1} but less than 5 mm h^{-1} (Rodgers and Adler 1981; Rhudy 1989); and, 2) the ratio of rain rate pixels greater than 5 mm h^{-1} to the total number of pixels in the area. The PIP is a measure of the relative contributions of stratiform (1 mm $h^{-1} \leq \mathbf{R} <$ 5 mm h^{-1}) and convective ($\mathbf{R} \geq$ 5 mm h^{-1}) rain. The second parameter addresses the impact of just the convective rain. This convective cut-off value of 5 mm h^{-1} is slightly higher than the 3 mm h^{-1} value suggested by Willoughby *et al.* 1982. In

order to compare these parameters with previous work (Rhudy 1989; MacArthur 1991) the 5 mm h^{-1} value will be used. These LHR parameters are shown in Figs. 24-25.

Calculations of LHR parameters were only performed for rings and azimuths with full scan coverage. Therefore, some calculations for individual SSM/I observations do not include complete radial or azimuthal coverage. Also, azimuthally stratified rain rates for the direction-of-motion rotated grid were calculated for the inner core (rings 1 and 2), stratified by motion of the tropical cyclone (fast movers [>5 knots] and slow movers [$\leq$ 5 knots]) and are shown in Figs. 26-27. Additionally, in Figs. 28-32 inner core azimuthal rain rates were stratified by the stage in which they occurred during Freda's lifetime (i.e., disturbance/depression [$\mathbf{P_{min}}$ > 1000 mb], tropical storm [$\mathbf{P_{min}}$ 1000-978 mb], weak typhoon [$\mathbf{P_{min}}$ 977-950 mb], and strong typhoon [$\mathbf{P_{min}}$ < 950 mb]). Fig. 33 illustrates average radial rain rates that were calculated for each of these stages.

3. ECMWF Grids

The ECMWF runs a global spectral model every 12 hours at 0000 and 1200 UTC. This model is full physics (based upon the primitive equations) and had a resolution of 2.5° by 2.5° in 1987. An analysis of the ECMWF model by Reed *et al.* (1988) found that it has an impressive ability in forecasting the synoptic scale circulation of the tropics,

even in data sparse regions. Chang and Lam (1989) used the ECMWF model to predict the movement of Typhoon Wayne (1986). They determined that the model provided a rather accurate prediction of Wayne's movement and the large scale environmental flow. Additional research by Ploshay *et al.* (1992) judged the ECMWF's performance in the tropics as being more faithful to the actual data than other global atmospheric models (i.e., GFDL and NMC).

Using the GEneral Meteorological software PAcKage (GEMPAK), a number of products were created from the initialization fields of ECMWF model runs for September 3-14, 1987. Plots of geopotential heights at numerous pressure levels, potential vorticity, wind shear between 250 and 850 mb, moisture convergence, and other meteorological parameters were generated. These were done in order to access the over all synoptic patterns. See Fig. 34 for an example of the 200 mb geopotential height plots, note Freda's location indicated by the dot. Tables to evaluate tropospheric moisture flux convergence and ERFC were also generated.

Tropospheric water vapor flux convergence was calculated by summing the influx of moisture at the 300, 500, 700, 850, and 1000 mb pressure levels. These levels encompass most of the tropospheric moisture flux since only a negligible amount of moisture occurs above 300 mb (Frank 1977). The radius chosen to perform the calculation was 222

km since research by Frank (1977) indicates that evaporation is nearly four times less than precipitation within the core; so that the water vapor budget can be approximated as: flux = precipitation. An example MFC calculation using Eq. 12 is contained in Appendix C.

Vertical shear was calculated by averaging the difference between the magnitude of the horizontal wind (**u** and **v** components) at 250 and 850 mb (i.e., Eq. 13) at five points. These points included the corners of a 5° box centered on the storm and a fifth point in the middle of the storm. This scheme was used to eliminate vertical shear created by the tropical cyclone itself.

Using Eq. 14, ERFC was calculated on an annulus 600-1000 km from the center of the tropical cyclone at the 200 mb level. This allowed the calculations to be outside of the Central Dense Overcast (CDO) region to prevent effects due to the storm itself. Also, research by DeMaria *et al.* (1991) found that ERFC in this annulus had a high correlation with future intensity change. Calculation of ERFC is illustrated by an example in Appendix C.

CHAPTER IV

RESULTS/DISCUSSION

1. Convective Ring Cycle Validated

In general, the convective ring cycle (Willoughby *et al.* 1982; Willoughby 1988; Willoughby 1990) was observed in this study. The cycle is illustrated by this single case study of Freda in Figs. 35-36. Fig. 35 shows the average rain rate according to ring number and time of the SSM/I observation. The data gaps are indicated by empty white grid boxes. Rain rates within ring 1 reach a peak of 9.61 mm h^{-1} at 2100 UTC on September 5, indicating the formation of the eye wall or inner convective ring ($R \geq 3$ mm h^{-1}). The maximum rain rate remains within the core region until 0900 UTC on September 7. Then, a gap in the coverage prevents observation until 2100 UTC on September 9.

Fig. 36 further illustrates the convective ring cycle for the more contiguous data from 2100 on UTC September 9 until 2100 UTC on September 14. Rain rate maxima of 7.13 mm h^{-1} and 6.14 mm h^{-1} occur in ring 1 and 2, respectively, on September 9. Just as the intensity reaches its peak at 0000 UTC on September 10, a convective ring forms in rings 5 and 6. This ring propagates inward to ring 3 until 2100 on

September 10 and the previous inner convective ring disappears. Intensity during this period decreased slightly.

Next, another convective ring forms in rings 5 and 6 as the second ring disappears and the eye radius increases (depicted by the large radius of less than 1 mm h^{-1} rain rates, indicative of increasing subsidence within the eye region). This third convective ring contracts, intensifies, and enters the inner core region at 0900 UTC on September 13. This causes the eye radius to constrict. While the third convective ring formed and later contracted, intensity decreased from 115 knots to 55 knots. This is not what is predicted by the convective ring cycle, however.

2. Latent Heat Release and Intensification

To explain this departure, the effects of LHR on intensity were examined. Also, the environmental forcing on the inner and outer core LHR was studied. The temporal changes in total LHR were plotted with respect to changes in MSLP (intensity) in Fig. 37. Although no observations occurred on September 8, the oscillations in LHR and intensity coincide with previous studies (Rodgers and Adler 1981; MacArthur 1991) relating the two variables. The figure shows that rapid increases of inner core LHR precede intensification. A similar pattern is observed in the other LHR parameters shown in Figs. 24-25. The patterns shown by the other LHR parameters concur with previous research by

Rhudy (1989) and MacArthur (1991) which showed that the majority of LHR appears to be caused by convection ($R \geq 5$ mm h^{-1}).

On September 10, a rapid decrease in LHR precedes a period of rapid decrease in intensity (Fig. 37). However, an increase in LHR on the September 13 has little influence on the intensity of Freda. It should be remembered that these LHR fluctuations are only for the inner core and reflect instances where convective rings are inside rings 1 and 2. The influence of the four environmental parameters in this study on LHR are illustrated in Figs. 38, 41, 43, and 45 (inner core) and Figs. 39, 42, 44, and 46 (outer core--an annulus from 111-222 km).

3. *SST*

In both the inner and outer core, LHR does not appear to be controlled by SST. This is because Freda stayed over warm open ocean waters (>26 °C) throughout the period of September 3-14 (Figs. 38-39). The only significant point concerning SST is that the maximum intensity of 125 knots (63 m s^{-1}) occurs on September 10 when SST is at a maximum value of 29.2 °C, as shown in Fig. 40. This SST value yields a potential intensity of 171 knots (86 m s^{-1}) using Eq. 11.

4. Vertical Shear

Vertical shear has little effect on LHR in both the inner and outer core until after September 9 (i.e., shear is

increasing while LHR increases). However, extreme values of vertical shear after 0000 UTC on September 10 correspond to a decline in the second peak in inner core LHR (Fig. 41). In the outer core from September 10 onward (Fig. 42), oscillations in vertical shear and LHR appear to suggest that as shear increased, LHR decreased--as expected. In summary, values of shear above 20 m s^{-1} increasingly affect core LHR and intensity as Freda moves farther north into the Westerlies of the midlatitudes, especially after September 13 when the third peak in inner core LHR diminishes as shear reaches it maximum value.

5. Moisture Flux Convergence

Moisture flux convergence appears to have different effects on the inner and outer core regions. Within the inner core (Fig. 43), positive values of moisture flux do not relate to inner core convection or diabatic heating associated with LHR due to condensation and precipitation. However, within the outer core (Fig. 44), a large influx of moisture precedes LHR from September 10-14. This differential effect may be explained by the fact that strong inner core inertial stability of intense tropical cyclones prevents horizontal middle and lower tropospheric transport of moisture from occurring in the inner core (Holland and Merrill 1984). The LHR in the outer core is indicative of the role in the formation of convective rings played by moisture flux convergence. Also, the resolution of the

ECMWF model initialization data is about 250 km and therefore may not be fine enough to resolve the effects of moisture flux convergence in the inner core (within 111 km).

6. ERFC

ERFC appears to be the major factor that determines total core LHR. In both the inner and outer core, positive and negative values of ERFC precede or are concurrent with corresponding increases and decreases in LHR (Figs. 45-46). This is true only until September 13, afterward, extremely high values of vertical shear prevent LHR despite large positive ERFC values. Similar results were found by DeMaria *et al.* (1991) where a confounding effect due to vertical shear prevented the use of just ERFC as a predictor of future intensification.

7. Precipitation Structure

Figs. 26 and 27 depict the direction-of-motion, azimuthally stratified average rain rates in terms of fast moving and slow moving periods of Freda's life cycle. The values obtained in these figures compare favorably with other research by Marks (1985), and Burpee and Black (1989). Like the aforementioned studies, slow moving storms (Fig. 26) have a maximum rain rate on the left side of the tropical cyclone, while, maximum rain rate occurs on the right side of the faster moving tropical cyclone (Fig. 27).

Figs. 28-32 illustrate evolution of the structure and distribution of precipitation throughout Freda's various

stages and overall life span with regards to azimuth. These results are consistent with Frank (1977), Marks (1985), and Burpee and Black (1989) in both magnitude and azimuthal location of rain rate maxima. The only exceptions are the low rain rates in the weak typhoon stage (Fig. 30) and the high rain rates in the tropical storm stage (Fig. 29). This departure will be explained below as a result of ERFC.

Motion and intensity of tropical cyclones tend to be negatively related, especially in Freda's case (See Fig. 3). This means that because of the slower translation speeds of Freda during its more intense stages (weak and strong typhoon) rain rate maxima should be on the left side, which is the case as shown in Figs. 30-31. The opposite effect is seen by the rain rate maximum in the faster moving tropical storm stage occurring on the right side (Fig. 29).

The azimuthal distribution of rain rate throughout Freda's life span is similar to previous research (Frank 1977; Marks 1985; and Burpee and Black 1989). As the above research suggests, a slight asymmetry of rain rates causes the rain rates on the right side to be slightly greater as shown in Fig. 32. The average rain rate for Freda's inner core is 1.8 mm h^{-1}, which compares to 3.9, 2.7, and 3.6 mm h^{-1} (Frank 1977; Marks 1985; Burpee and Black 1989, respectively). The disparity in the rain rate from those of Frank (1977) and Burpee and Black (1989) may be the result of different definitions of inner core area those

researchers used. The lower rain rate for Freda may also be due to the tendency for the SSM/I-based algorithm to underestimate rain rate slightly (Adler *et al.* 1992).

Average radial rain rates for all eight rings stratified by storm stage are contained in Fig. 33. The results indicated in this figure are very similar to those found in research by Rodgers and Adler (1981), except that the maximum average rain rate occurs during the tropical storm stage instead of the strong typhoon stage.

Lastly, ERFC may explain why the average radial rain rates in Fig. 33 depart from previous research by Rodgers and Adler (1981). They found that the radius of maximum rain rates for Northern Pacific tropical cyclones tended to contract as the storm intensified. Fig. 33 shows a similar relationship except for the tropical storm stage average radial rain rates. However, an extremely high ERFC value occurred on September 5-6 (59.3 m s^{-1} day^{-1}) which was during the tropical storm stage of Freda. This caused a spike in the ring 2 tropical storm average radial rain rate and, therefore, the inner core rain rate. From this result, it appears that ERFC can have a very dramatic impact on the rain rate and, therefore, LHR with its subsequent intensification.

CHAPTER V

CONCLUSION

This one case study confirmed the importance of latent heating due to convection in the inner core and future intensification. SST was not found to be an inhibiting factor since Tropical Cyclone Freda remained over warm open ocean its entire life span. The differential effects of tropospheric moisture flux in the outer and inner core were attributed to lower and middle tropospheric inertial stability considerations. That is, the strong inertial stability of the inner core prevents MFC from impacting LHR, while MFC appears to help increase LHR in the outer core. Upper level ERFC was highly related to changes in LHR except in the presence of strong vertical shear which counters any positive influence ERFC may have on increasing LHR (an effect seen before by DeMaria *et al.* [1991]).

Willoughby's (*et al.* 1982, 1988, and 1990) convective ring cycle was verified and departures from it were explained in terms of environmental forcing mechanisms which, in this case study, prevented re-intensification as the outer convective ring contracted. Further research into the upper tropospheric adjustment between tropical cyclones

and midlatitudinal troughs and TUTT's may illuminate the complex interaction between vertical shear and upper level ERFC.

Limitations of the SSM/I's coverage and reliability on the coarse resolution of the ECMWF model data are factors that should be taken into account when comparing this research with other research on this topic. With the launch of DMSP F9-F11 satellites, the new constellation of SSM/I sensors will allow better spatial and temporal coverage of the tropics. This will eliminate many of the problems with missing or incomplete data. Also, improved algorithms are allowing researchers to better utilize SSM/I data and take advantage of geostationary infrared (IR) satellite data to "fill in the data gaps" (Manobianco *et al.* 1991; Adler *et al.* 1991). Increased ECMWF model resolution of 1.25° x 1.25° and insertion of a tropical cyclone bogus in the years since 1987 will allow a more complete and accurate analysis of environmental forcing parameters and their interaction with the tropical cyclone, especially within the inner core.

This research validated the convective ring cycle (Willoughby *et al.* 1982) in a manner never before accomplished. The combination of satellite sensors and numerical models may provide an effective method for forecasters to predict intensity changes in tropical cyclones, even with the projected curtailment of aerial reconnaissance due to budgetary constraints.

APPENDIX A

TABLES

TABLE 1. SSM/I Channel Characteristics

Frequency (GHz)	Polarization	Resolution along-track (km)	Resolution cross-track (km)	Spatial sampling (km)
19.4	vertical	69	43	25
19.4	horizontal	69	43	25
22.2	vertical	50	40	25
37.0	vertical	37	28	25
37.0	horizontal	37	29	25
85.5	vertical	15	13	12.5
85.5	horizontal	15	13	12.5

TABLE 2. SSM/I Observations of Tropical Cyclone Freda

Date (Sept)	Time (UTC)	Direction of Motion	Speed of Motion (knots)	Latitude	Longitude	Stage
3	2030	293	12	10.4	147.5	Disturbance
4	2021	307	12	12.5	145.0	Disturbance
5	0853	307	13	14.3	143.3	Storm
5	2008	270	9	14.8	141.2	Storm
6	0840	090	2	14.8	140.8	Storm
7	0828	301	1	15.4	141.1	Weak Typhoon
9	2101	284	3	17.1	137.3	Strong Typhoon
10	0933	330	3	17.3	137.0	Strong Typhoon
10	2049	001	2	17.8	136.9	Strong Typhoon
11	0920	018	2	18.2	137.3	Strong Typhoon
11	2036	046	4	18.9	138.1	Strong Typhoon
12	0908	042	5	19.4	138.5	Weak Typhoon
12	2024	030	5	20.7	139.0	Weak Typhoon
13	0856	009	5	21.9	139.7	Weak Typhoon
13	2012	008	7	22.9	139.9	Storm
14	0843	007	8	24.4	140.0	Storm
14	1959	357	10	26.2	140.0	Storm

APPENDIX B

FIGURES

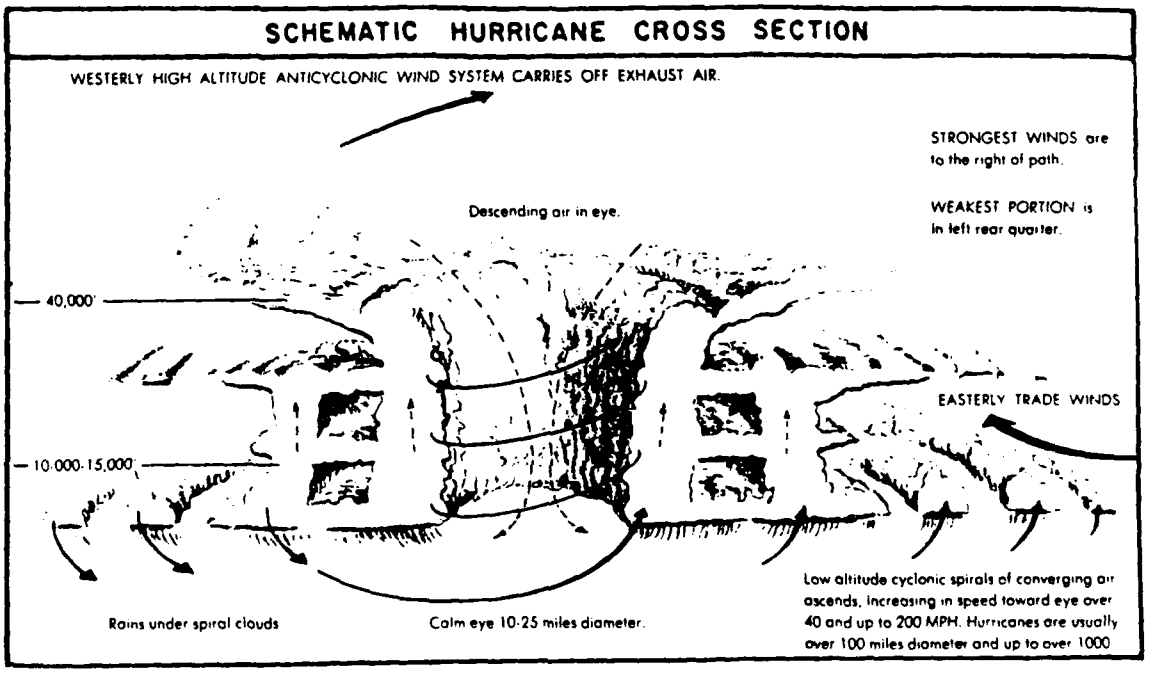
SCHEMATIC HURRICANE CROSS SECTION
WESTERLY HIGH ALTITUDE ANTICYCLONIC WIND SYSTEM CARRIES OFF EXHAUST AIR.
STRONGEST WINDS are to the right of path.
WEAKEST PORTION is in left rear quarter.
Descending air in eye.
40,000'
10,000-15,000'
EASTERLY TRADE WINDS
Rains under spiral clouds
Calm eye 10-25 miles diameter.
Low altitude cyclonic spirals of converging air ascends, increasing in speed toward eye over 40 and up to 200 MPH. Hurricanes are usually over 100 miles diameter and up to over 1000

FIGURE 1

Environmental Parameters That Influence Tropical Cyclones

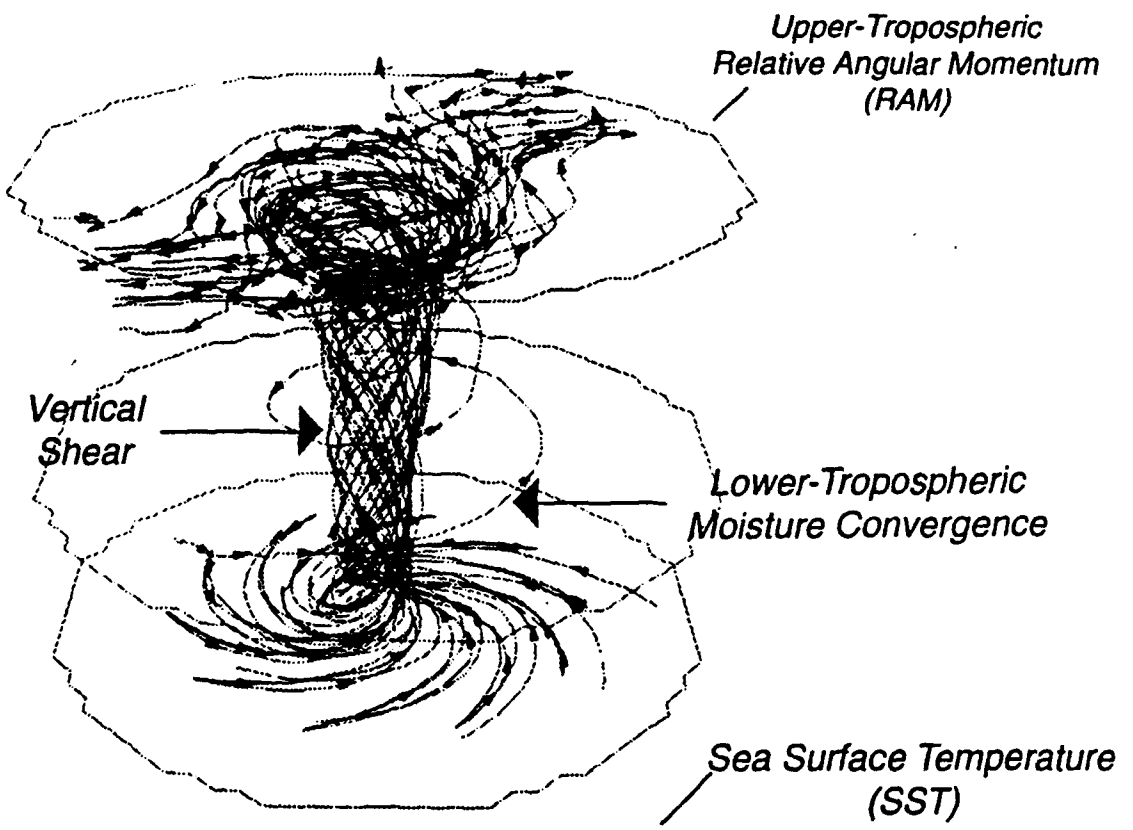

FIGURE 2

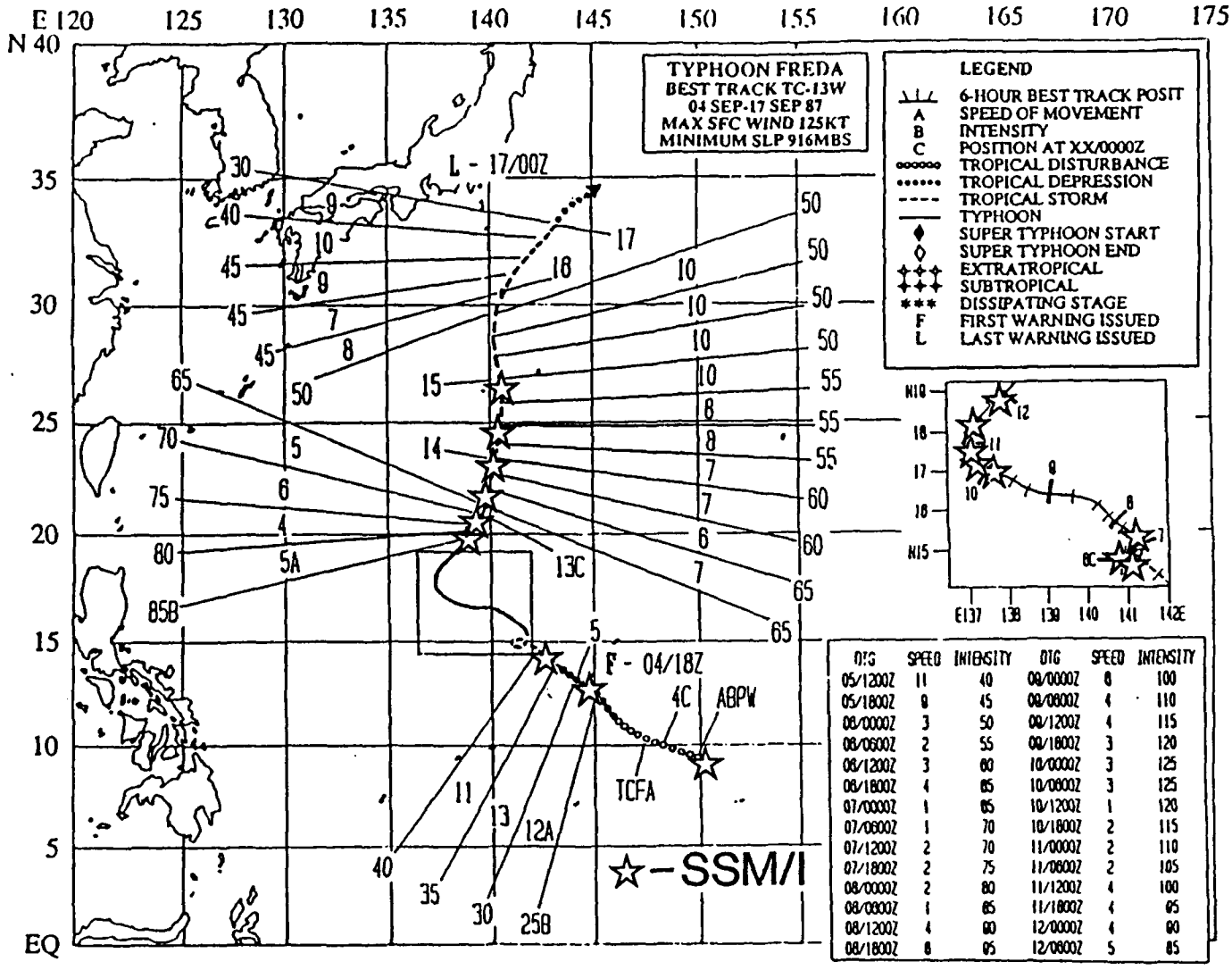

DTG	SPEED	INTENSITY	DTG	SPEED	INTENSITY
05/1200Z	11	40	08/0000Z	8	100
05/1800Z	9	45	08/0800Z	4	110
06/0000Z	3	50	08/1200Z	4	115
06/0600Z	2	55	08/1800Z	3	120
06/1200Z	3	60	10/0000Z	3	125
06/1800Z	4	65	10/0800Z	3	125
07/0000Z	1	65	10/1200Z	1	120
07/0600Z	1	70	10/1800Z	2	115
07/1200Z	2	70	11/0000Z	2	110
07/1800Z	2	75	11/0800Z	2	105
08/0000Z	2	80	11/1200Z	4	100
08/0600Z	1	85	11/1800Z	4	95
08/1200Z	4	90	12/0000Z	4	90
08/1800Z	8	95	12/0800Z	5	85

FIGURE 3

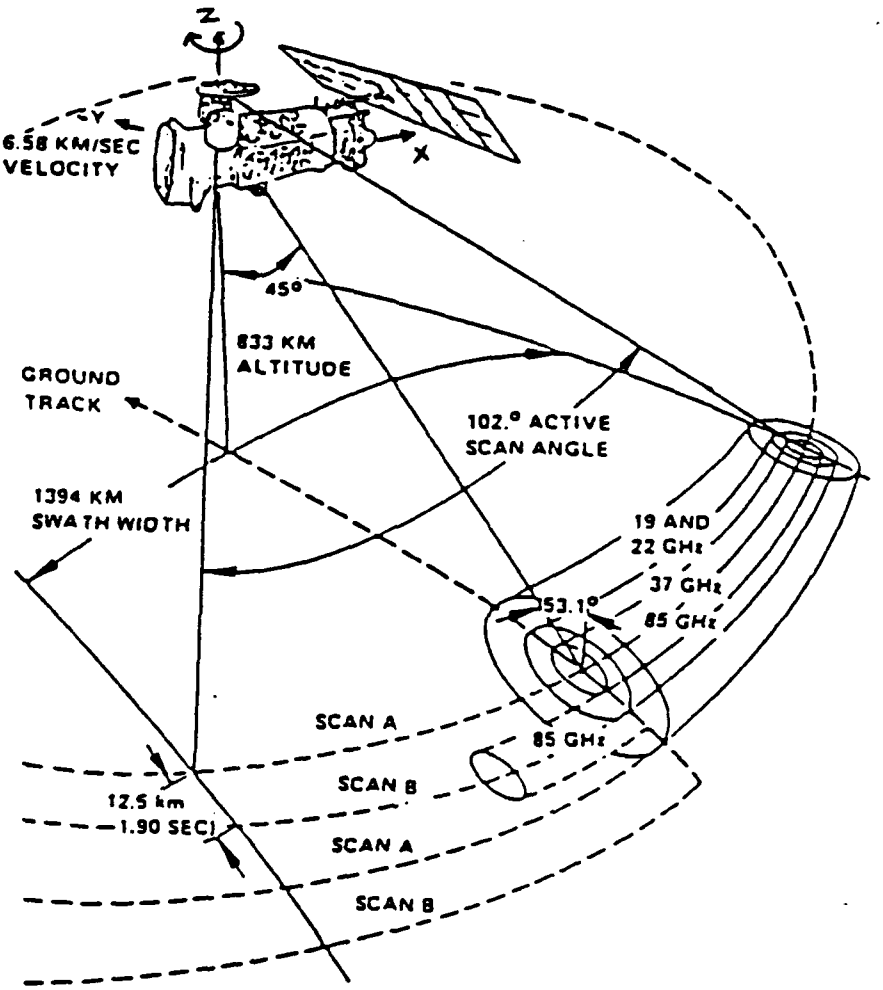
Z
-Y
6.58 KM/SEC
VELOCITY
X
45°
833 KM
ALTITUDE
GROUND
TRACK
102.° ACTIVE
SCAN ANGLE
1394 KM
SWATH WIDTH
19 AND
22 GHz
37 GHz
53.1°
85 GHz
SCAN A
85 GHz
SCAN B
12.5 km
(1.90 SEC)
SCAN A
SCAN B

FIGURE 4

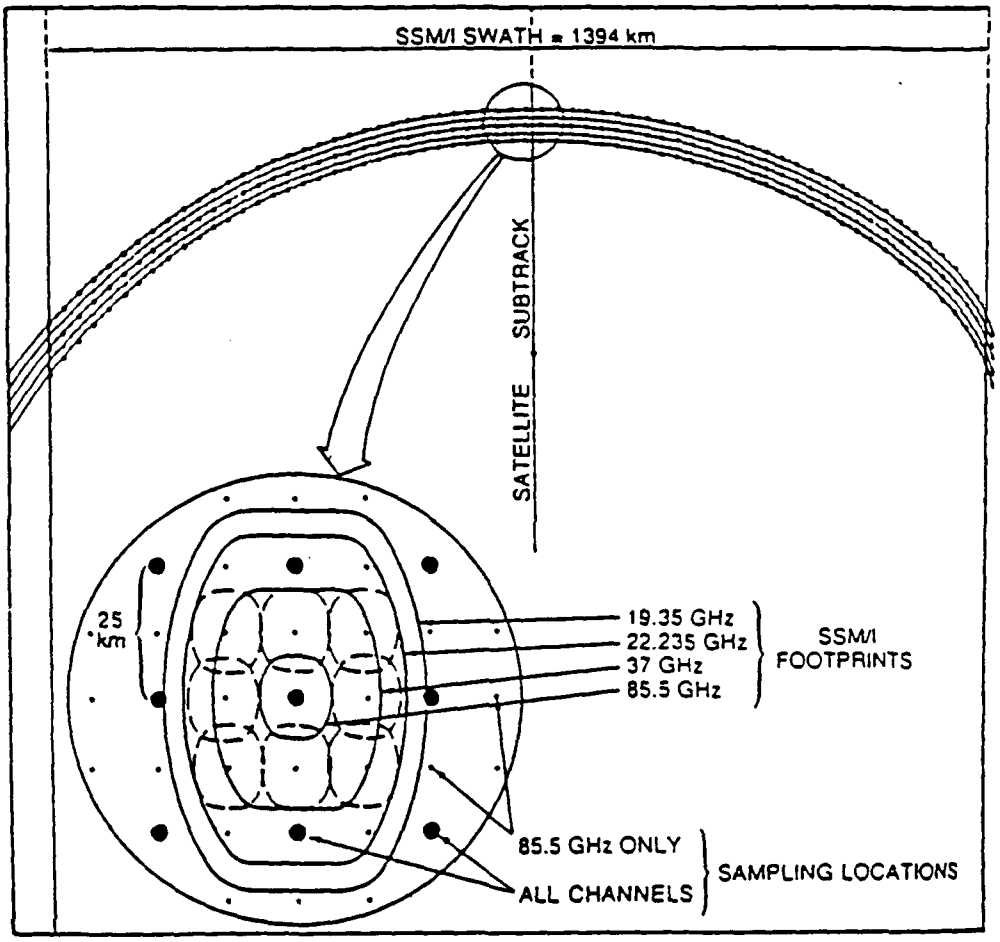
SSM/I SWATH = 1394 km
SATELLITE SUBTRACK
25 km
19.35 GHz
22.235 GHz
37 GHz
85.5 GHz
SSM/I FOOTPRINTS
85.5 GHz ONLY
ALL CHANNELS
SAMPLING LOCATIONS

FIGURE 5

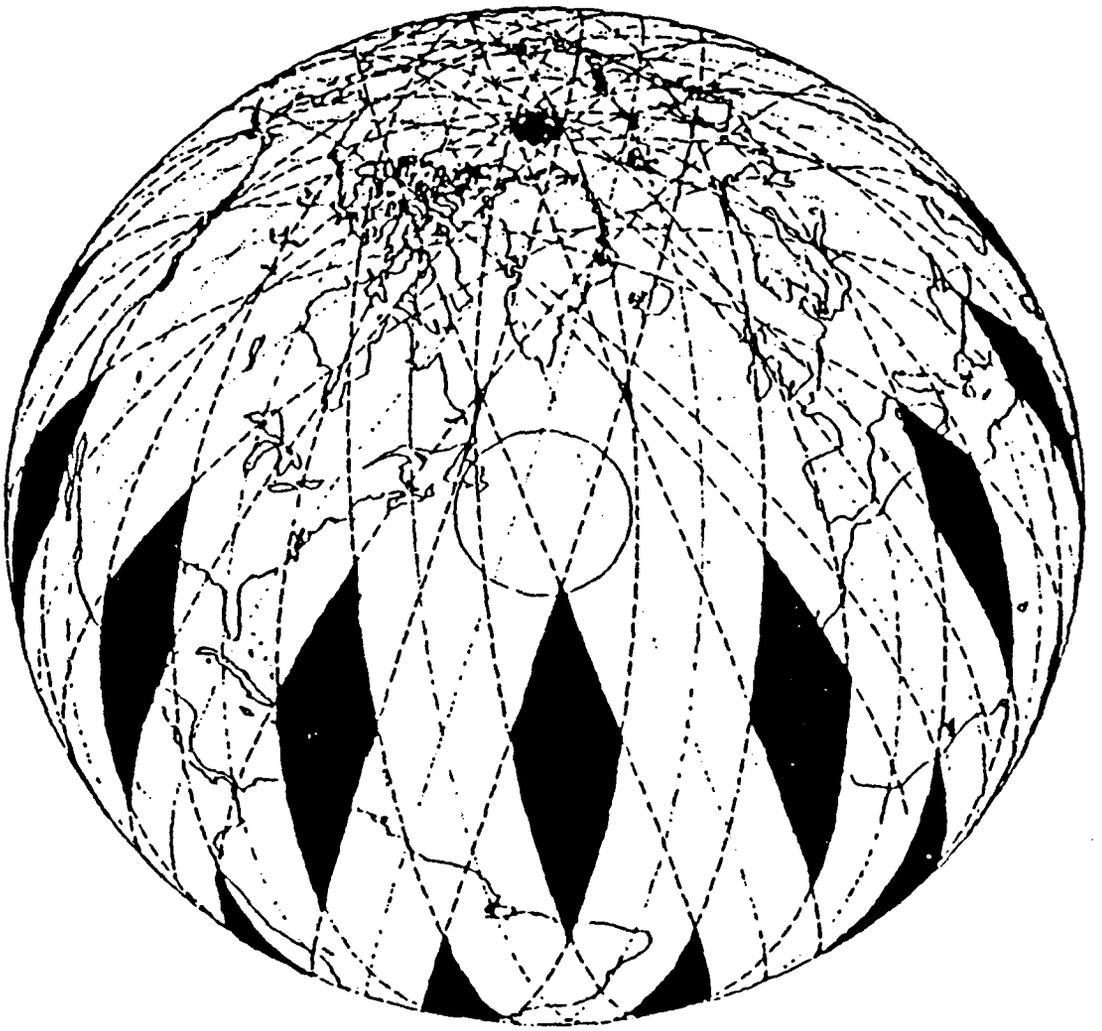

FIGURE 6

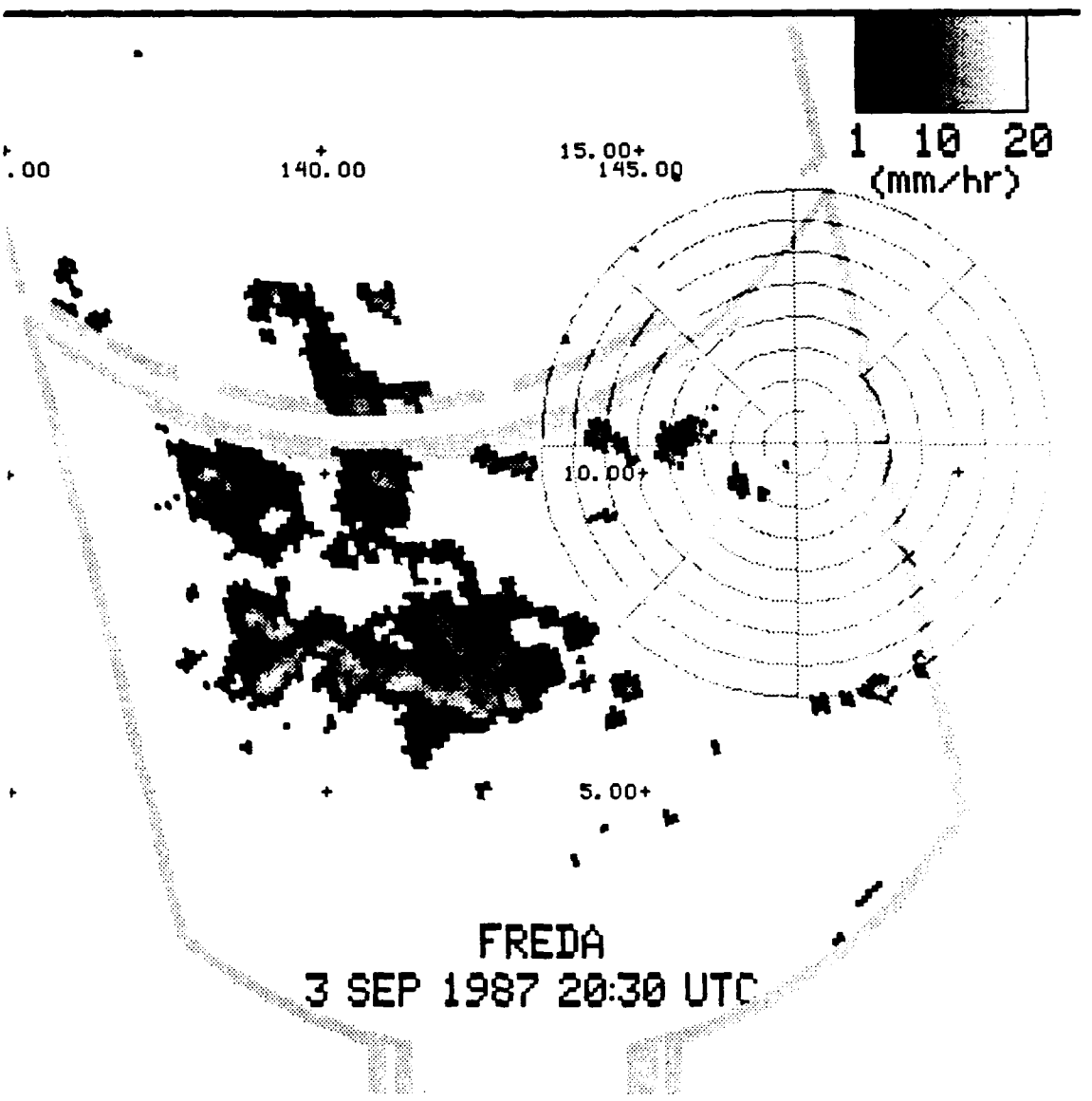
1 10 20
(mm/hr)
.00
140.00
15.00+
145.00
10.00+
5.00+
FREDA
3 SEP 1987 20:30 UTC

FIGURE 7

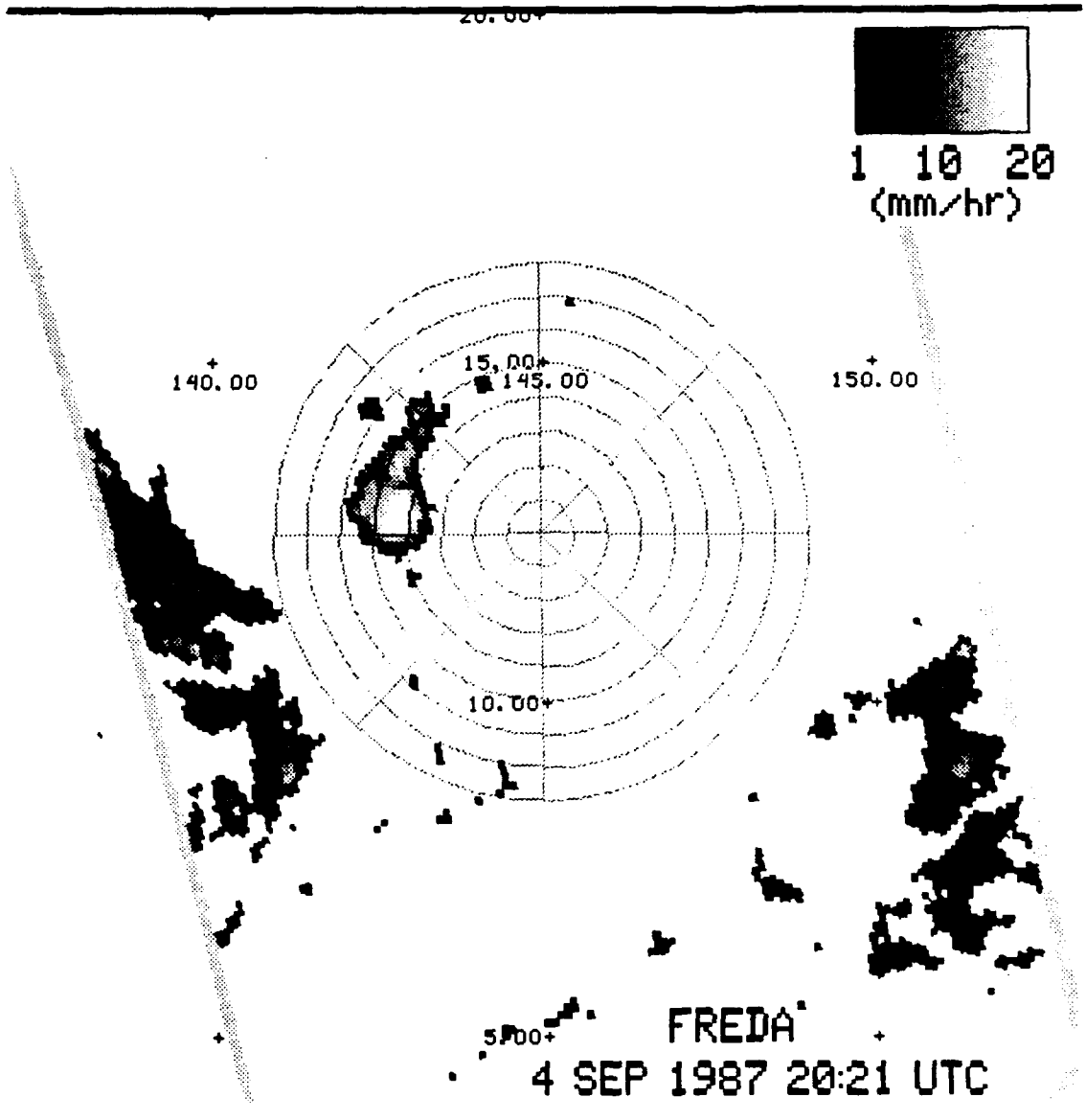
1 10 20
(mm/hr)
140.00
145.00
150.00
15.00
10.00
5.00
FREDA
4 SEP 1987 20:21 UTC

FIGURE 8

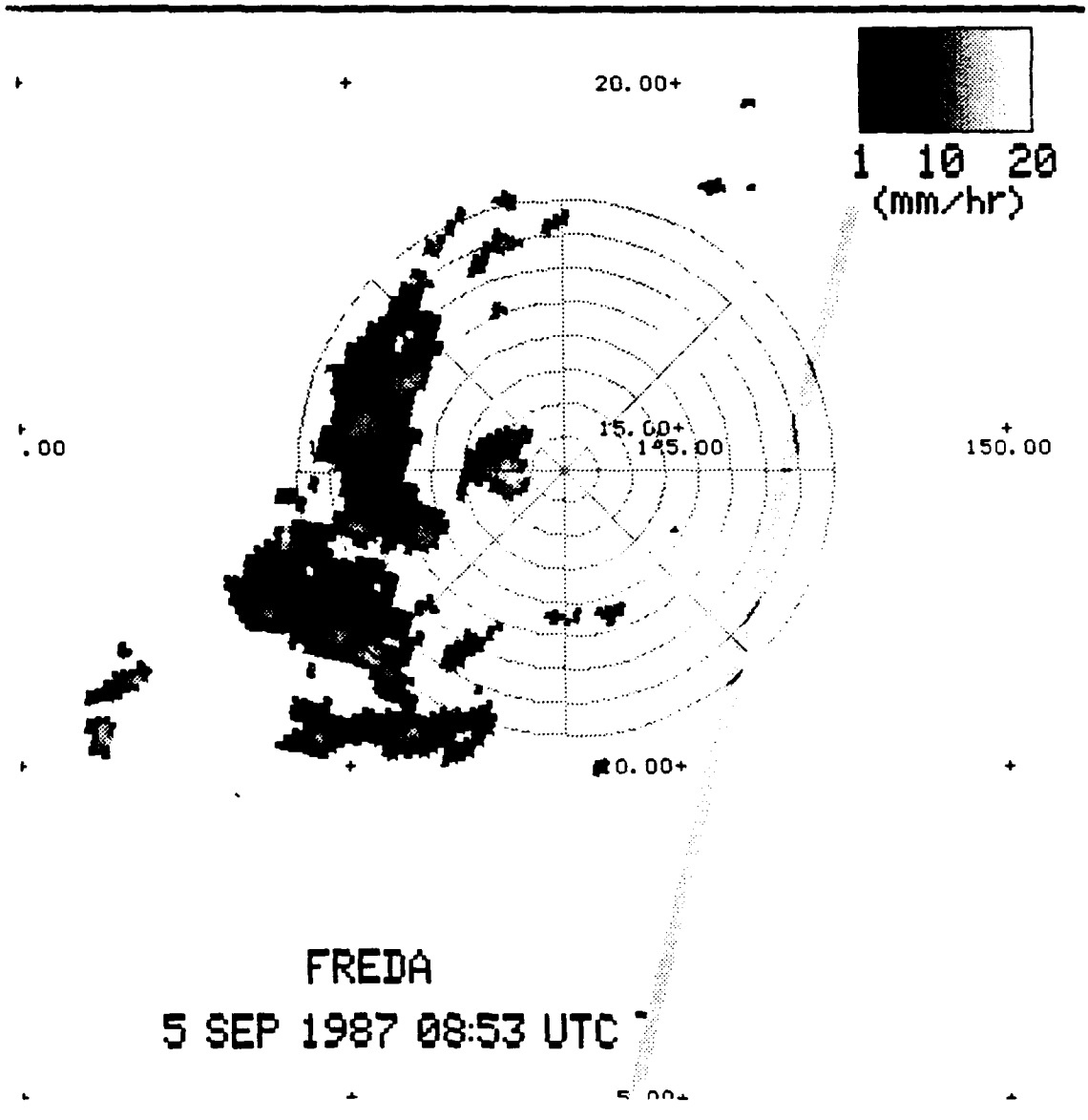
20.00+
1 10 20
(mm/hr)
15.00+
145.00
.00
150.00
0.00+
FREDA
5 SEP 1987 08:53 UTC

FIGURE 9

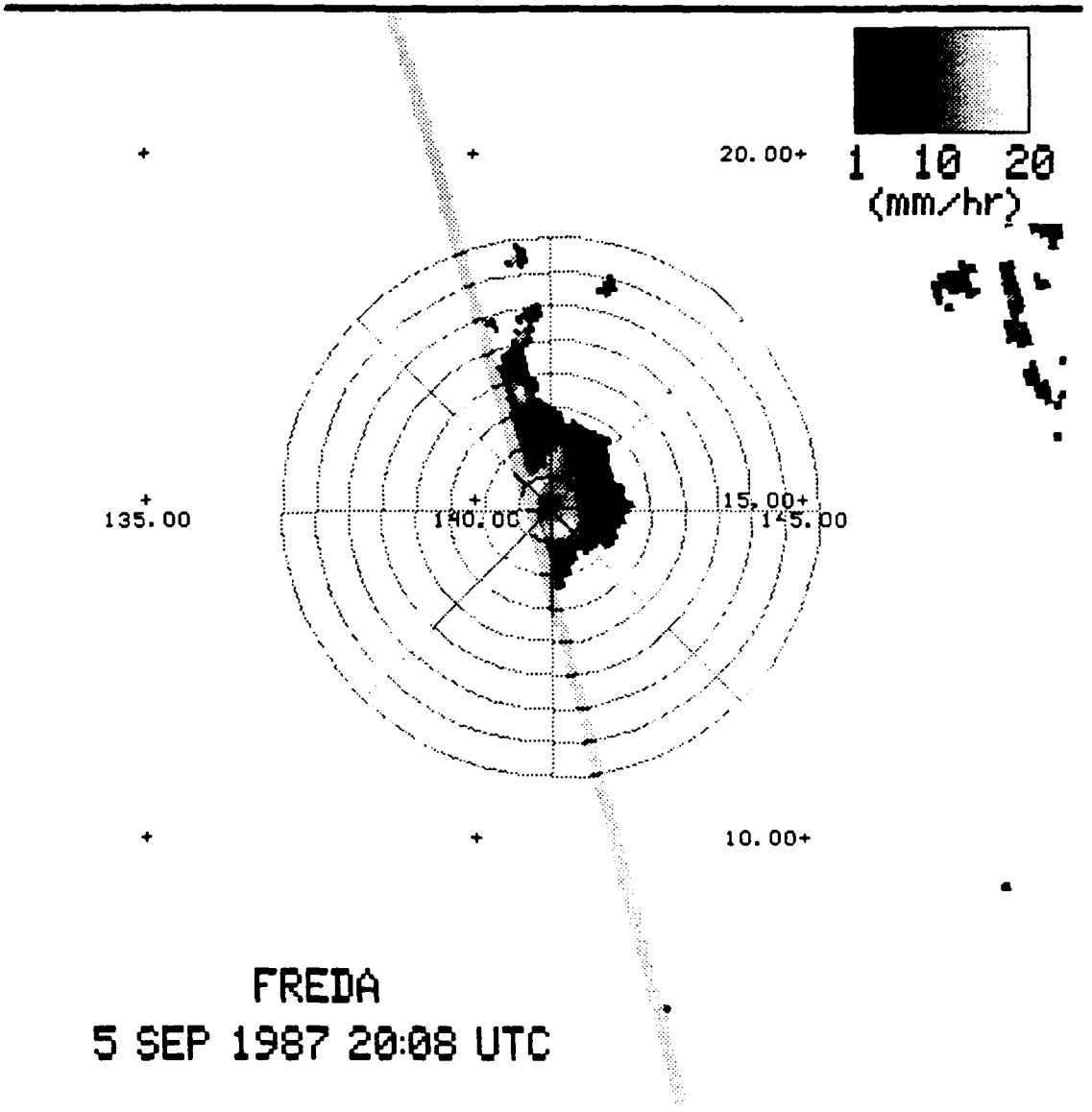
20.00+
1 10 20
(mm/hr)
135.00
140.00
145.00
15.00+
10.00+
FREDA
5 SEP 1987 20:08 UTC

FIGURE 10

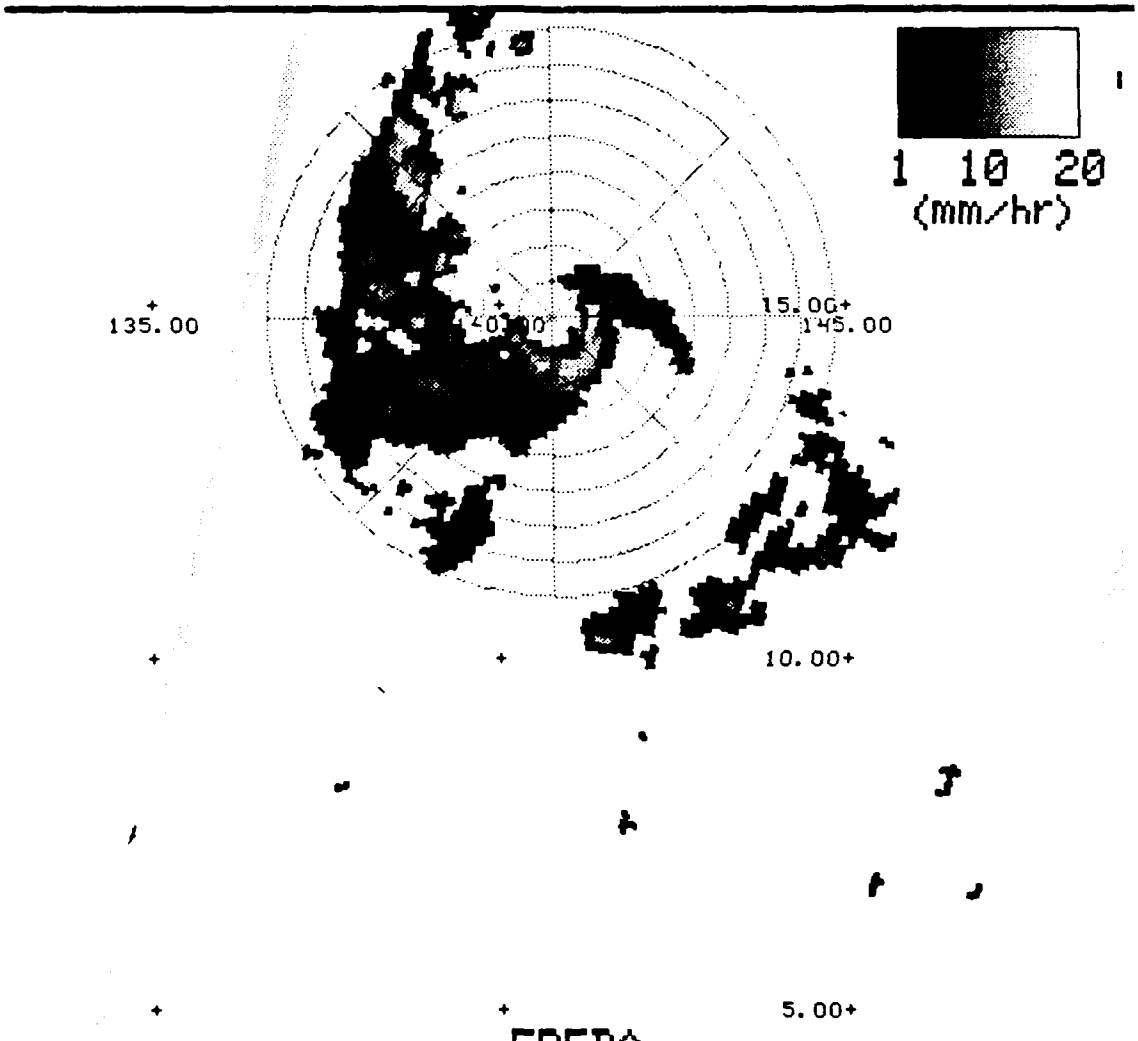
1 10 20
(mm/hr)
135.00
15.00+
145.00
10.00+
5.00+
FREDA
6 SEP 1987 08:40 UTC

FIGURE 11

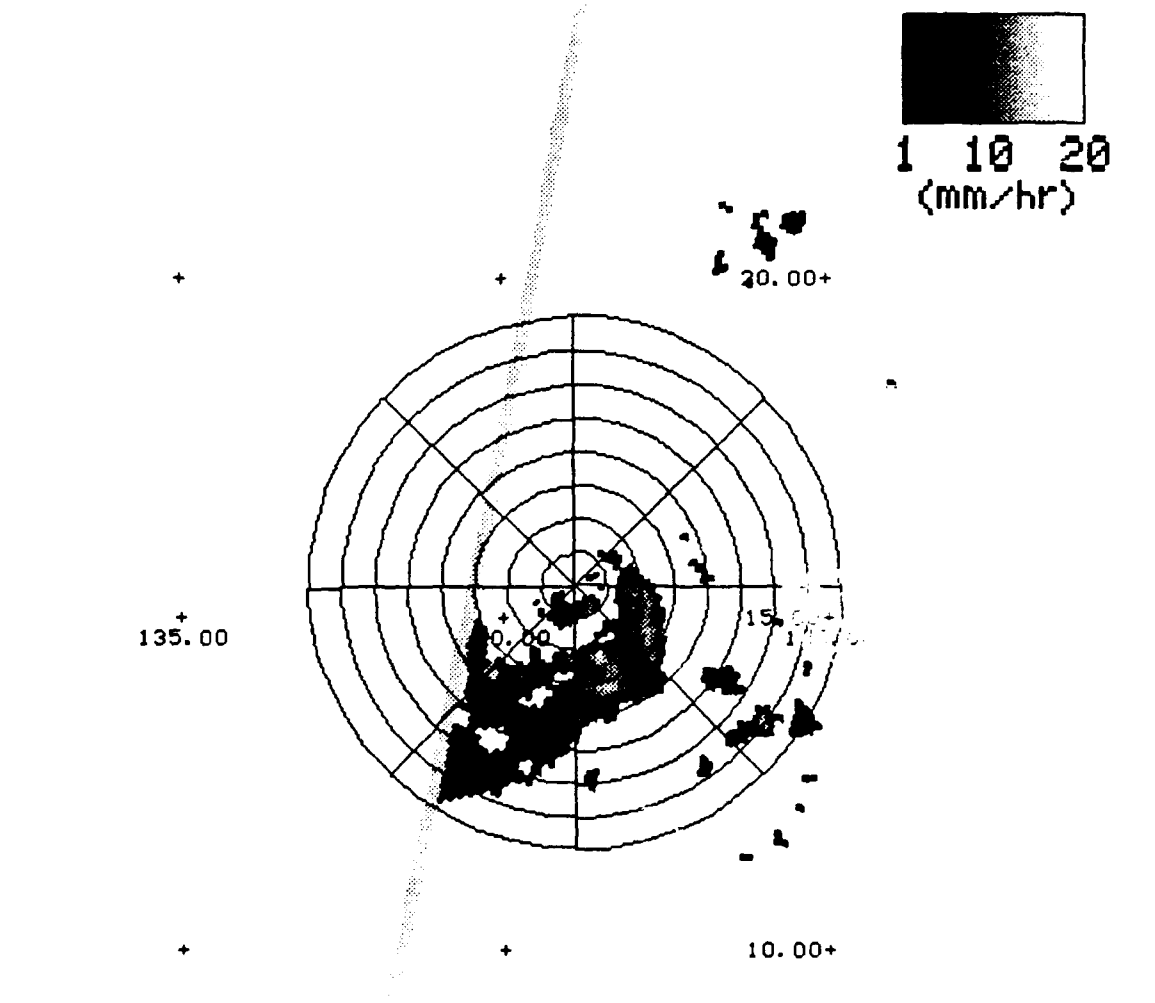

FIGURE 12

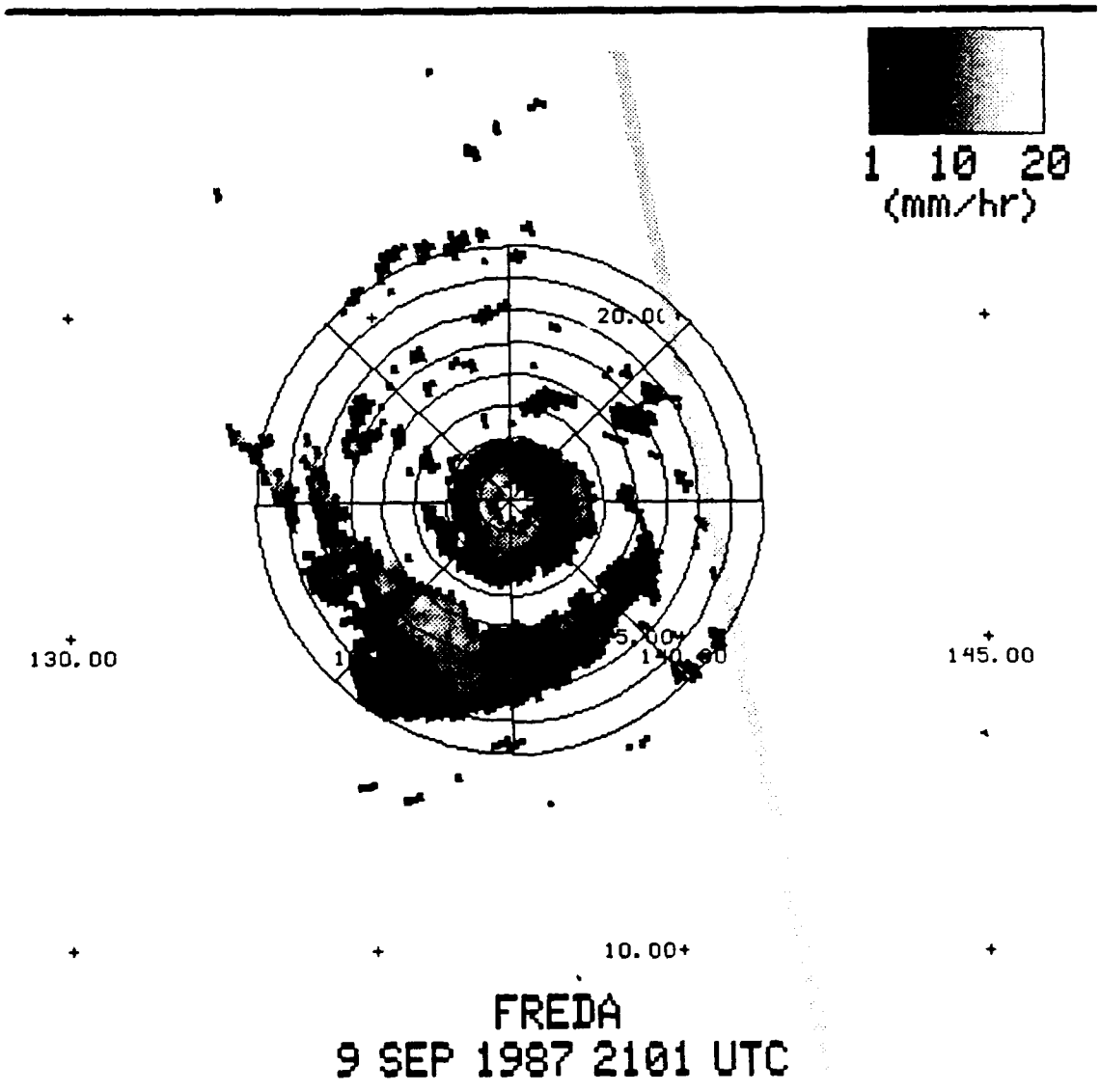

FIGURE 13

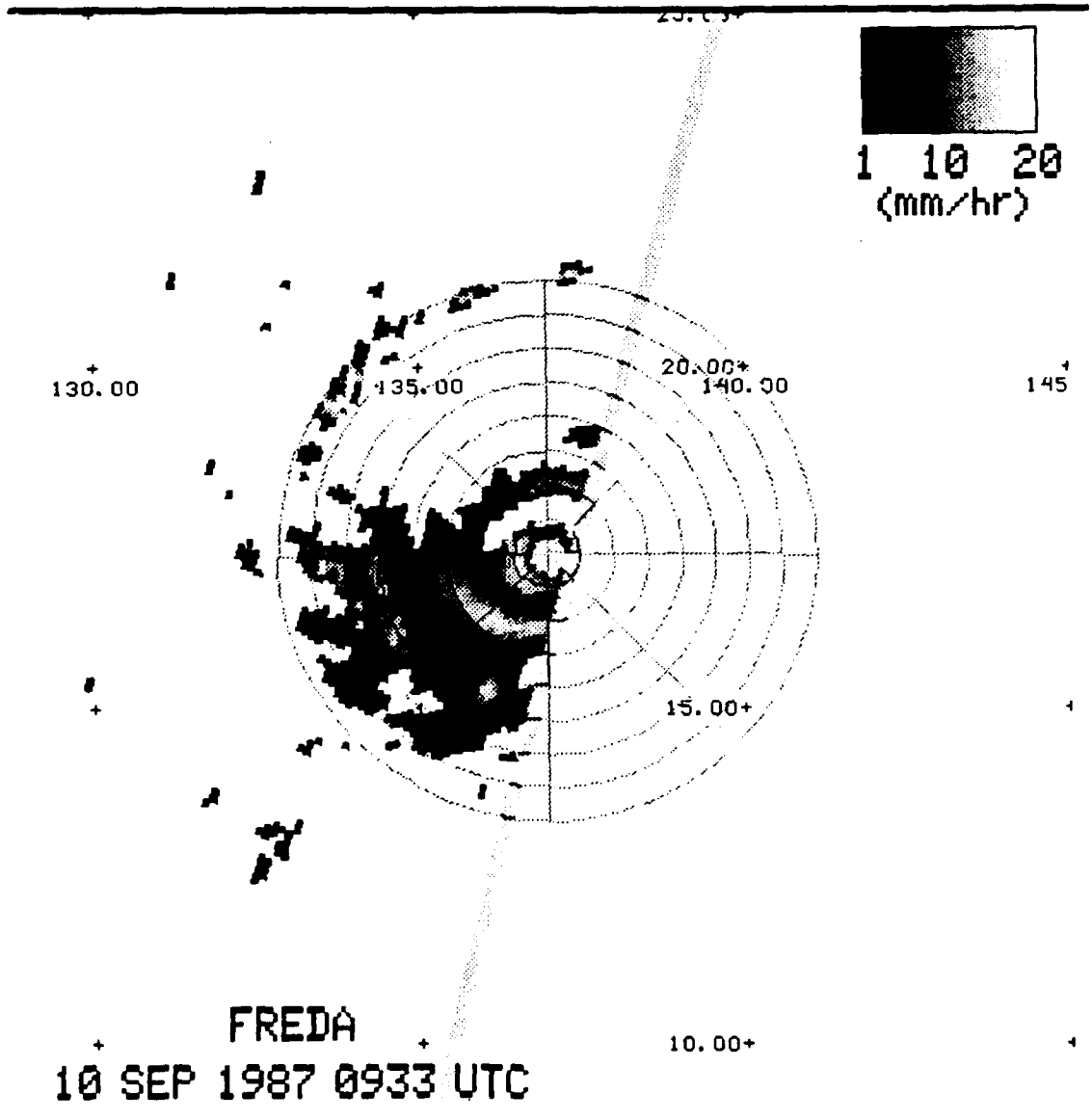
1 10 20
(mm/hr)
130.00
135.00
140.00
145
20.00+
15.00+
10.00+
FREDA
10 SEP 1987 0933 UTC

FIGURE 14

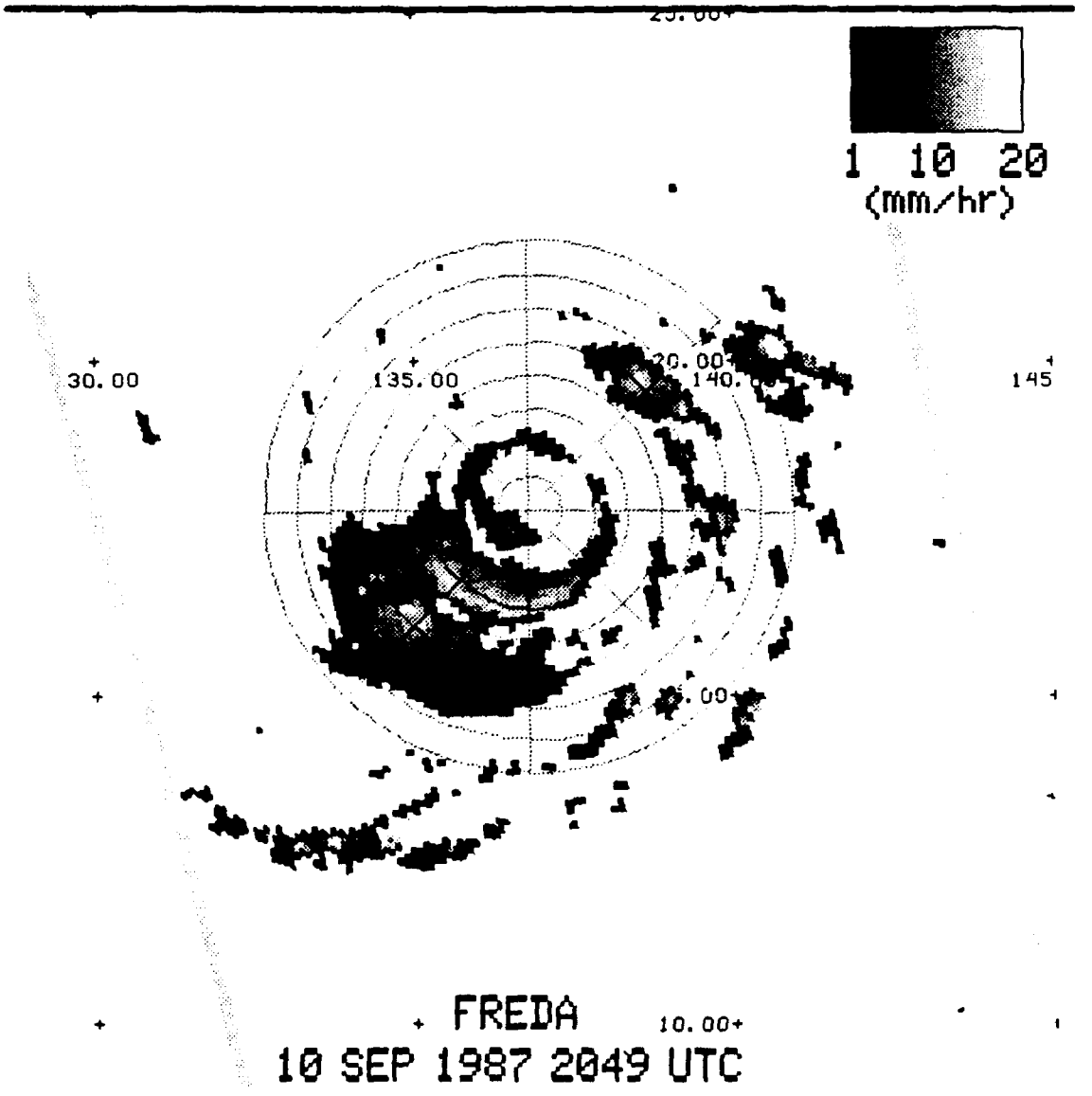

FIGURE 15

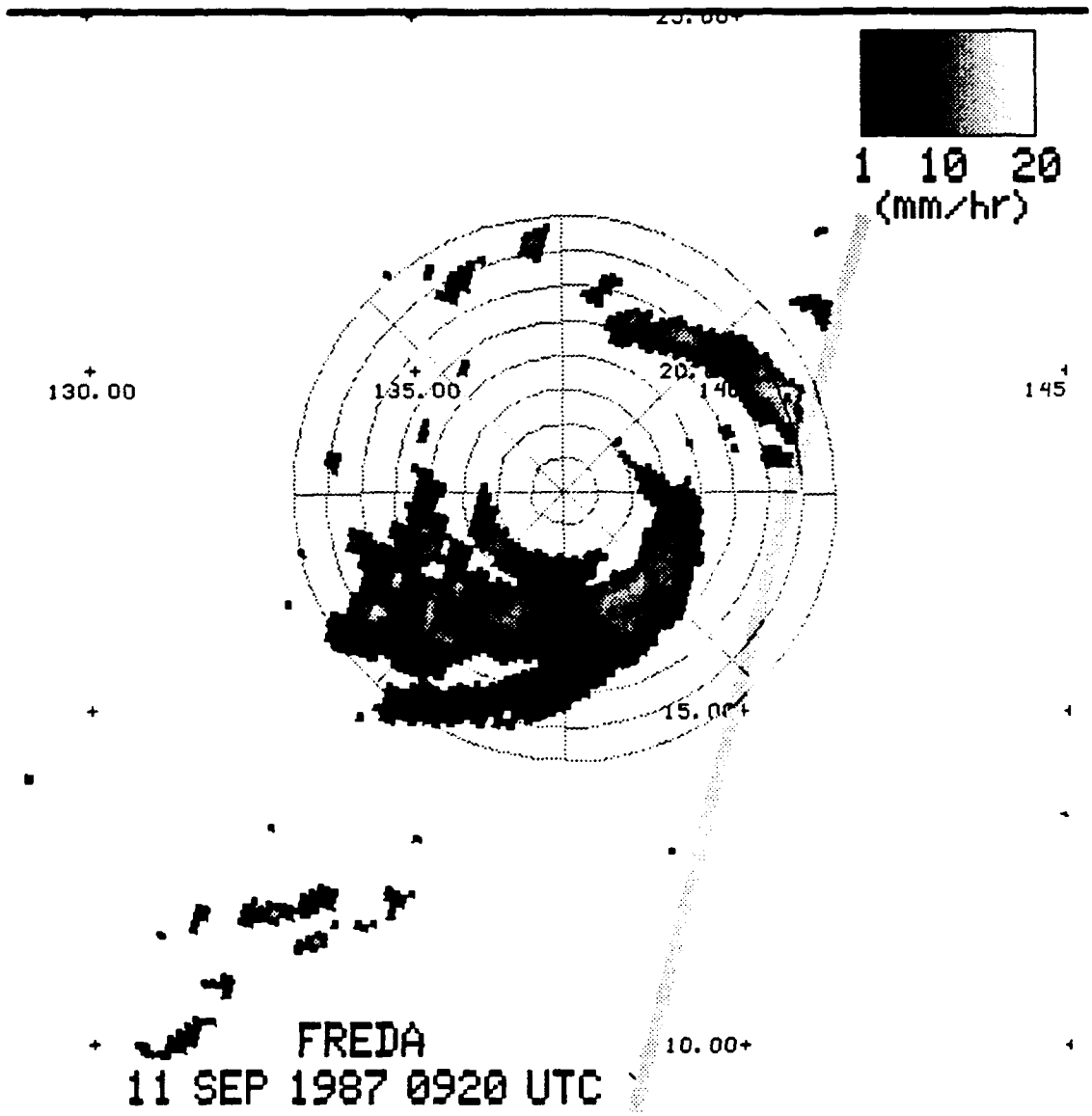
1 10 20
(mm/hr)
130.00
135.00
145
15.00
10.00
FREDA
11 SEP 1987 0920 UTC

FIGURE 16

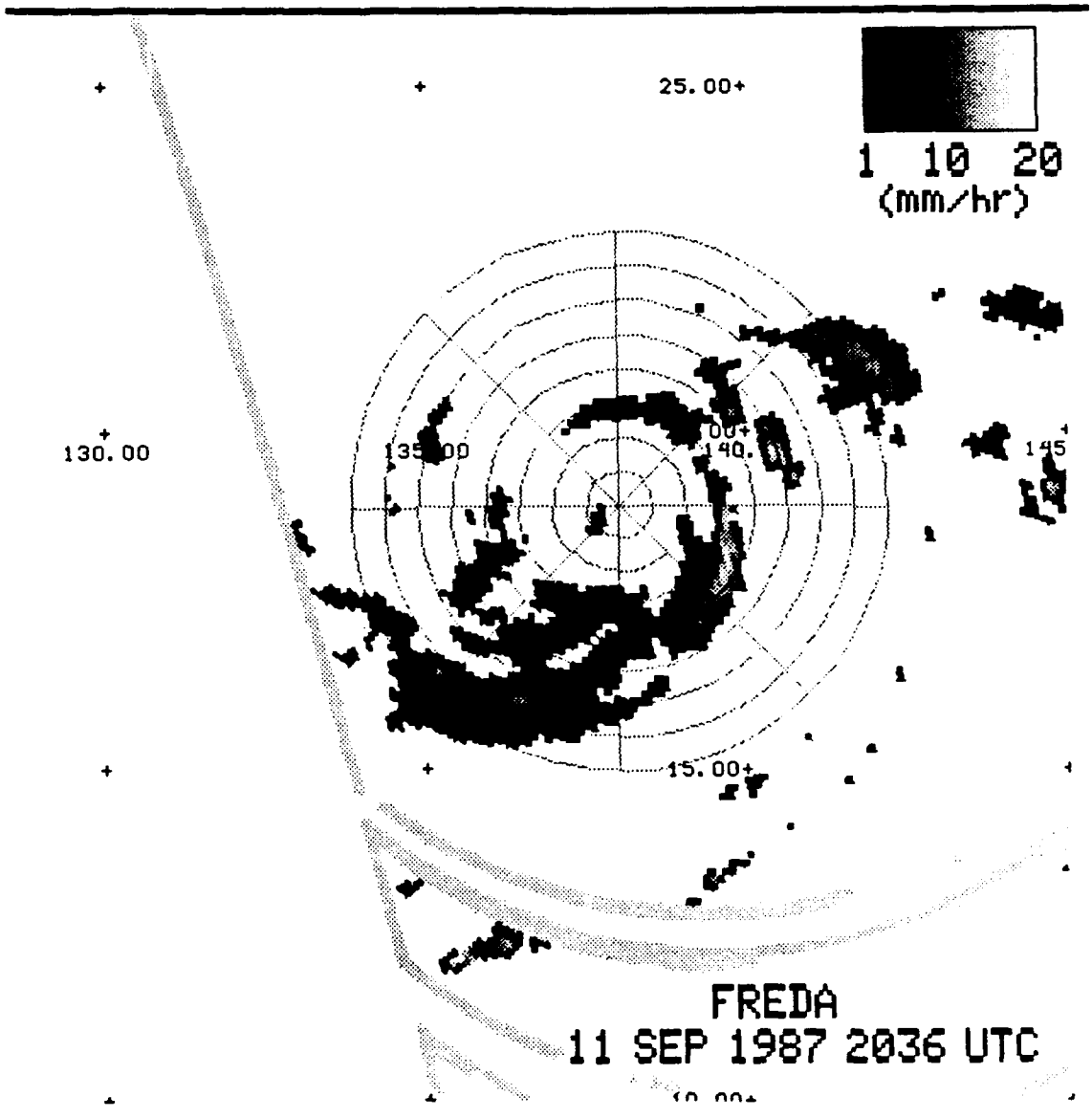
25.00+
1 10 20
(mm/hr)
130.00
135.00
140.00
145
15.00+
FREDA
11 SEP 1987 2036 UTC

FIGURE 17

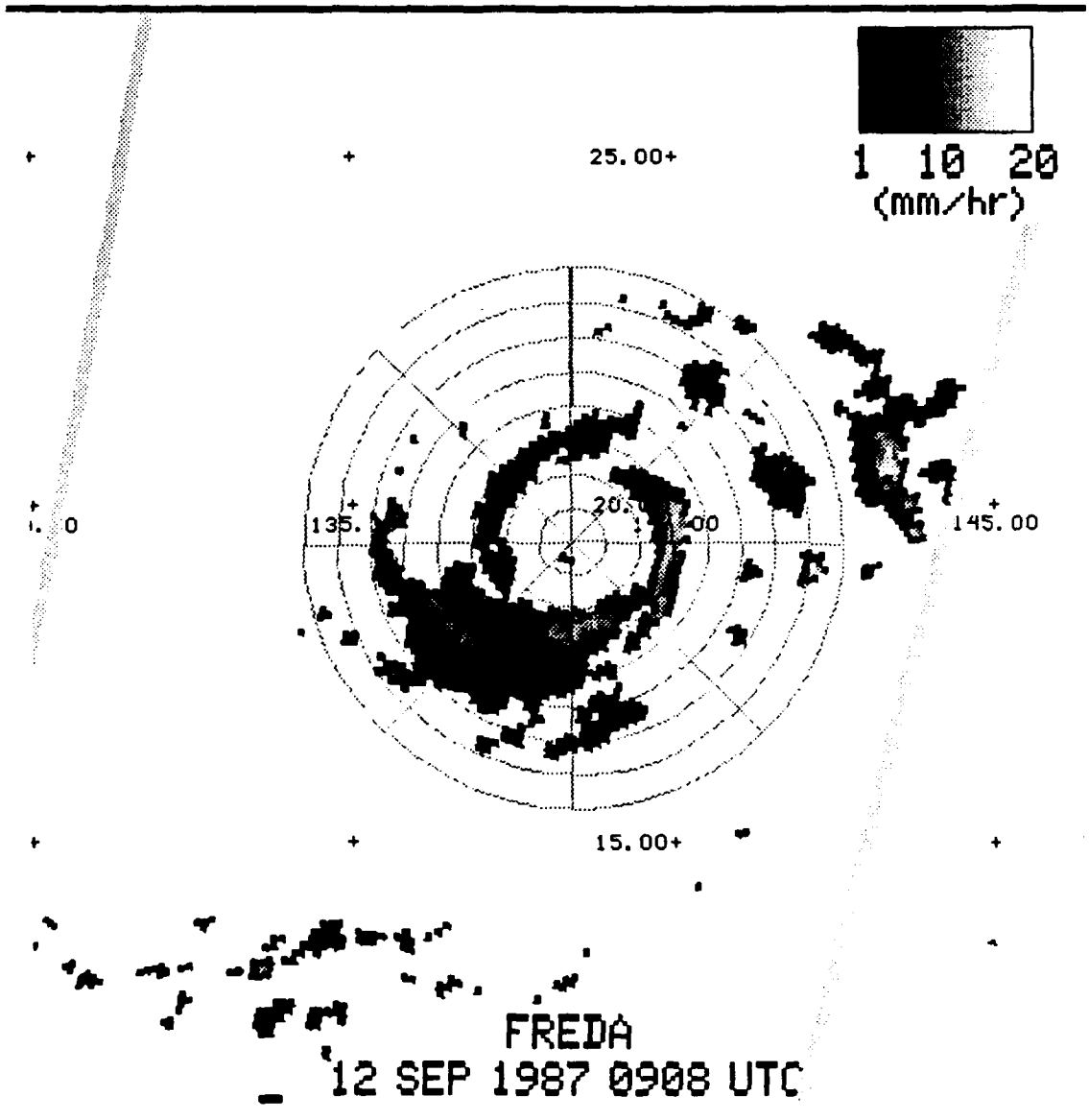

FIGURE 18

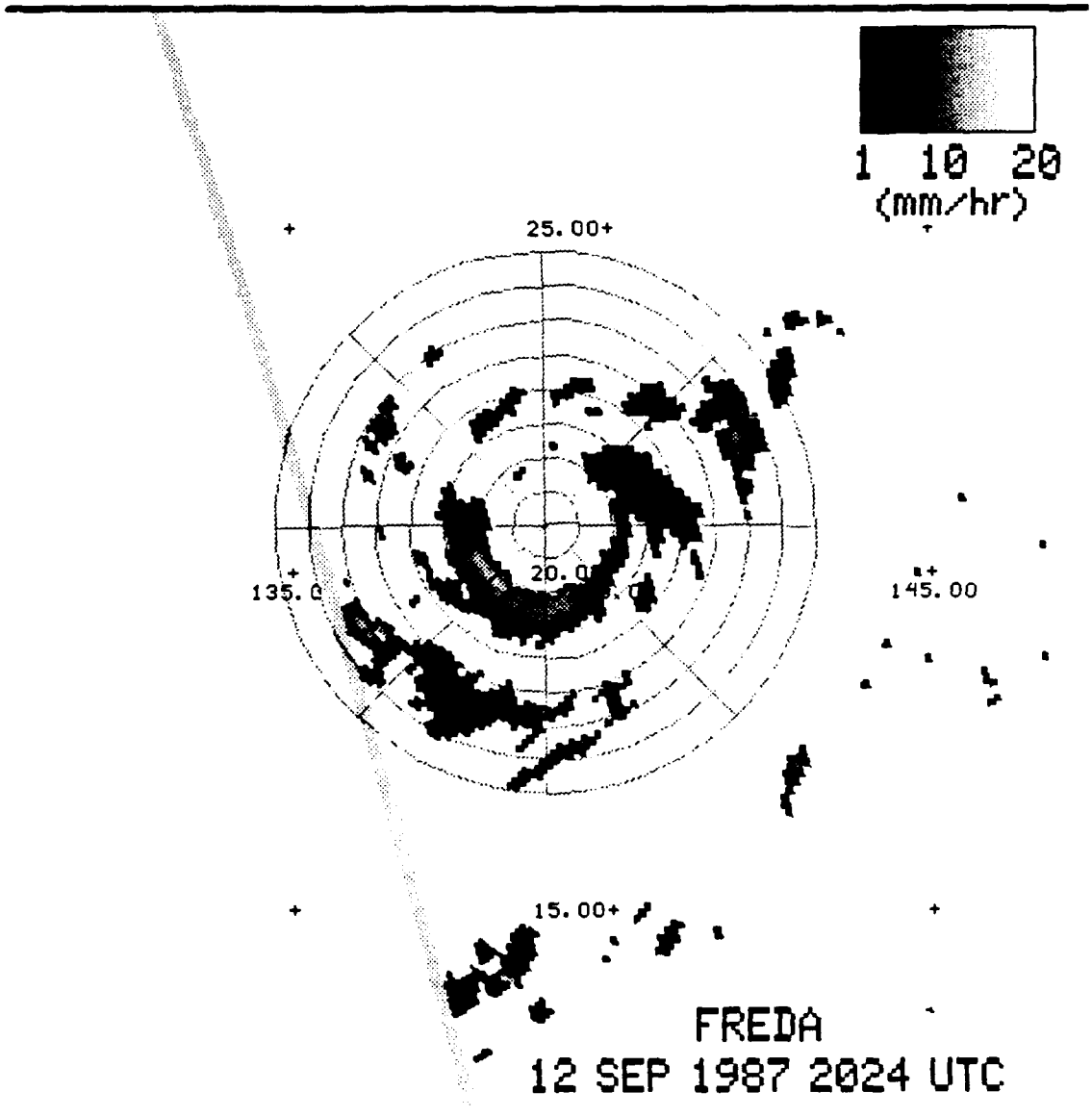
1 10 20
(mm/hr)
25.00+
20.0
135.0
145.00
15.00+
FREDA
12 SEP 1987 2024 UTC

FIGURE 19

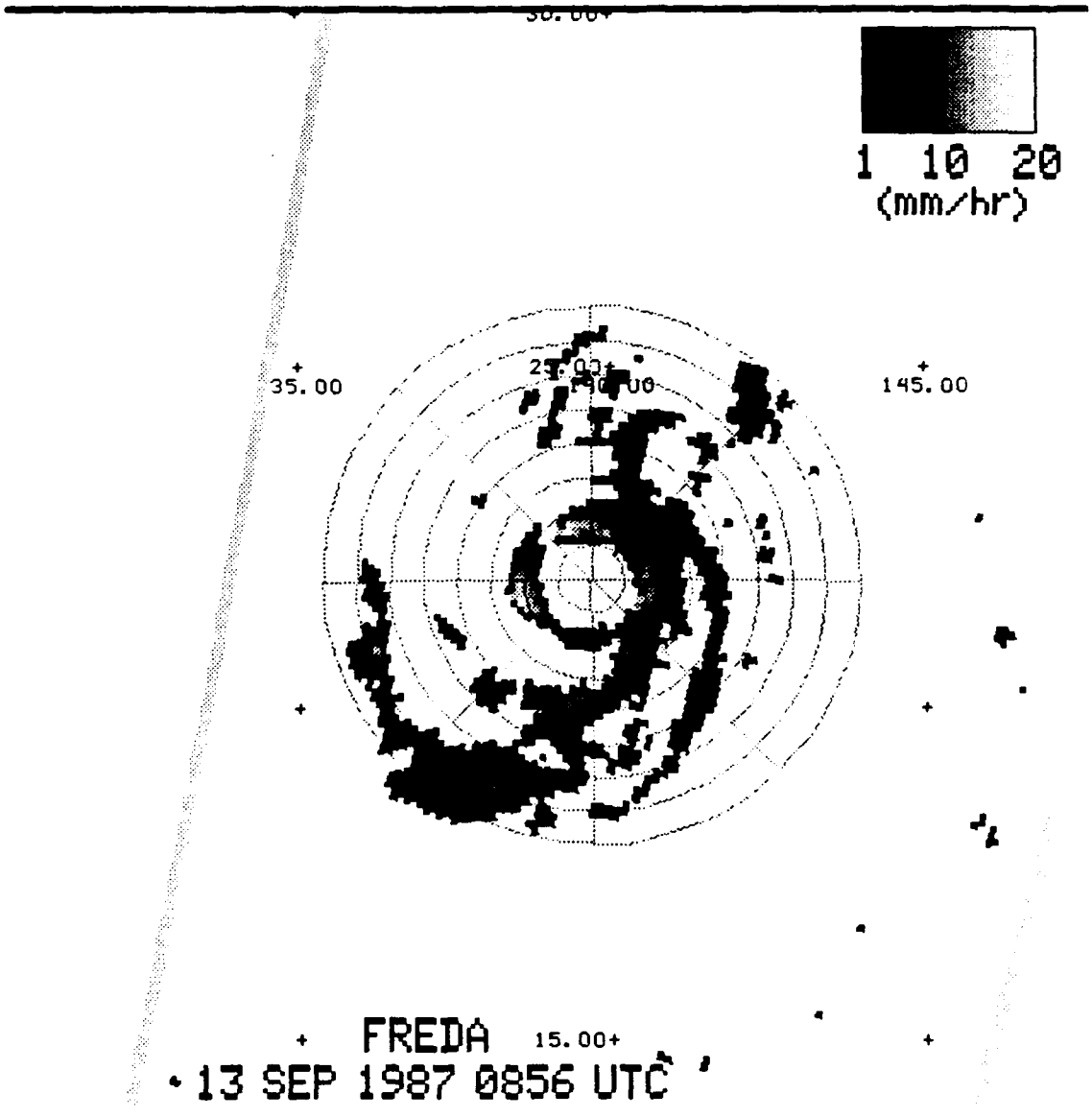

FIGURE 20

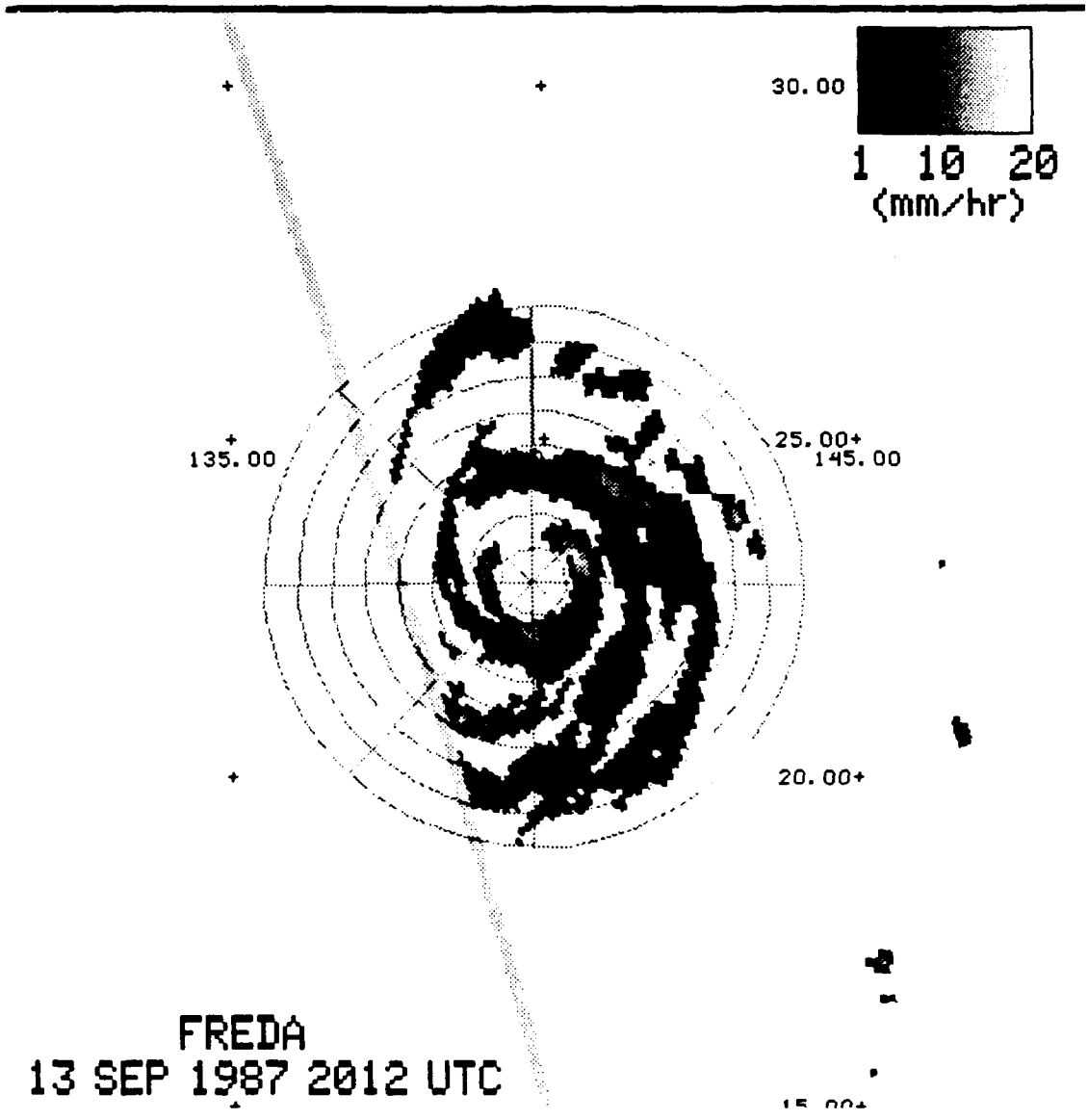
30.00
1 10 20
(mm/hr)
135.00
25.00
145.00
20.00
FREDA
13 SEP 1987 2012 UTC

FIGURE 21

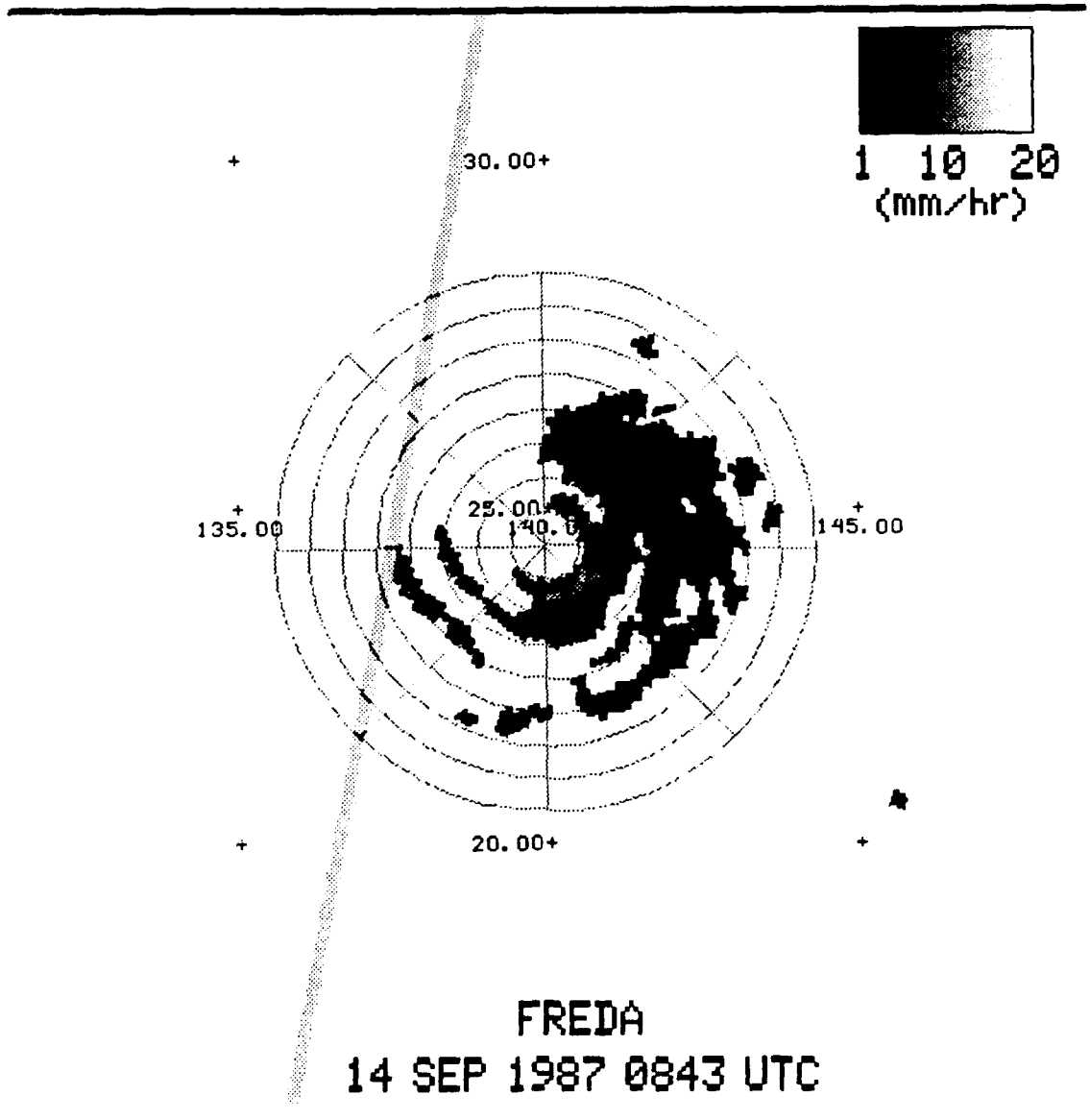

FIGURE 22

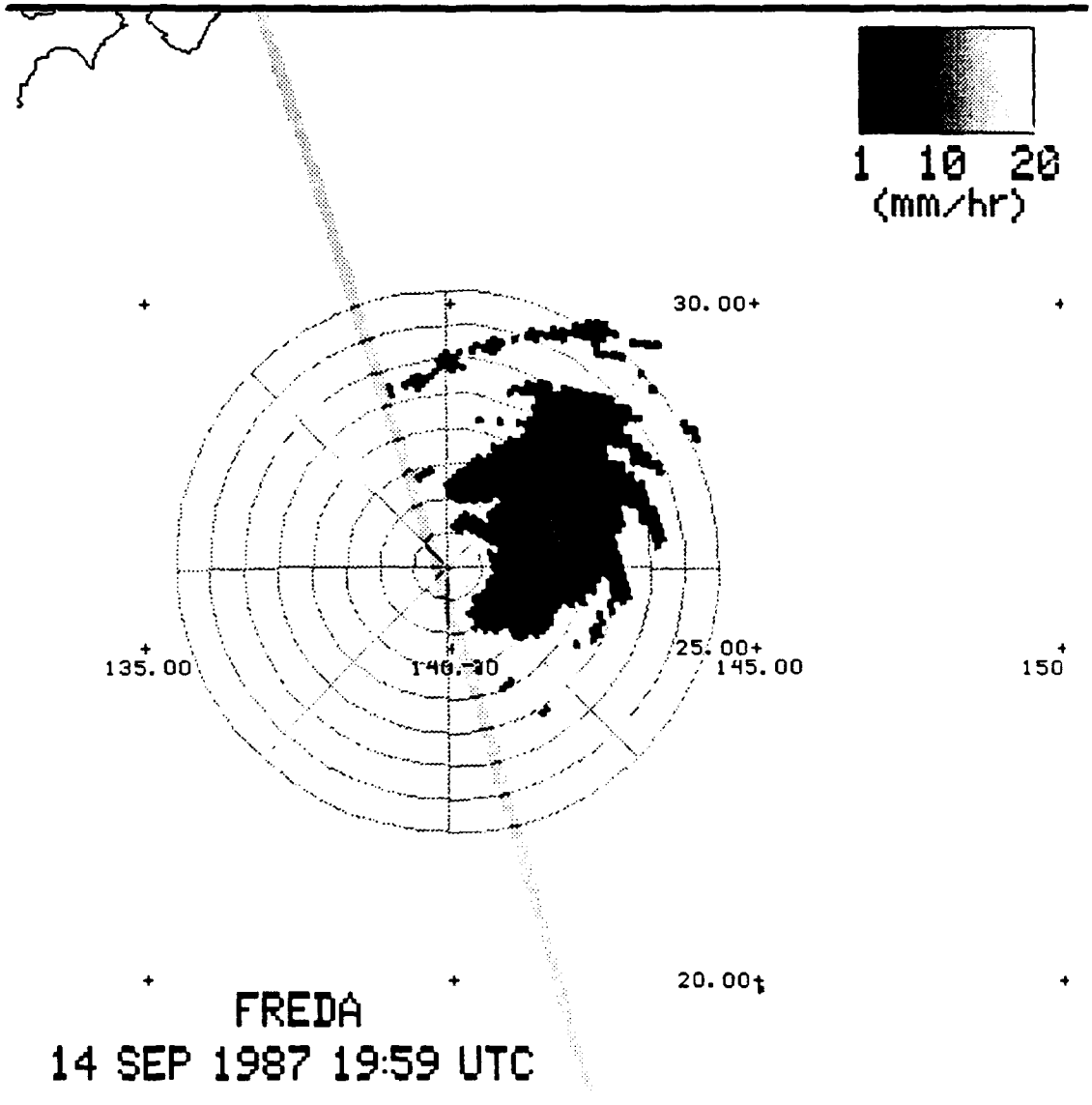
1 10 20
(mm/hr)
30.00
25.00
20.00
135.00
140.00
145.00
150
FREDA
14 SEP 1987 19:59 UTC

FIGURE 23

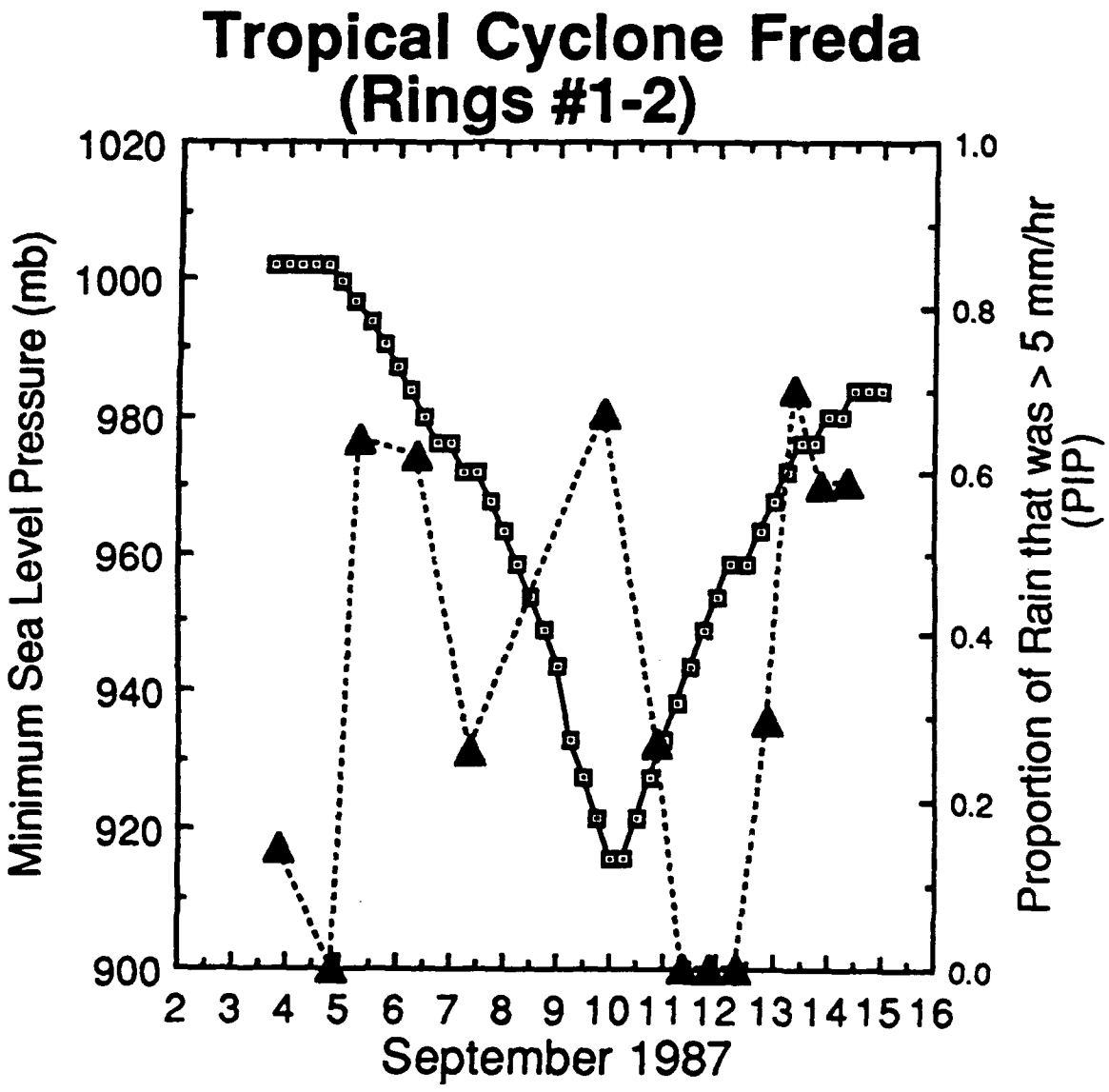
Tropical Cyclone Freda
(Rings #1-2)
Minimum Sea Level Pressure (mb)
1020
1000
980
960
940
920
900
Proportion of Rain that was > 5 mm/hr
(PIP)
1.0
0.8
0.6
0.4
0.2
0.0
2 3 4 5 6 7 8 9 10 11 12 13 14 15 16
September 1987

FIGURE 24

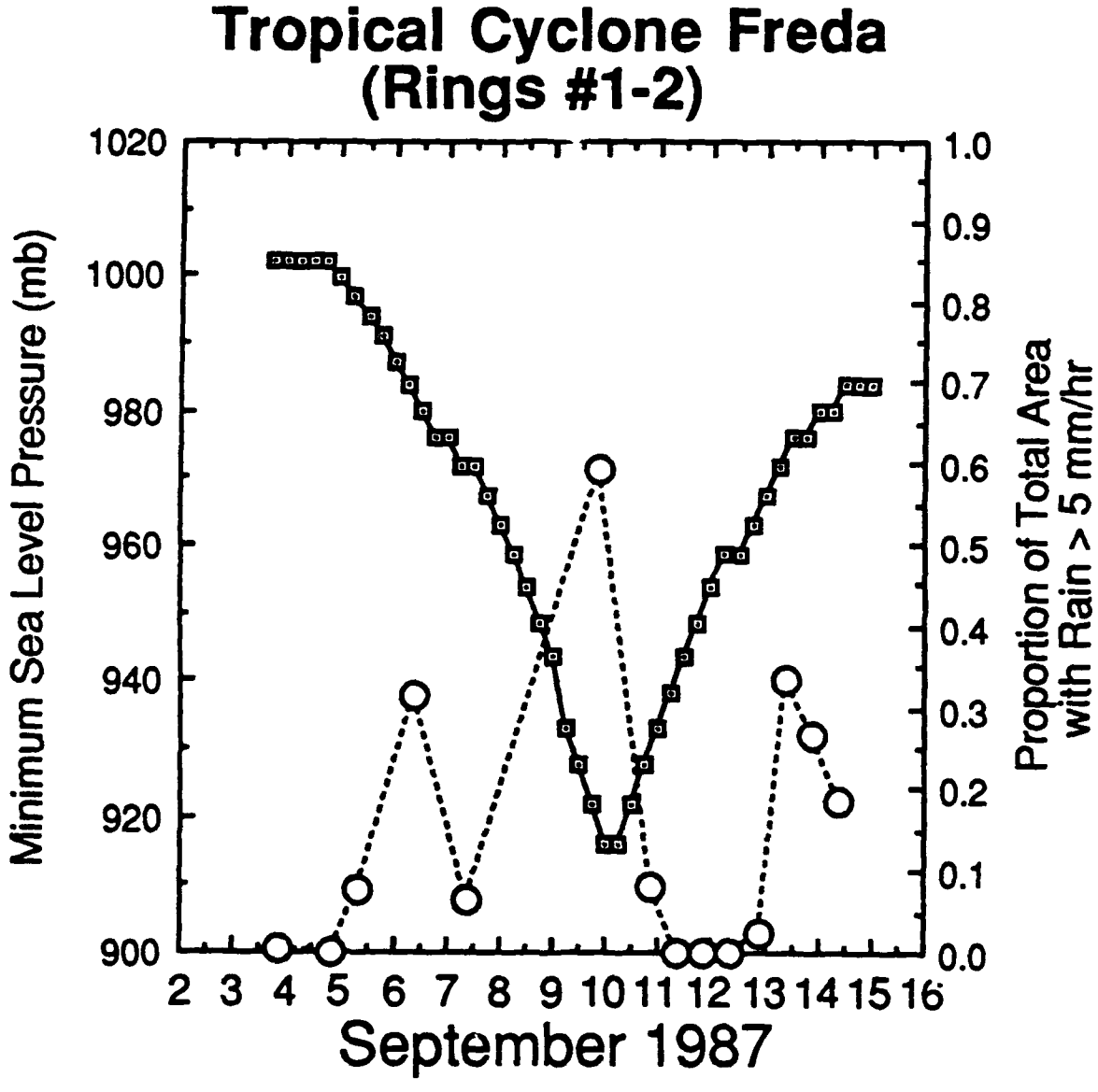
Tropical Cyclone Freda
(Rings #1-2)
Minimum Sea Level Pressure (mb)
1020
1000
980
960
940
920
900
Proportion of Total Area
with Rain > 5 mm/hr
1.0
0.9
0.8
0.7
0.6
0.5
0.4
0.3
0.2
0.1
0.0
2 3 4 5 6 7 8 9 10 11 12 13 14 15 16
September 1987

FIGURE 25

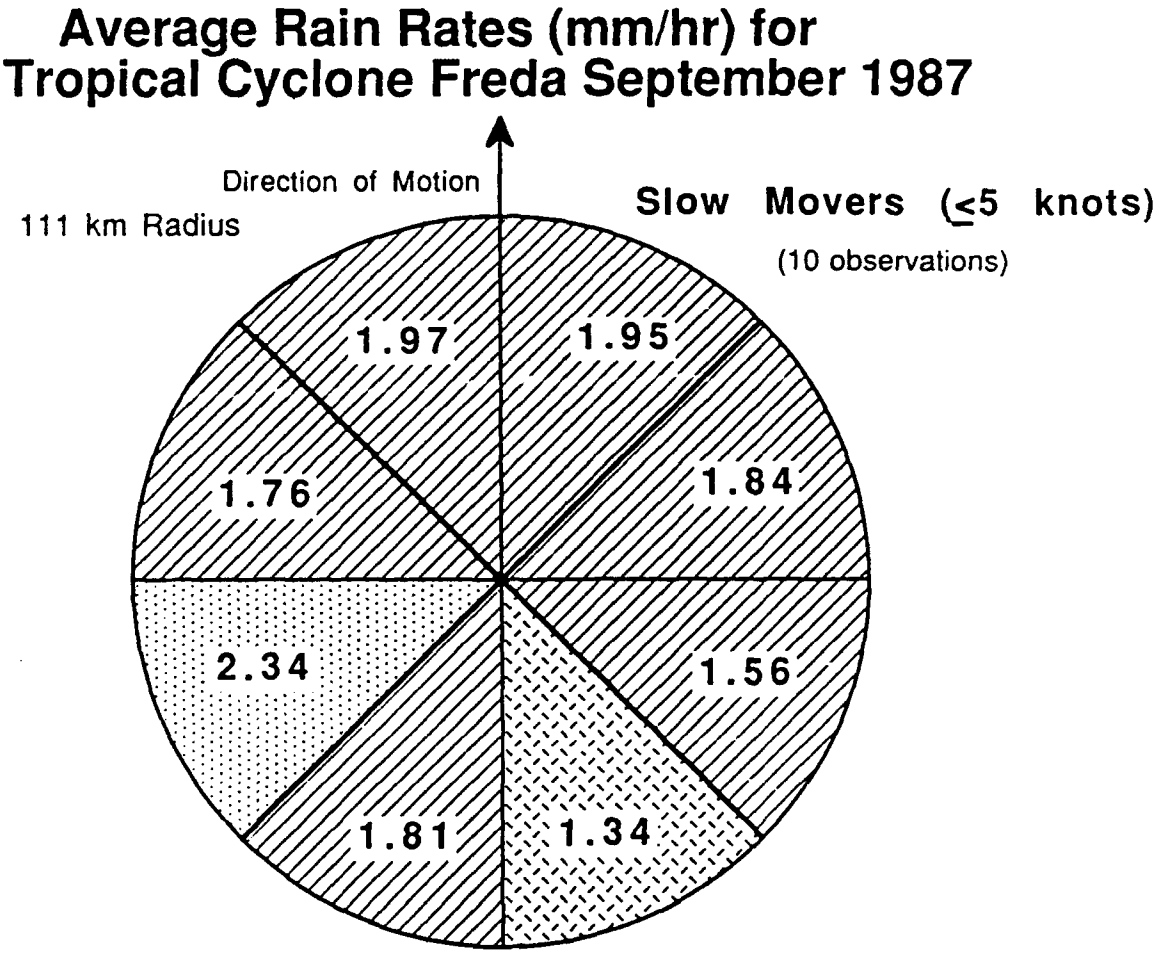
Average Rain Rates (mm/hr) for
Tropical Cyclone Freda September 1987
Direction of Motion
111 km Radius
Slow Movers (≤5 knots)
(10 observations)
1.97
1.95
1.76
1.84
2.34
1.56
1.81
1.34

FIGURE 26

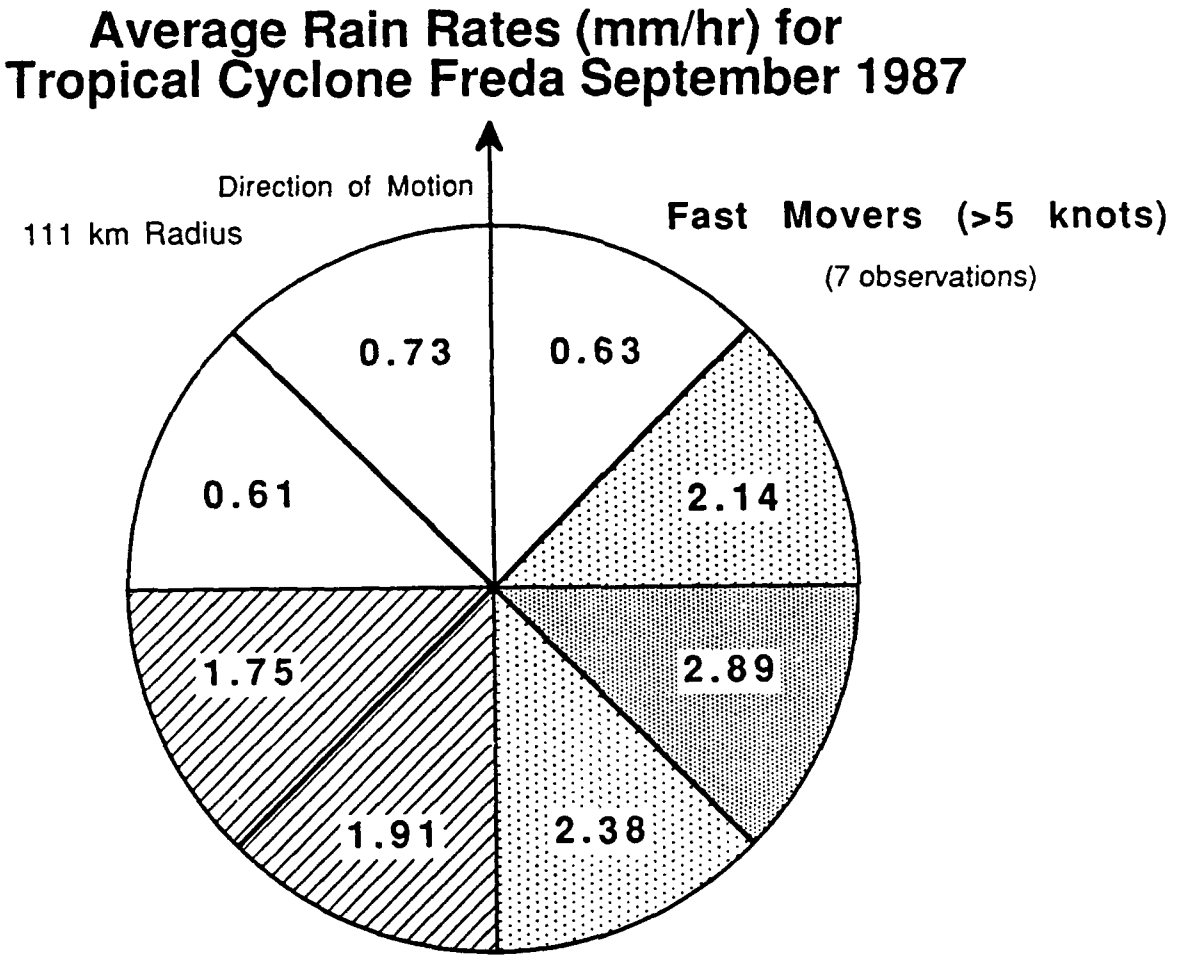
Average Rain Rates (mm/hr) for
Tropical Cyclone Freda September 1987
Direction of Motion
111 km Radius
Fast Movers (>5 knots)
(7 observations)
0.73
0.63
0.61
2.14
1.75
2.89
1.91
2.38

FIGURE 27

Average Rain Rates (mm/hr) for Tropical Disturbance/Depression Freda

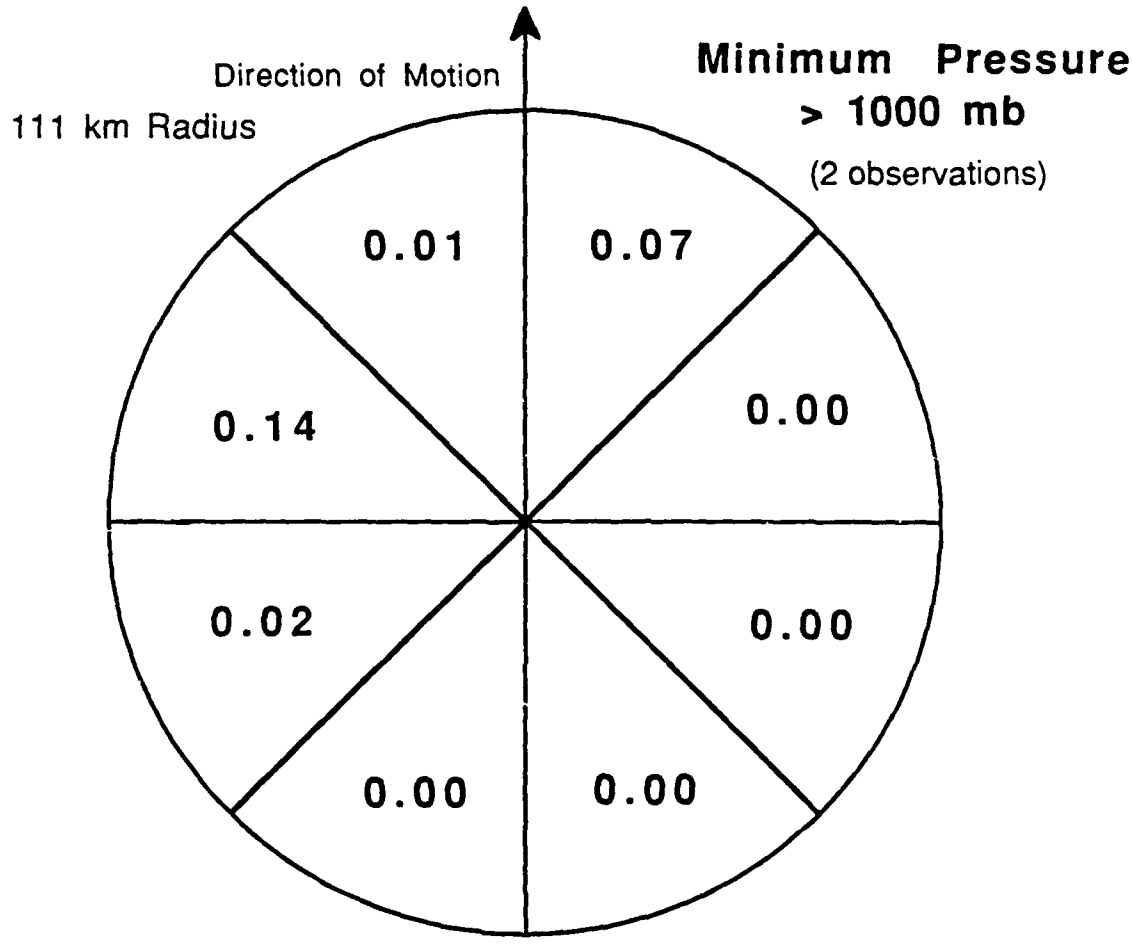

FIGURE 28

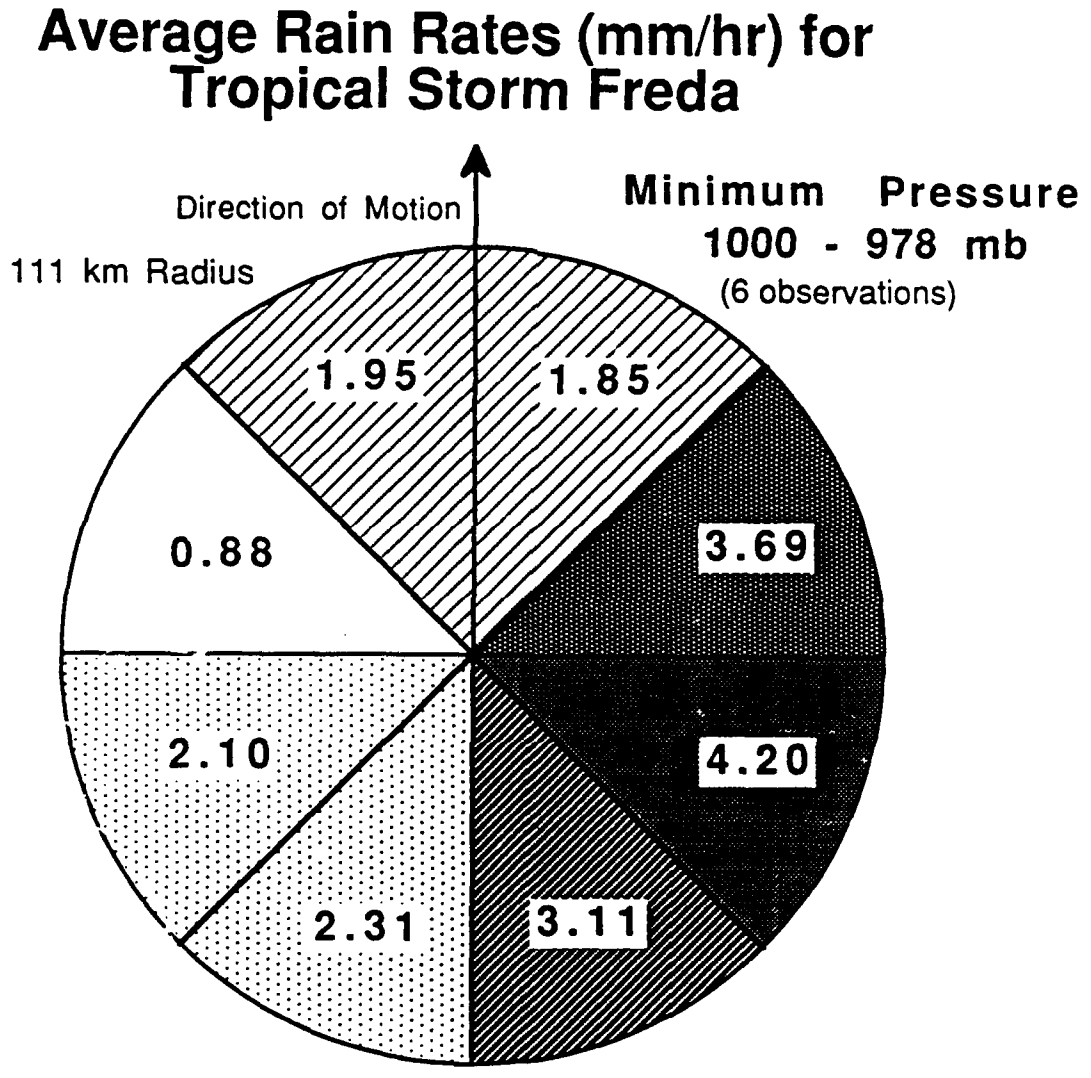
Average Rain Rates (mm/hr) for
Tropical Storm Freda
Direction of Motion
111 km Radius
Minimum Pressure
1000 - 978 mb
(6 observations)
1.95
1.85
0.88
3.69
2.10
4.20
2.31
3.11

FIGURE 29

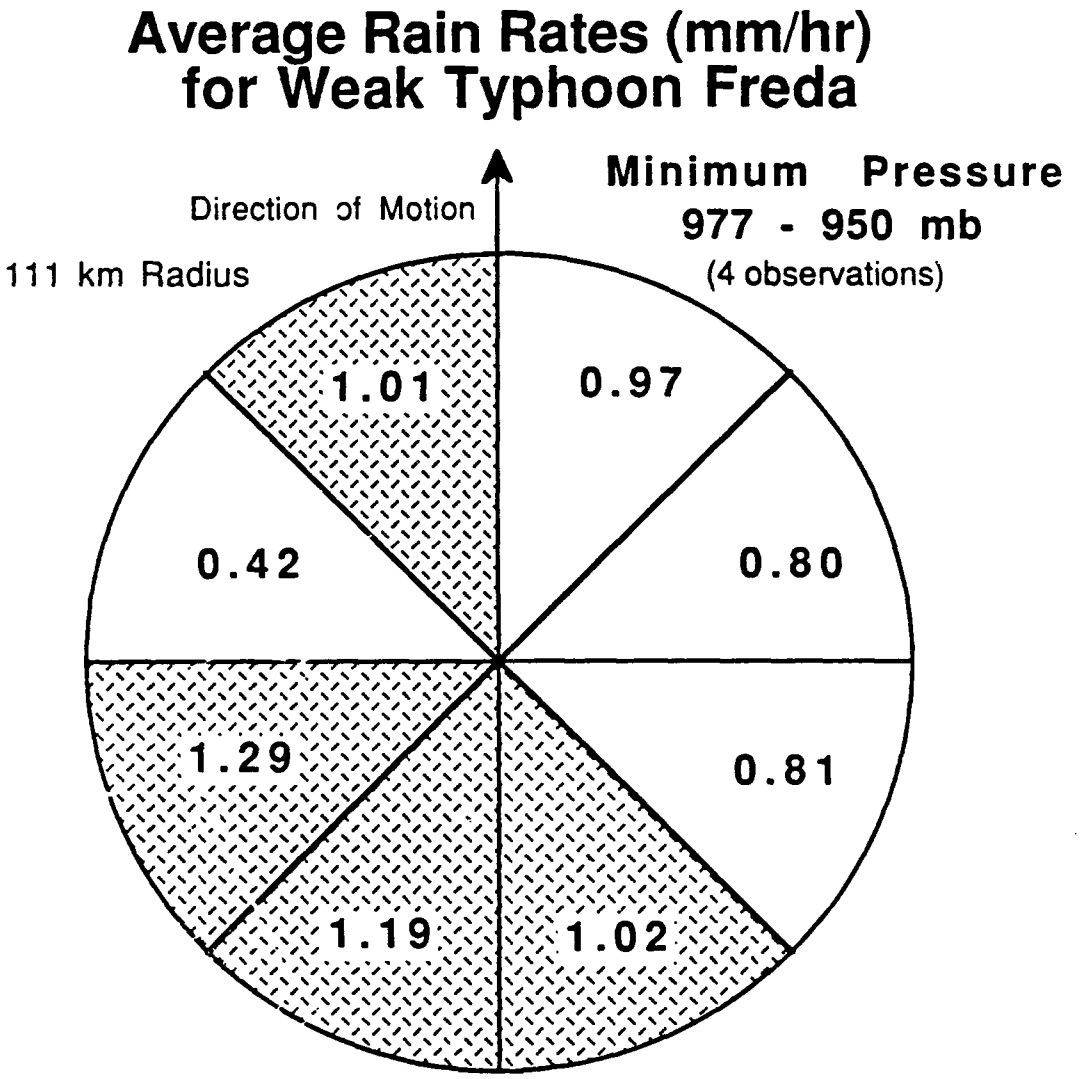
Average Rain Rates (mm/hr)
for Weak Typhoon Freda
Direction of Motion
111 km Radius
Minimum Pressure
977 - 950 mb
(4 observations)
1.01
0.97
0.42
0.80
1.29
0.81
1.19
1.02

FIGURE 30

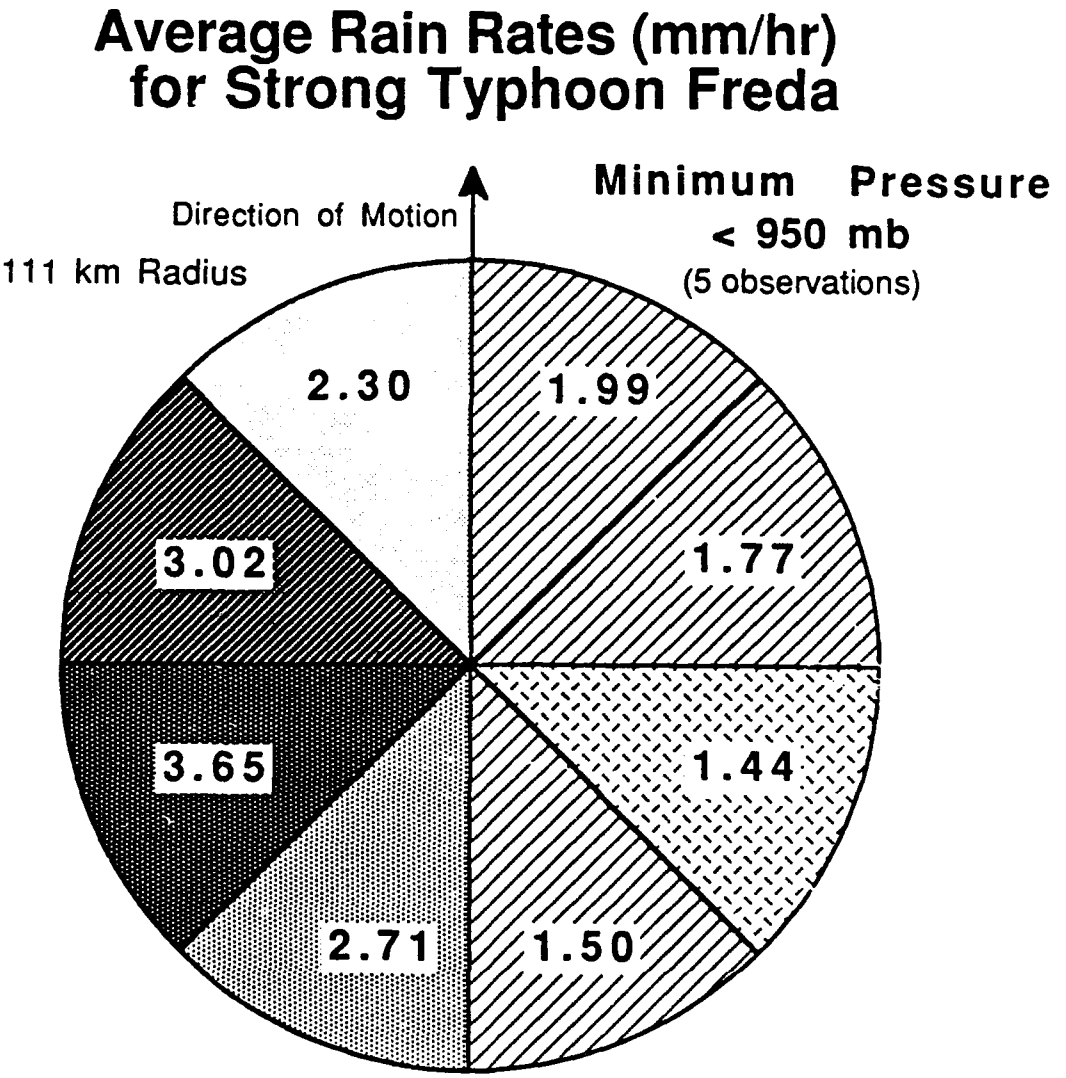
Average Rain Rates (mm/hr)
for Strong Typhoon Freda
Minimum Pressure
< 950 mb
(5 observations)
Direction of Motion
111 km Radius
2.30
1.99
3.02
1.77
3.65
1.44
2.71
1.50

FIGURE 31

Average Rain Rates (mm/hr) for Tropical Cyclone Freda (September 3-14, 1987)

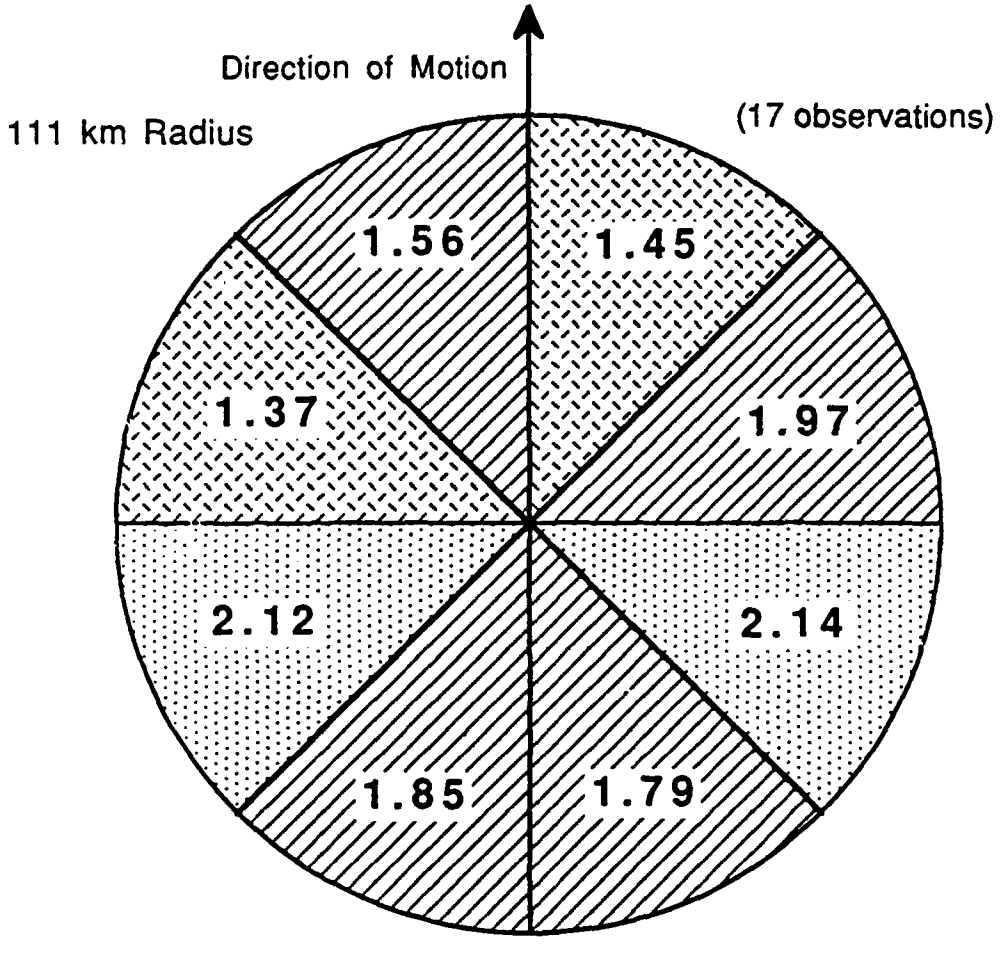

FIGURE 32

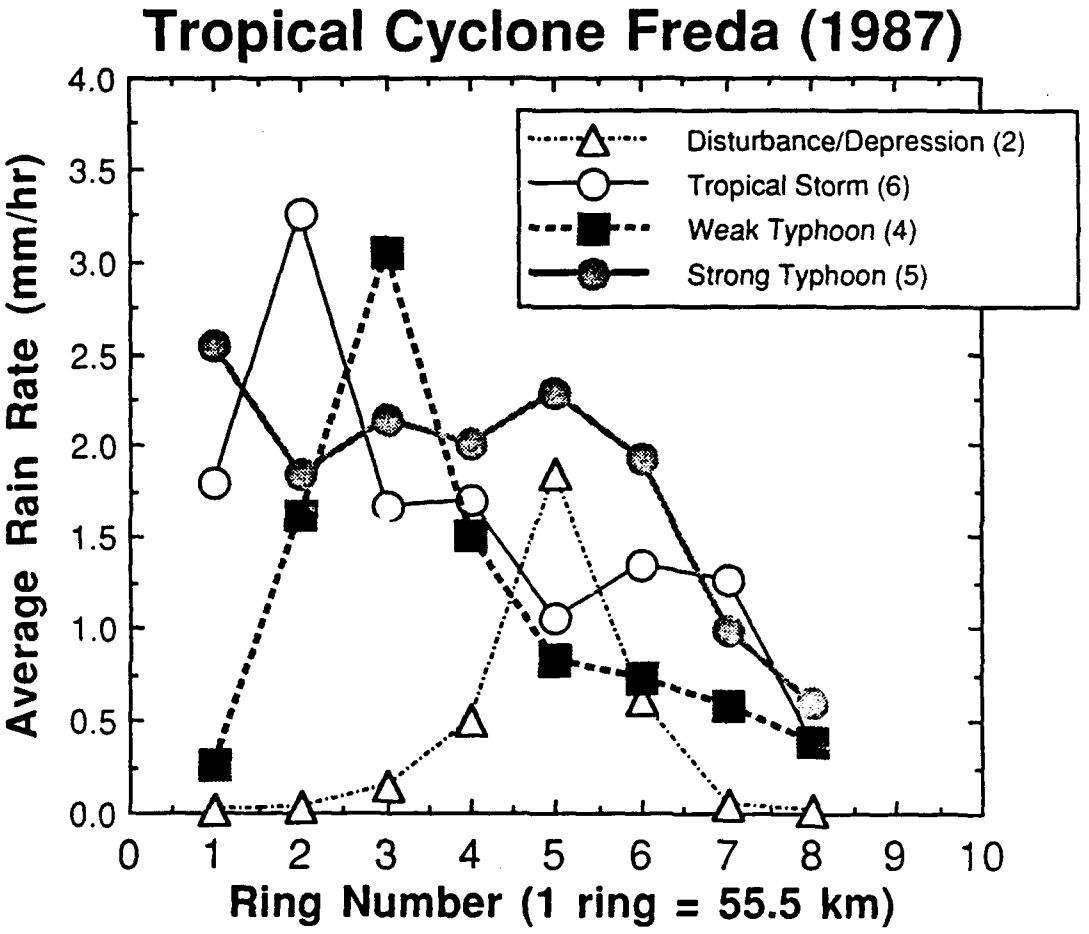
Tropical Cyclone Freda (1987)
Average Rain Rate (mm/hr)
4.0
3.5
3.0
2.5
2.0
1.5
1.0
0.5
0.0
0
1
2
3
4
5
6
7
8
9
10
Ring Number (1 ring = 55.5 km)
Disturbance/Depression (2)
Tropical Storm (6)
Weak Typhoon (4)
Strong Typhoon (5)

FIGURE 33

200 MB HGHT (00 GMT 09/SEP/87)
200 MB HGHT (00 GMT 10/SEP/87)
200 MB HGHT (12 GMT 09/SEP/87)
200 MB HGHT (12 GMT 10/SEP/87)

FIGURE 34

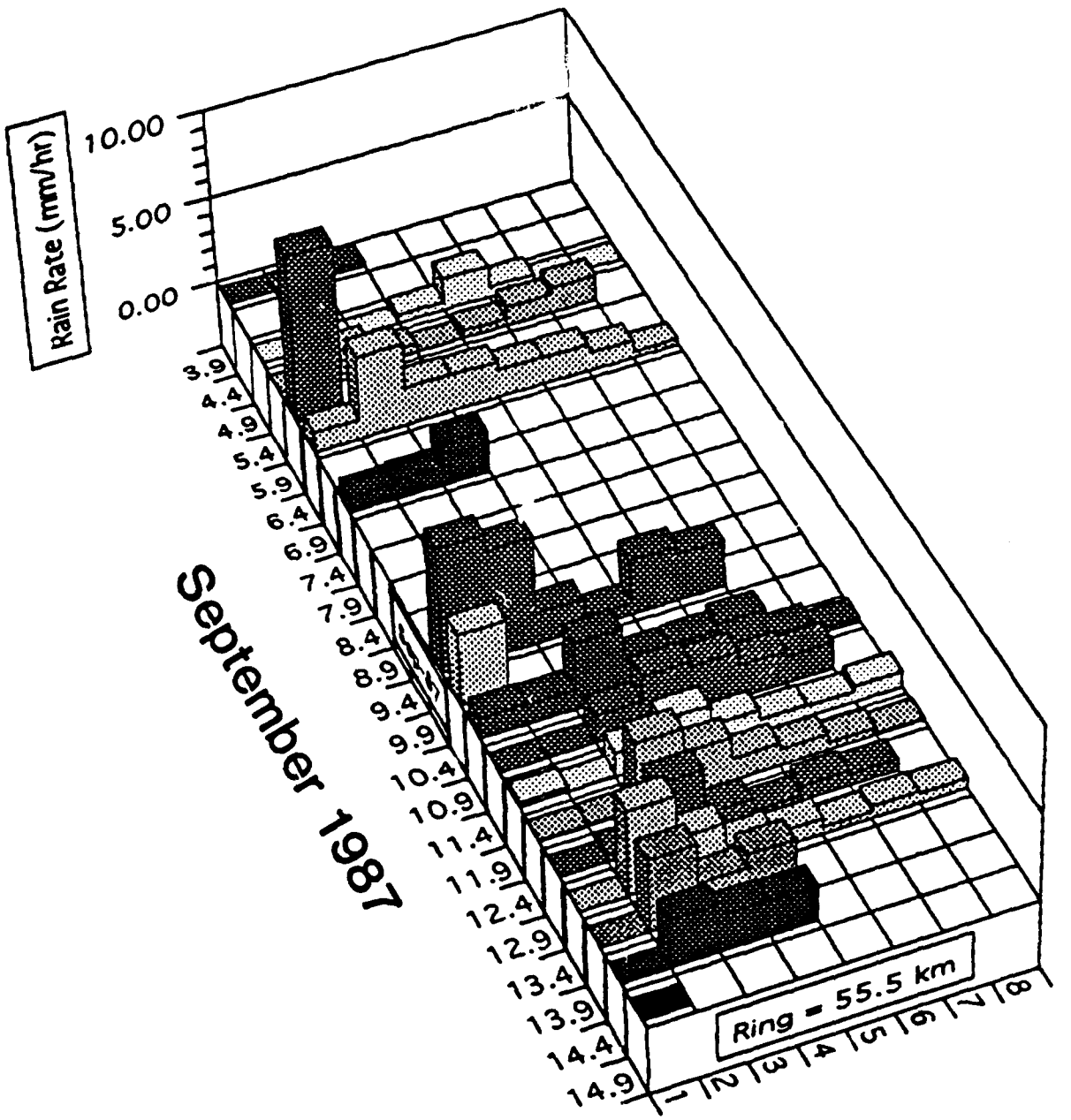
Rain Rate (mm/hr)
10.00
5.00
0.00
3.9
4.4
4.9
5.4
5.9
6.4
6.9
7.4
7.9
8.4
8.9
9.4
9.9
10.4
10.9
11.4
11.9
12.4
12.9
13.4
13.9
14.4
14.9
September 1987
Ring = 55.5 km
1
2
3
4
5
6
7
8

FIGURE 35

Tropical Cyclone Freda (September 1987)

Radial Distribution of Mean Rain Rate (mm/h) Vmax (kts)

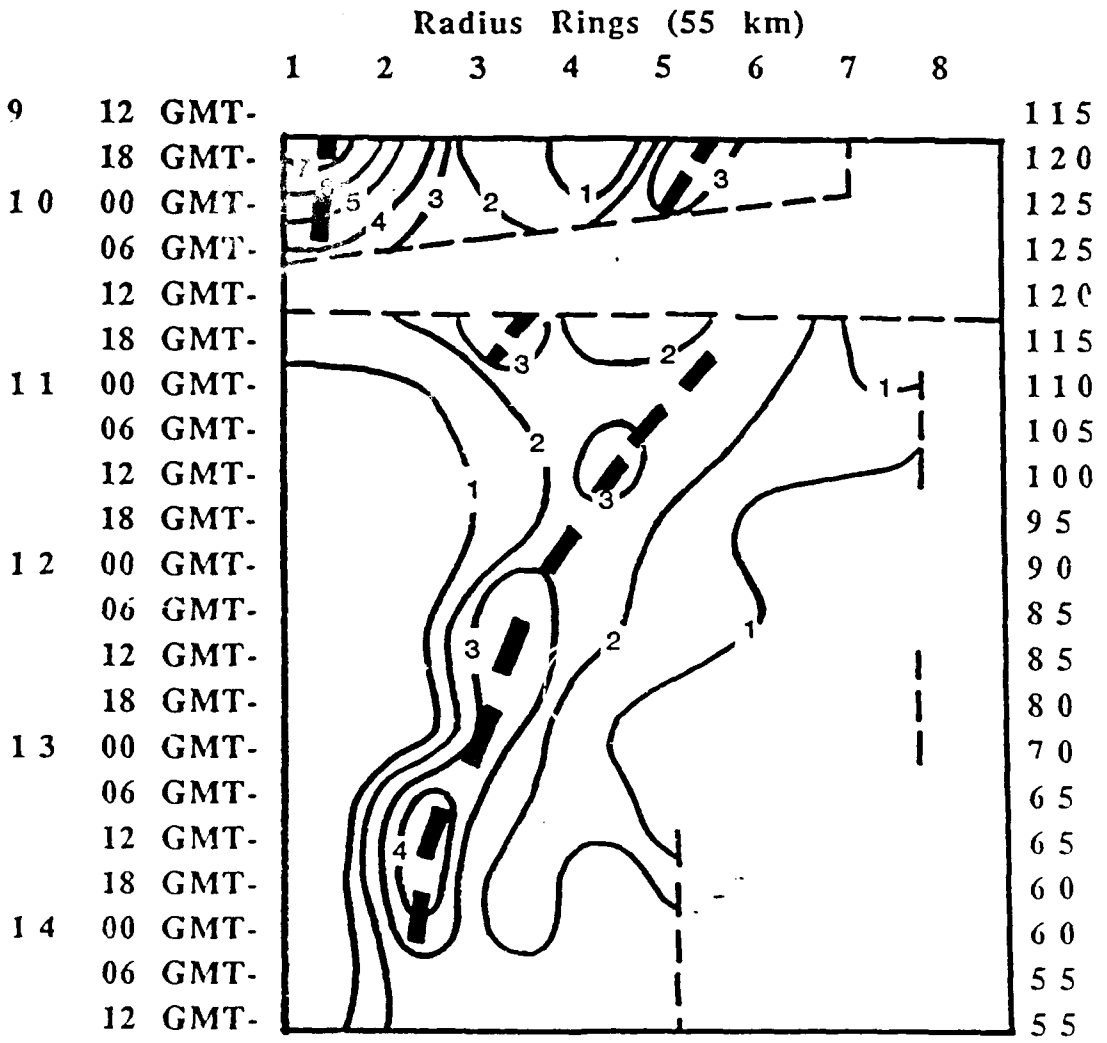

Dashed lines indicate missing data.

Bold dashed lines illustrate three convective rings.

FIGURE 36

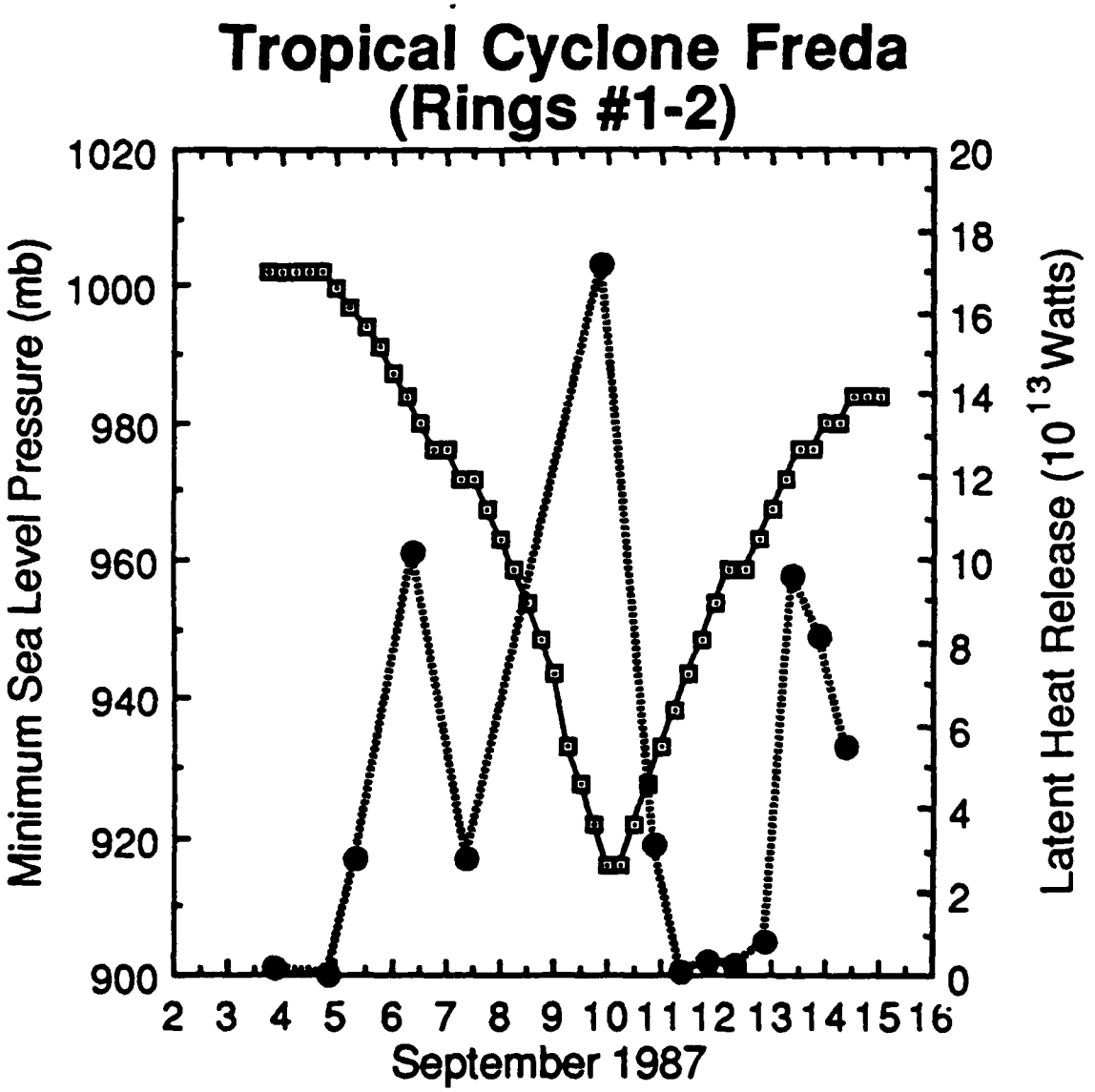
Tropical Cyclone Freda
(Rings #1-2)
Minimum Sea Level Pressure (mb)
1020
1000
980
960
940
920
900
Latent Heat Release (10^{13} Watts)
20
18
16
14
12
10
8
6
4
2
0
2 3 4 5 6 7 8 9 10 11 12 13 14 15 16
September 1987

FIGURE 37

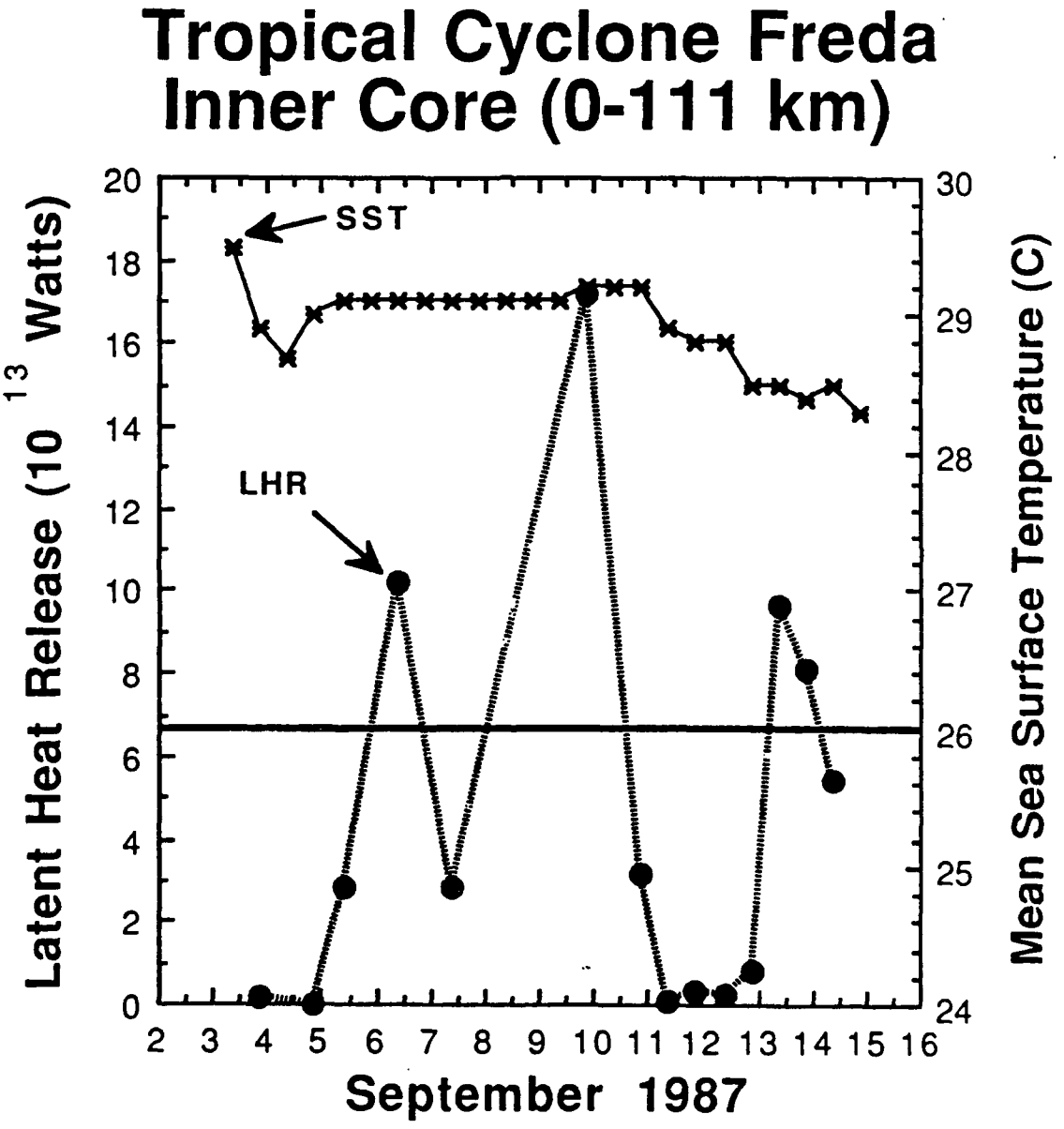
Tropical Cyclone Freda
Inner Core (0-111 km)
Latent Heat Release (10^{13} Watts)
Mean Sea Surface Temperature (C)
SST
LHR
20
18
16
14
12
10
8
6
4
2
0
30
29
28
27
26
25
24
2 3 4 5 6 7 8 9 10 11 12 13 14 15 16
September 1987

FIGURE 38

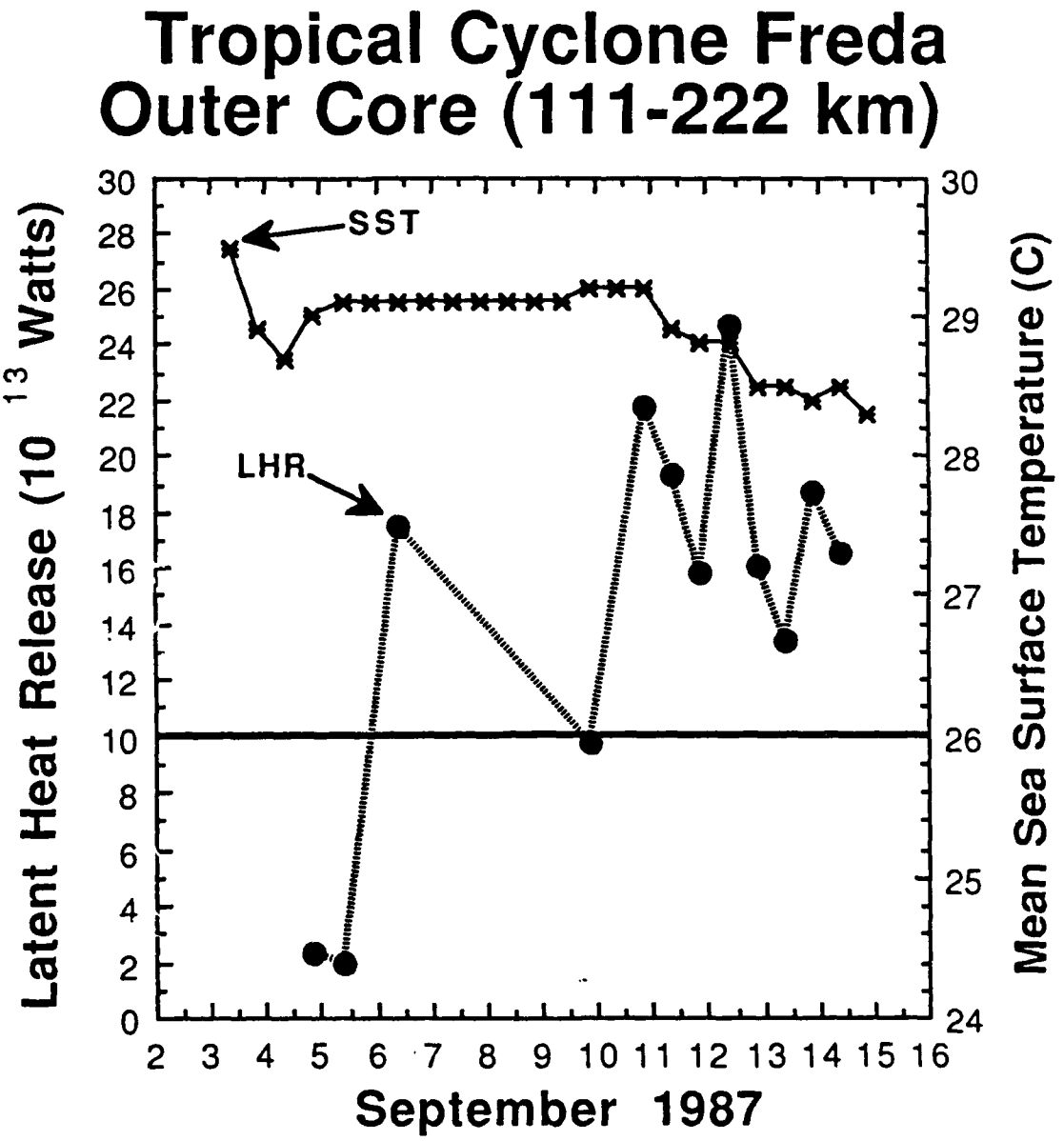
Tropical Cyclone Freda
Outer Core (111-222 km)
Latent Heat Release (10 13 Watts)
Mean Sea Surface Temperature (C)
SST
LHR
30
28
26
24
22
20
18
16
14
12
10
8
6
4
2
0
29
27
25
2 3 4 5 6 7 8 9 10 11 12 13 14 15 16
September 1987

FIGURE 39

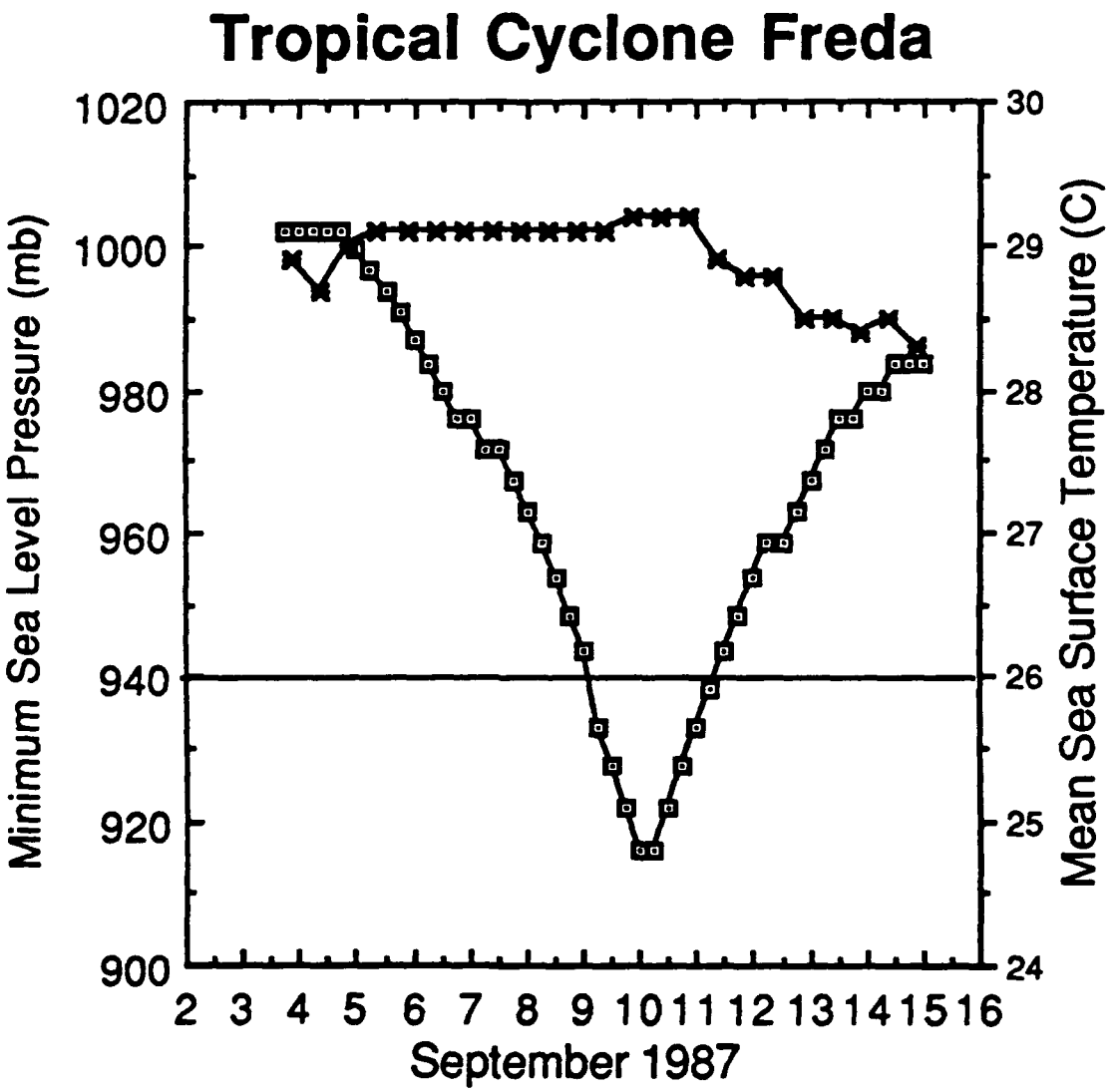
Tropical Cyclone Freda
Minimum Sea Level Pressure (mb)
Mean Sea Surface Temperature (C)
1020
1000
980
960
940
920
900
30
29
28
27
26
25
24
2 3 4 5 6 7 8 9 10 11 12 13 14 15 16
September 1987

FIGURE 40

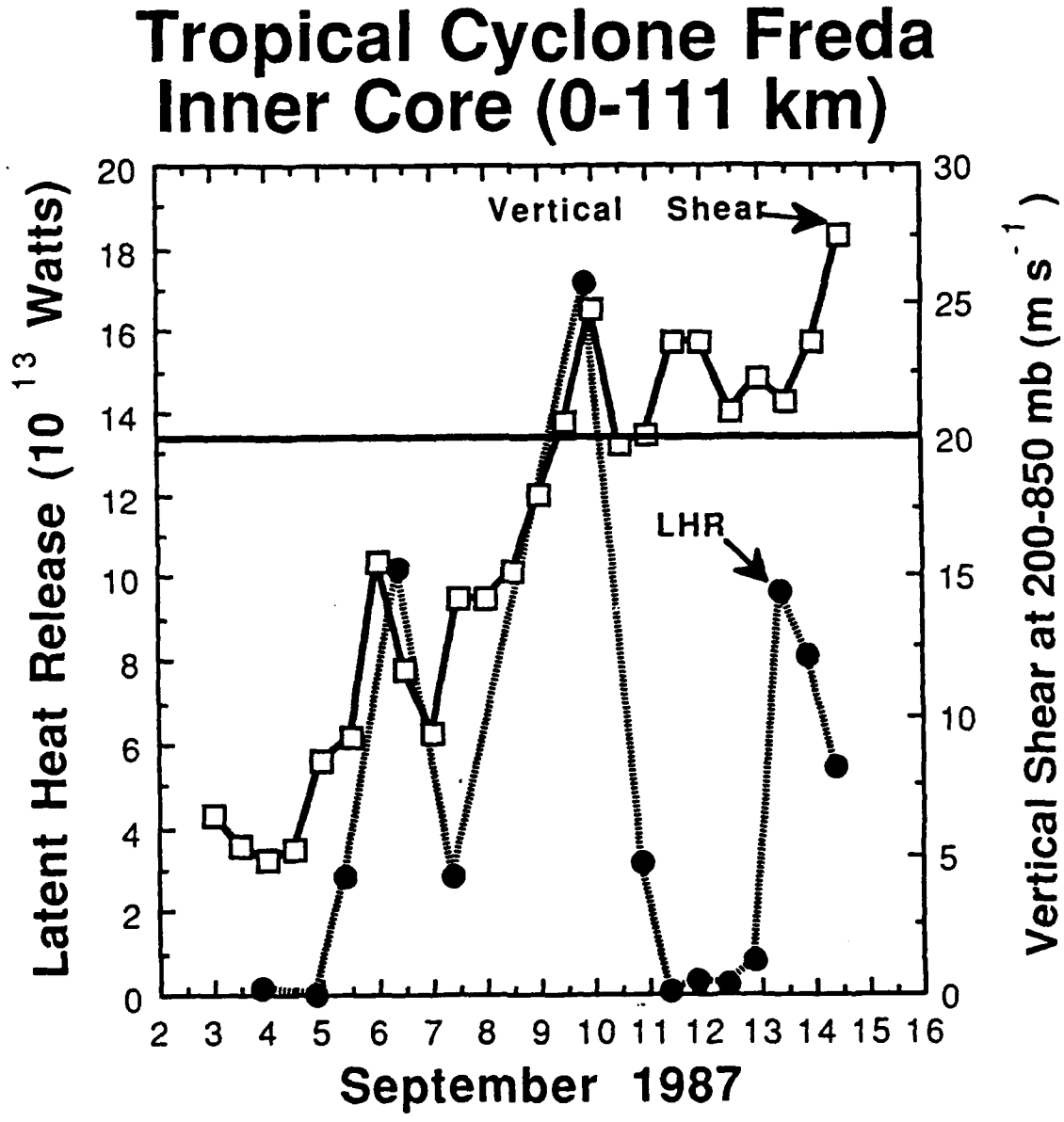
Tropical Cyclone Freda
Inner Core (0-111 km)
Latent Heat Release (10 13 Watts)
Vertical Shear at 200-850 mb (m s-1)
Vertical Shear
LHR
20
18
16
14
12
10
8
6
4
2
0
30
25
20
15
10
5
0
2 3 4 5 6 7 8 9 10 11 12 13 14 15 16
September 1987

FIGURE 41

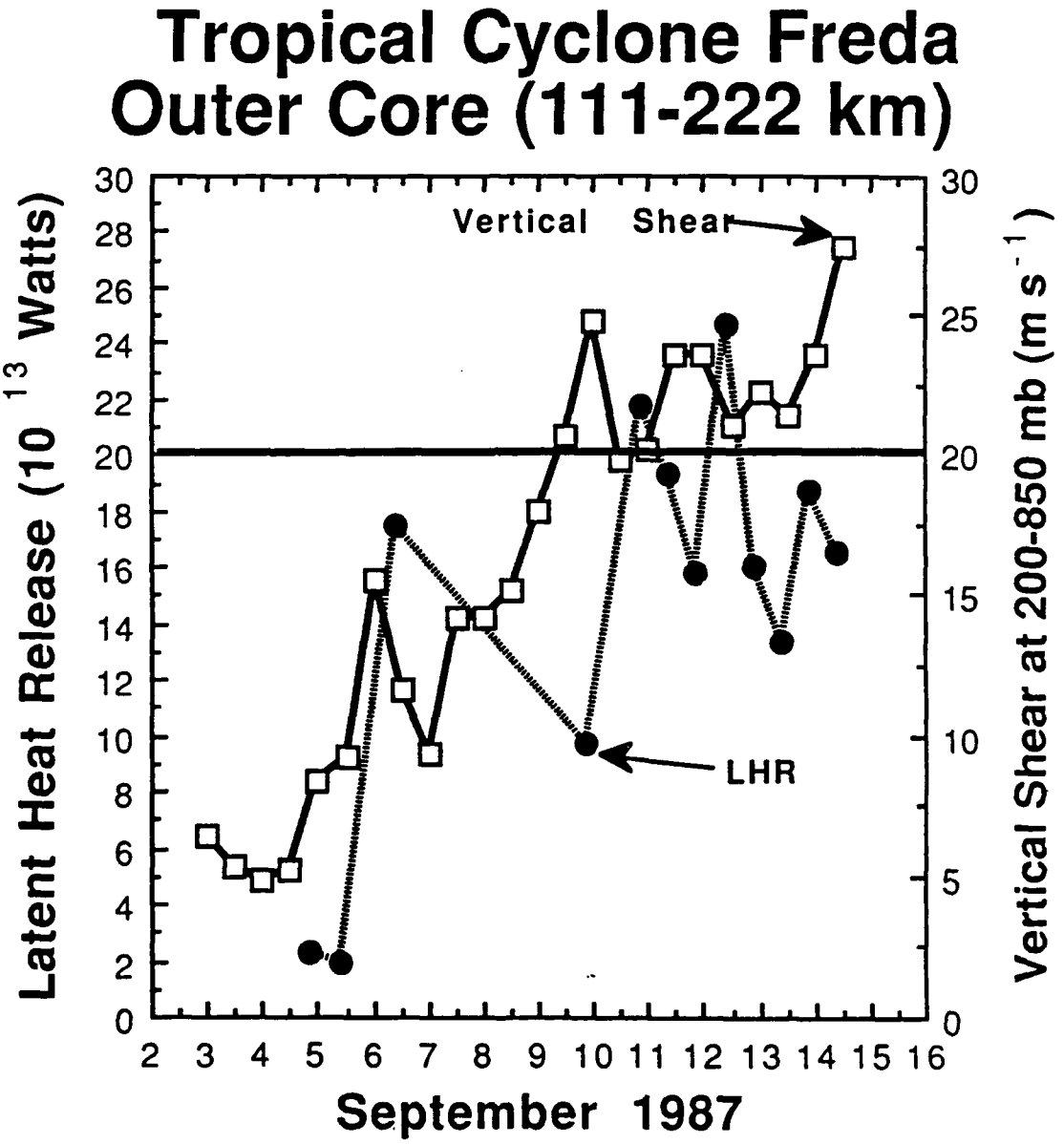
Tropical Cyclone Freda
Outer Core (111-222 km)
Latent Heat Release (10^{13} Watts)
Vertical Shear at 200-850 mb ($m\ s^{-1}$)
Vertical Shear
LHR
0 2 4 6 8 10 12 14 16 18 20 22 24 26 28 30
0 5 10 15 20 25 30
2 3 4 5 6 7 8 9 10 11 12 13 14 15 16
September 1987

FIGURE 42

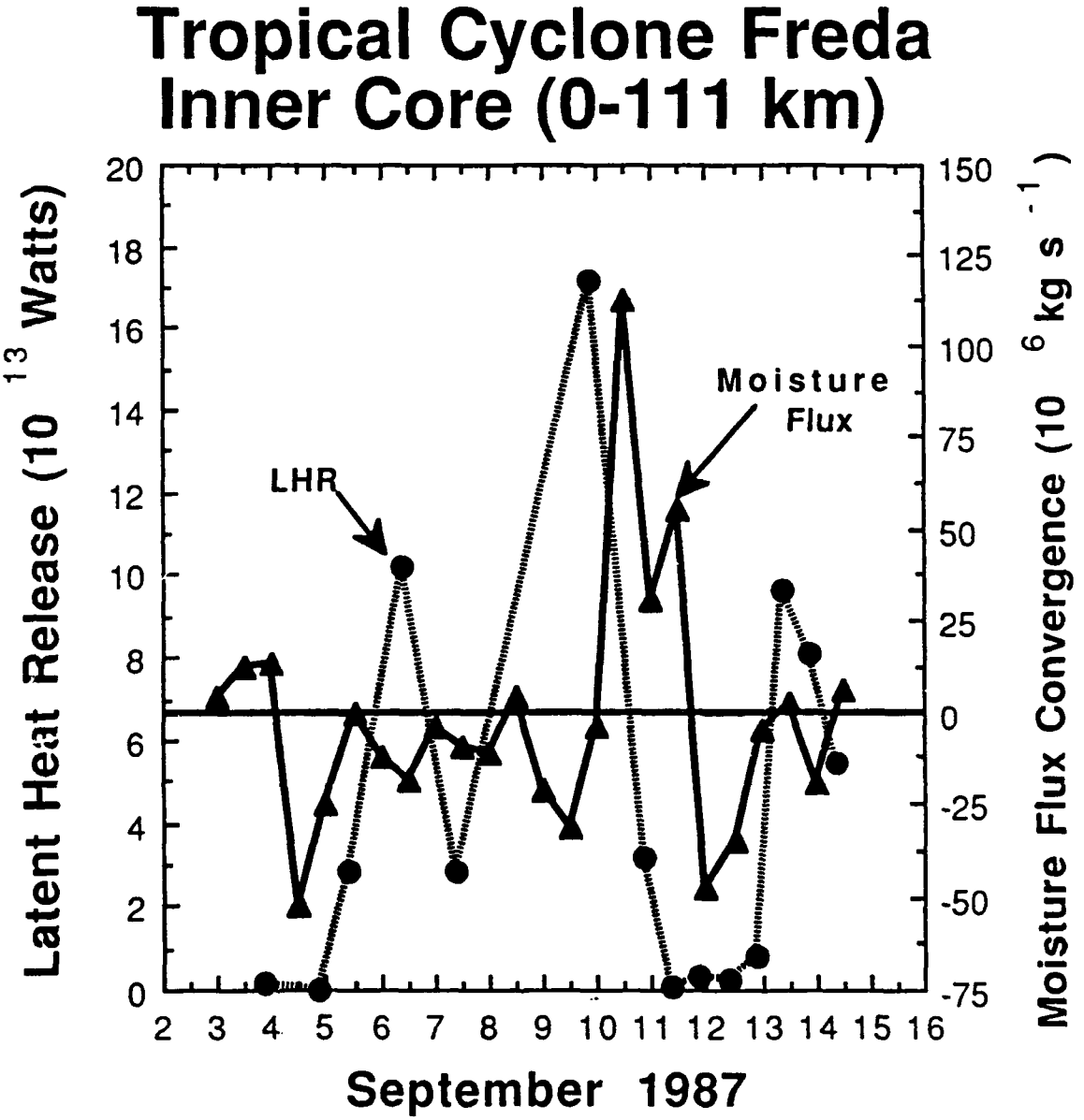
Tropical Cyclone Freda
Inner Core (0-111 km)
Latent Heat Release (10 13 Watts)
Moisture Flux Convergence (10 6 kg s -1)
LHR
Moisture Flux
20
18
16
14
12
10
8
6
4
2
0
150
125
100
75
50
25
0
-25
-50
-75
2 3 4 5 6 7 8 9 10 11 12 13 14 15 16
September 1987

FIGURE 43

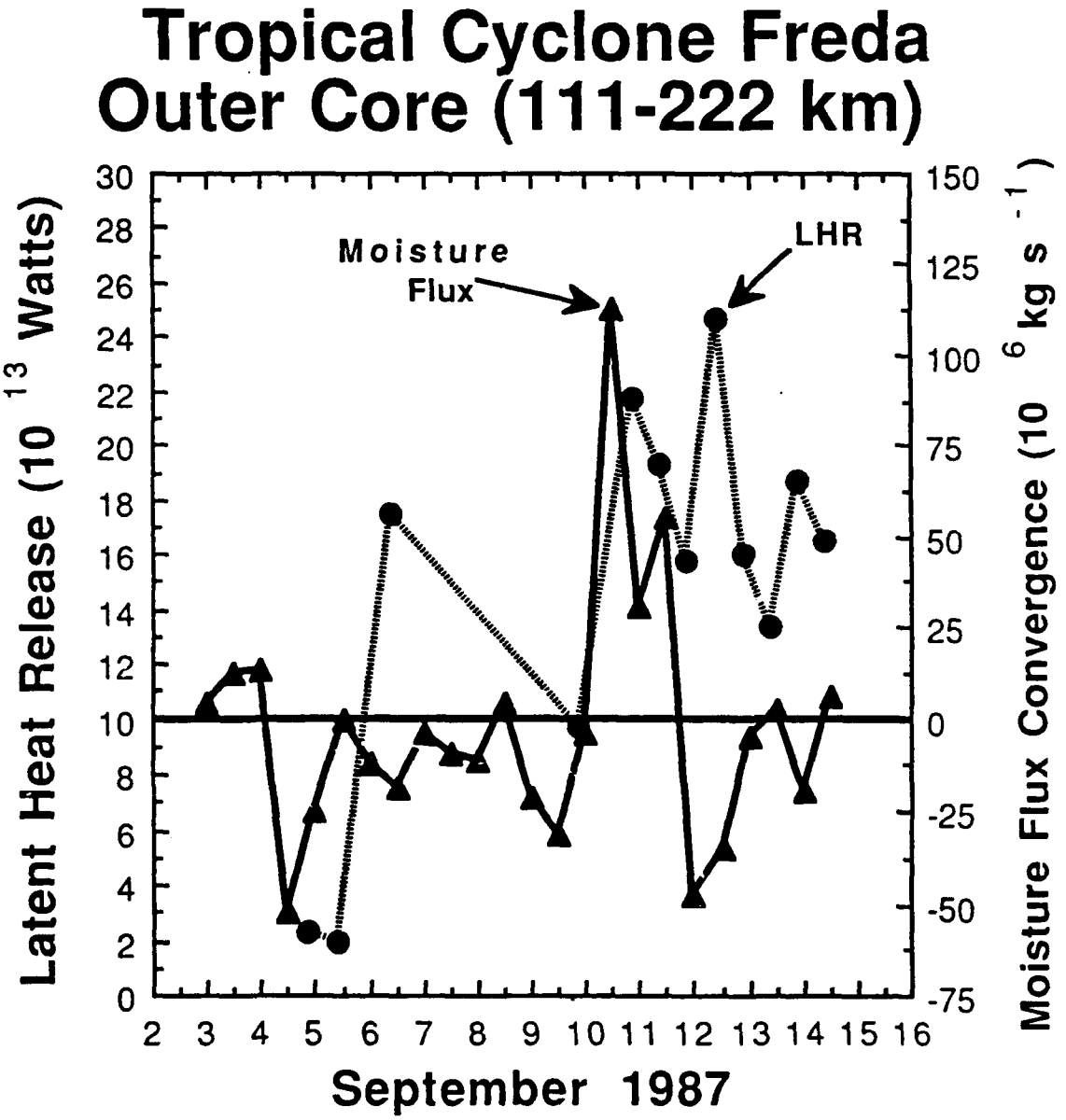
Tropical Cyclone Freda
Outer Core (111-222 km)
Latent Heat Release (10 13 Watts)
Moisture Flux Convergence (10 6 kg s -1)
Moisture Flux
LHR
30
28
26
24
22
20
18
16
14
12
10
8
6
4
2
0
150
125
100
75
50
25
0
-25
-50
-75
2 3 4 5 6 7 8 9 10 11 12 13 14 15 16
September 1987

FIGURE 44

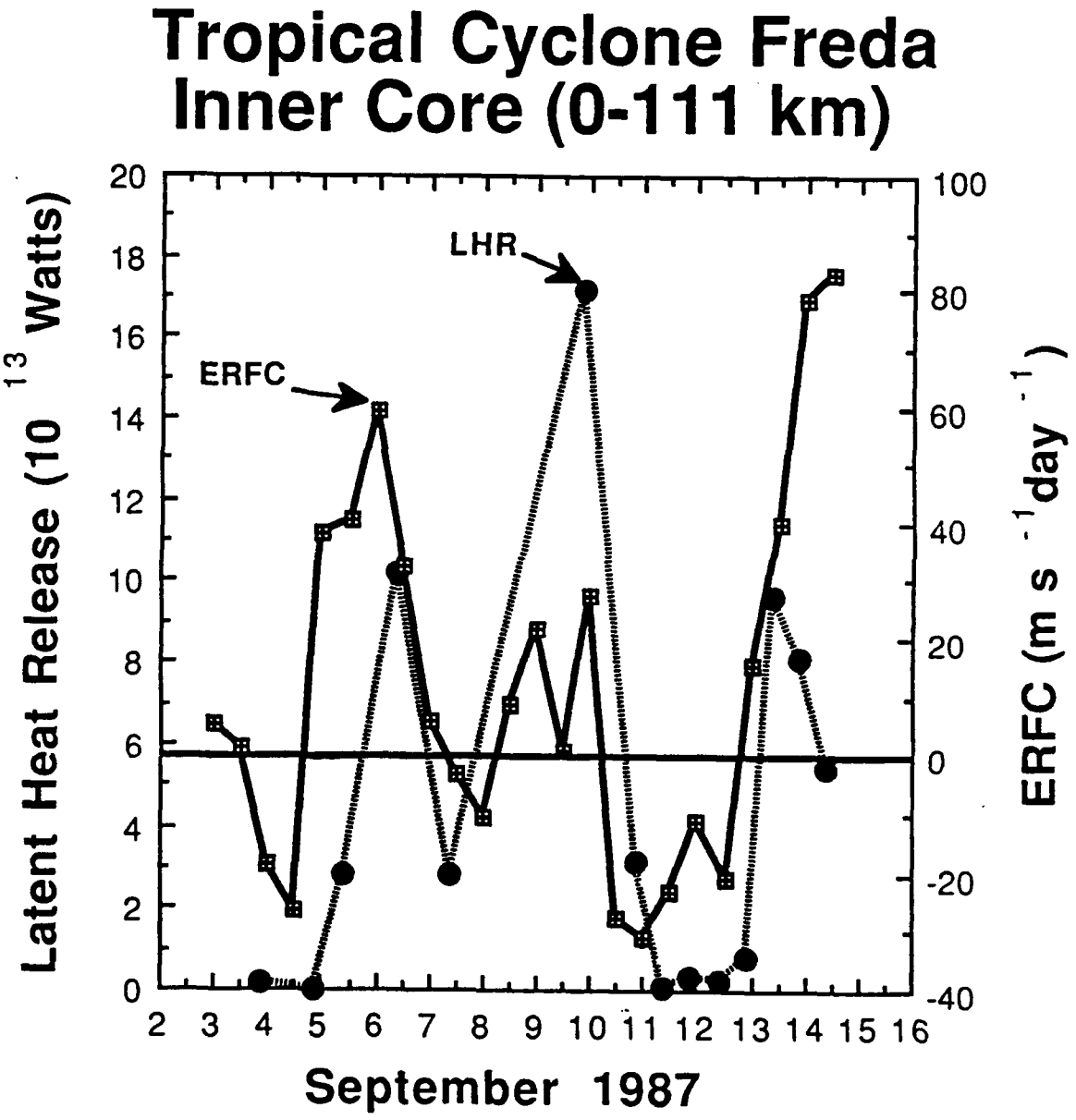
Tropical Cyclone Freda
Inner Core (0-111 km)
Latent Heat Release (10 13 Watts)
ERFC (m s -1 day -1)
LHR
ERFC
20
18
16
14
12
10
8
6
4
2
0
100
80
60
40
20
0
-20
-40
2 3 4 5 6 7 8 9 10 11 12 13 14 15 16
September 1987

FIGURE 45

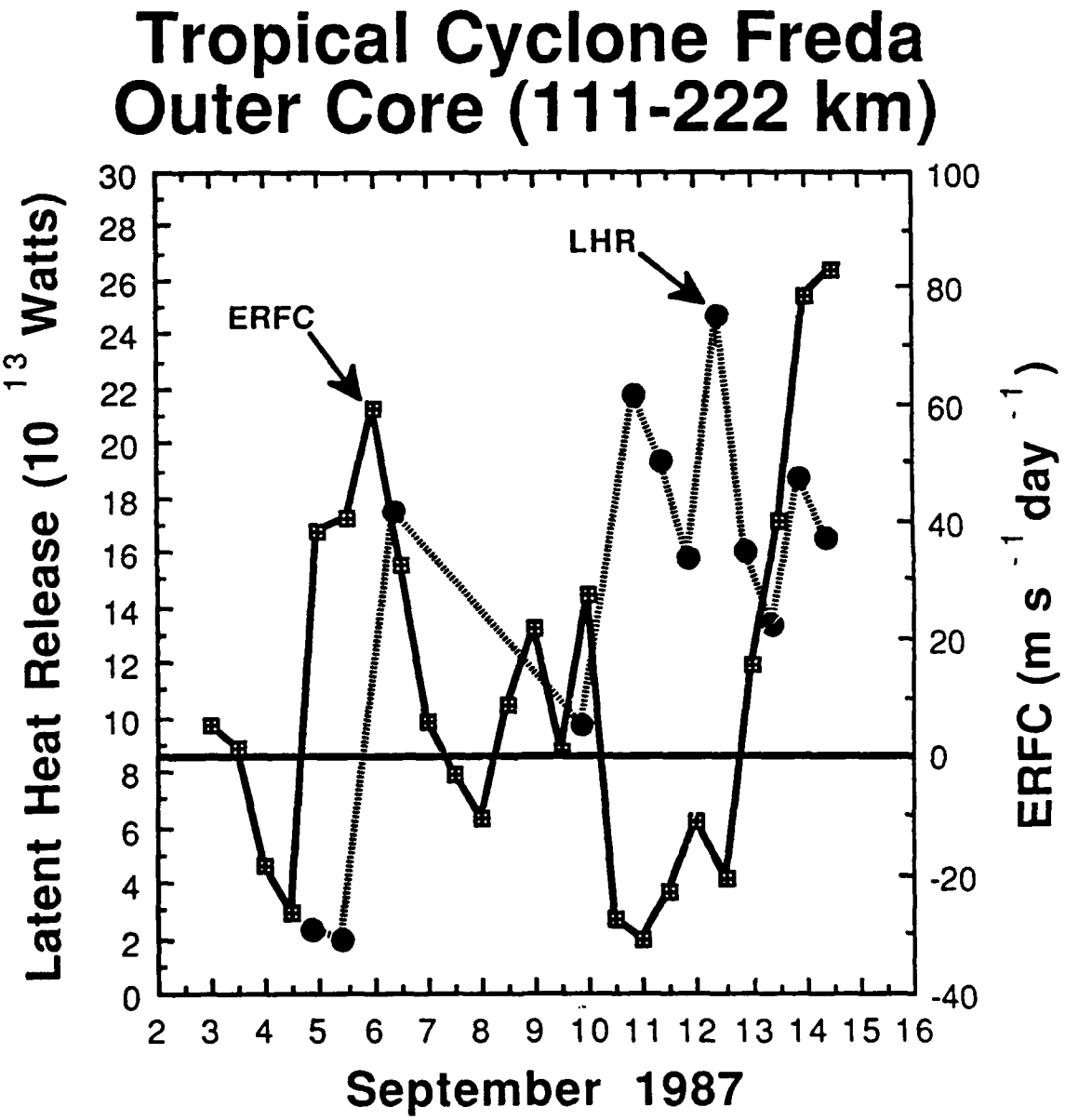
Tropical Cyclone Freda
Outer Core (111-222 km)
Latent Heat Release (10 13 Watts)
ERFC (m s -1 day -1)
LHR
ERFC
30
28
26
24
22
20
18
16
14
12
10
8
6
4
2
0
100
80
60
40
20
0
-20
-40
2 3 4 5 6 7 8 9 10 11 12 13 14 15 16
September 1987

FIGURE 46

APPENDIX C

EXAMPLE CALCULATIONS

1. Example LHR Calculation

This example calculation is for the SSM/I observation that occurred at 0853 on September 5. Eq. 10 can be written:

$$LHR = L\rho\int_A \bar{R}\,da = L\rho\bar{R}\int_A da \qquad (18)$$

where $\bar{\mathbf{R}}$ is the average rain rate for the area of interest. The histogram produced by AOIPS II gives an average rain rate, $R_{1\text{-}2}$, for the inner core (rings 1 and 2). $\int_A \mathbf{da}$ can be written as πr^2 (where $\mathbf{r}$ is the radius for the circular area of interest). Eq. 18 can then be written as:

$$LHR = L\rho\bar{R}\pi r^2 \qquad (19)$$

$\mathbf{L}$ = 2.5×10^6 J kg^{-1}
ρ = 1.0×10^3 kg m^{-3}
$\bar{\mathbf{R}}$ = $R_{1\text{-}2}$ ~~mm~~ ~~h^{-1}~~ $(3600\ s)^{-1}$ ~~h~~ 1000 m ~~mm^{-1}~~ = $R_{1\text{-}2}$ 0.278 m s^{-1}
$\mathbf{r}$ = 111000 m.

Inserting the above values into Eq. 19 yields the following computational formula:

LHR = 2.5 x 10^6 J ~~kg^{-1}~~ 1000 ~~kg~~ ~~m^{-3}~~ $R_{1\text{-}2}$ 0.278 ~~m~~ s^{-1} π(111000 ~~m~~)^2

$$\mathbf{LHR} = 2.688 \times 10^{13}\ R_{1\text{-}2}\ \text{J}\ s^{-1}.$$

In this example, $R_{1\text{-}2}$ from the histogram is 1.05, which yields a LHR of 2.82×10^{13} watts.

2. Example MFC Calculation

The TAWIND function of GEMPAK was used in the calculation of tropospheric moisture flux convergence in for this research. TAWIND takes gridded data (x, y) and produces tabular output of the radial and tangential (r, λ) components of the wind in relation to storm center and motion (Lagrangian frame of reference). By including the scalar mixing ratio (q) as input, this data and the transport of the data across a radius circle (in this case, r = 222 km) are calculated and output in the form of a table. The following is a list of parameters input into the TAWIND function:

1) date/time (YYMMDD/HHMM)
2) pressure level (300, 500, 700, 850, or 1000 mb)
3) latitude/longitude of center
4) direction of motion (from)
5) speed of motion (m s^{-1})
6) radius of interest (222 km)
7) azimuthal increment (10°)
8) input scalar (q).

The table for each of the five pressure levels includes an average value around the radius of interest for the scalar product of q and u_L (i.e., $\overline{[q\ u_L]}_{300\ mb}$, $\overline{[q\ u_L]}_{500\ mb}$, $\overline{[q\ u_L]}_{700\ mb}$, $\overline{[q\ u_L]}_{850\ mb}$, or $\overline{[q\ u_L]}_{1000\ mb}$). The integral in Eq. 12 can be written as the sum of MFC within four pressure layers: Layer 1 (1000-850 mb), Layer 2 (850-700 mb), Layer 3 (700-500 mb), and Layer 4 (500-300 mb). Assuming an average value of $\overline{q\ u_L}$ for each layer and that $\int dp$ can be expressed

as Δp (p_{top} - p_{bottom}), Eq. 12 becomes the sum of the following layers:

Layer 1

$$2\pi\ (222000\ m)\ (9.8\ m\ s^{-2})^{-1}\ \tfrac{1}{2}(\overline{[q\ u_L]}_{1000\ mb} + \overline{[q\ u_L]}_{950\ mb})\ *$$
$$0.001\ g\ g^{-1}\ m\ s^{-1}\ 15000\ kg\ m^{-1}\ s^{-2}$$

Layer 2

$$2\pi\ (222000\ m)\ (9.8\ m\ s^{-2})^{-1}\ \tfrac{1}{2}(\overline{[q\ u_L]}_{950\ mb} + \overline{[q\ u_L]}_{700\ mb})\ *$$
$$0.001\ g\ g^{-1}\ m\ s^{-1}\ 15000\ kg\ m^{-1}\ s^{-2}$$

Layer 3

$$2\pi\ (222000\ m)\ (9.8\ m\ s^{-2})^{-1}\ \tfrac{1}{2}(\overline{[q\ u_L]}_{700\ mb} + \overline{[q\ u_L]}_{500\ mb})\ *$$
$$0.001\ g\ g^{-1}\ m\ s^{-1}\ 20000\ kg\ m^{-1}\ s^{-2}$$

Layer 4

$$2\pi\ (222000\ m)\ (9.8\ m\ s^{-2})^{-1}\ \tfrac{1}{2}(\overline{[q\ u_L]}_{500\ mb} + \overline{[q\ u_L]}_{300\ mb})\ *$$
$$0.001\ g\ g^{-1}\ m\ s^{-1}\ 20000\ kg\ m^{-1}\ s^{-2}$$

Simplifying and summing the above layers yields the following computational formula for MFC:

$$\mathbf{MFC} = \{4.27 \times 10^6\ kg\ s^{-1}\ \tfrac{1}{2}\{(\overline{[q\ u_L]}_{1000\ mb} + \overline{[q\ u_L]}_{950\ mb}) + (\overline{[q\ u_L]}_{950\ mb} + \overline{[q\ u_L]}_{700\ mb})\}\} + \{5.70 \times 10^6\ kg\ s^{-1}\ *$$
$$\tfrac{1}{2}\{(\overline{[q\ u_L]}_{700\ mb} + \overline{[q\ u_L]}_{500\ mb}) + (\overline{[q\ u_L]}_{500\ mb} + \overline{[q\ u_L]}_{300\ mb})\}\}.$$

For example, at 1200 UTC on September 10 the computation is as follows:

$$\mathbf{MFC} = \{4.27 \times 10^6\ kg\ s^{-1}\ 0.5([27.10 + 10.43] + [10.43 + 1.47])\} + \{5.70 \times 10^6\ kg\ s^{-1}\ 0.5([1.47 + 0.40] + [0.40 + 0.07])\} = 112.2 \times 10^6\ kg\ s^{-1}.$$

3. Example ERFC Calculation

The TAWIND function was used in the ERFC calculations in much the same way as in the previous MFC calculations. The exception is that no input scalar quantity was used and the pressure level was 200 mb and two radii of interest were examined (600 and 1000 km). Eddy RAM is given by the following expression:

$$u'v' = \overline{uv} - \overline{u}\,\overline{v} \qquad (20)$$

where the over-bar represents average and the prime denotes eddy term. The first right hand side term is the total RAM and the second term is the mean RAM. TAWIND produces average values of **u**, **v**, and their product **u v**. For computational purposes, Eq. 14 can be rewritten as:

$$ERFC = \frac{1}{(r_{outer} - r_{inner})^2}\left(\frac{r_{outer}^2\,(\overline{u'v'})_{outer} - r_{inner}^2\,(\overline{u'v'})_{inner}}{(r_{outer} - r_{inner})}\right) \qquad (21)$$

where $\mathbf{r}_{outer}$ is the outer 1000 km radius and $\mathbf{r}_{inner}$ is the inner 600 km radius. Inserting the values and manipulating the numbers, including unit analysis, yields the following:

ERFC = 0.0135 $(100[\overline{\mathbf{u'v'}}]_{outer} - 36[\overline{\mathbf{u'v'}}]_{inner})$ m s^{-1} day^{-1}.

For example, on September 4 at 0000 UTC the average outer eddy term was -13.105 and the inner was 2.117. Inserting these into the above formula yields an ERFC of -18.72 m s^{-1} day^{-1}.

LIST OF REFERENCES

Adler, R. F. and E. B. Rodgers, 1977: Satellite-observed latent heat release in a tropical cyclone. *Mon. Wea. Rev.*, **105**, 956-963.

--------, H-Y. M. Yeh, N. Prasad, W-K. Tao, and J. Simpson, 1991: Microwave simulations of a tropical rainfall system with a three-dimensional cloud model. *J. Appl. Meteor.*, **30**, 924-953.

--------, A. J. Negri, P. R. Keehn, and I. M. Hakkarinen, 1992: Estimation of monthly rainfall over Japan and surrounding waters from a combination of low-orbit microwave and geosynchronous IR data. *J. Appl. Meteor.* Accepted April 1992.

Alliss, R. J. and S. Raman, 1992: Special Sensor Microwave/Imager (SSM/I) observations of Hurricane Hugo. *Mon. Wea. Rev.*, **120**, 2723-2737.

--------, G. D. Sandlin, S. W. Chang, and S. Raman, 1992: Applications of SSM/I data in the analysis of Hurricane Florence (1988). North Carolina State University Paper.

Anthes, R. A., 1982: Tropical cyclones: Their evolution, structure and effects. *Meteorological Monographs*, **19** (41), Amer. Meteor. Soc., 208 pp.

Atkinson, G. D. and C. R. Holliday, 1977: Tropical cyclone minimum sea level pressure/maximum sustained wind relationship for the Western North Pacific. *Mon. Wea. Rev.*, **105**, 421-427.

Baik, J-J., M. DeMaria, and S. Raman, 1991: Observational evidence for upper-tropospheric asymmetric eddy momentum forcing and subsequent hurricane intensity change. *Preprints, 19th Conf. on Hurricanes and Tropical Meteorology*, Miami, Amer. Meteor. Soc., 478-481.

Black, P. G. and R. A. Anthes, 1971: On the asymmetric structure of the tropical cyclone outflow layer. *J. Atmos. Sci.*, **28**, 1348-1366.

Burpee, R. W. and M. L. Black, 1989: Temporal and spatial variations near the centers of two tropical cyclones. *Mon. Wea. Rev.*, **117**, 2204-2218.

Challa, M. and R. Pfeffer, 1980: Effects of eddy fluxes of angular momentum on model hurricane development. *J. Atmos. Sci.*, **37**, 1630-1618.

--------, and --------, 1990: Formation of Atlantic hurricanes from cloud clusters and depressions. *J. Atmos. Sci.*, **47**, 909-927.

Chang, J. C. L. and H. Lam, 1989: Performance of the ECMWF model in predicting the movement of Typhoon Wayne (1986). *Wea. Forecasting*, **4**, 234-245.

Chen L. and W. M. Gray, 1985: Global view of the upper level outflow patterns associated with tropical cyclone intensity changes during FGGE. Colorado State University, Atmospheric Science Paper 392, 126 pp.

Critchfield, H. J., 1983: *General Climatology*. 4th ed. Englewood Cliffs, NJ: Prentice-Hall, Inc.

DeMaria, M., J-J. Baik, and J. Kaplan, 1991: Upper-level eddy angular momentum fluxes and tropical cyclone intensity change. *J. Atmos. Sci.*, **30**.

--------, and J. Kaplan, 1991: A statistical model for predicting tropical cyclone intensity change. *Preprints, 19th Conf. on Hurricanes and Tropical Meteorology*, Miami, Amer. Meteor. Soc., 521-526.

Dvorak, V. F., 1975: Tropical cyclone intensity analysis and forecasting from satellite imagery. *Mon. Wea. Rev.*, **103**, 420-430.

Eagleman, J. R., 1983: *Severe and Unusual Weather*. New York: Van Nostrand Reinhold Company.

Elsberry, R. L., W. M. Frank, G. L. Holland, J. D. Jarrell, and R. L. Southern, 1987: *A Global View of Tropical Cyclones*. Office of Naval Research, Washington, D.C., 185 pp.

Emanuel, K. A., 1986: An air-sea interaction theory for tropical cyclones. Part I: steady-state maintenance. *J. Atmos. Sci.*, **43**, 585-604.

Felde, G. W. and M. Glass, 1991: SSM/I brightness temperature analysis of tropical cyclones. *Preprints, 19th Conf. on Hurricanes and Tropical Meteorology*, Miami, Amer. Meteor. Soc., 400-404.

--------, 1988: The maximum intensity of hurricanes. *J. Atmos. Sci.*, **45**, 1143-1155.

Frank, W. M., 1977: The structure and energetics of the tropical cyclone. Part I: storm structure. *Mon. Wea. Rev.*, **105**, 1119-1135.

--------, 1984: A composite analysis of the core of a mature hurricane. *Mon. Wea. Rev.*, **112**, 2401-2420.

Glass, M. and G. W. Felde, 1989: Structure of tropical cyclones and surrounding regions as determined from OLS and SSM/I imagery analysis. *Preprints, 4th Conf. on Satellite Meteorology and Oceanography*, San Diego, Amer. Meteor. Soc., 35-38.

--------, and --------, 1990: Tropical storm structure analysis using SSM/I and OLS data. *Preprints, 5th Conf. on Satellite Meteorology and Oceanography*, London, Amer. Meteor. Soc., 432-437.

--------, and --------, 1992: Intensity estimation of tropical cyclones using SSM/I brightness temperatures. *Preprints, Joint Symposium on Weather Forecasting and 6th Conf. on Satellite Meteorology and Oceanography*, Atlanta, Amer. Meteor. Soc., J8-J10.

Griffin, J. S., R. W. Burpee, J. L. Franklin, and F. D. Marks, 1991: Preliminary results of airborne analysis of observations in support of operational hurricane forecasting. *Preprints, 19th Conf. on Hurricanes and Tropical Meteorology*, Miami, Amer. Meteor. Soc., 144-147.

Gray, W. M., 1979: Hurricanes: their formation, structure, and likely role in the tropical circulation. Meteorology over the Tropical Oceans. D. B. Shaw, Ed., *Roy. Meteor. Soc.*, 155-218.

--------, C. Neumann, and T. L. Tsui, 1991: Assessment of the role of aircraft reconnaissance on tropical cyclone analysis and forecasting. *Bull. Amer. Meteor. Soc.*, **72**, 1867-1883.

Hack, J. J. and W. H. Schubert, 1986: On nonlinear response of atmospheric vorticities to heating by organized cumulus convection. *J. Atmos. Sci.*, **45**, 1559-1573.

Henderson-Sellers, A. and P. J. Robinson, 1986: *Contemporary Climatology*. New York: John Wiley and Sons, Inc.

Holland, G. L., 1983: Angular momentum transport in tropical cyclones. *Quart. J. Roy. Meteor. Soc.*, **109**, 187-210.

--------, and R. T. Merrill, 1984: On the dynamics of tropical cyclone structural changes. *Quart. J. Roy. Meteor. Soc.*, **110**, 723-45.

Hollinger, J. T., 1989: DMSP Special sensor microwave/imager calibration/validation. Final Report, Volume I of the Naval Research Laboratory, Washington, D.C., 177 pp.

--------, K. Lo, G. Poe, R. Savage, and J. Pierce, 1987: Special sensor microwave/imager user's guide. Dept. of the Navy, Naval Research Laboratory, Washington, D.C., 120 pp.

Kummerow, C. D. and D. Duffy, 1992: Computer program written in the "C" programming language which used input latitude and longitude to extract climatological SST from a global change modelling data base.

Kurihara, Y. and R. E. Tuleya, 1974: Structure of a tropical cyclone developed in a three-dimensional numerical simulation model. *J. Atmos. Sci.*, **31**, 893-919.

Lee, C. S., 1986: An observational study of tropical cloud cluster evolution and cyclogenesis in the Western North Pacific. Colorado State University, Atmospheric Science Paper 403, 250 pp.

MacArthur, P. D., 1991: Microwave derived rainrates in typhoons and their use in the diagnosis and prediction of typhoon intensity. M.S. Thesis, St. Louis University, Mo., 70 pp. Available from University Microfilms., Ann Arbor, Mi.

Malkus, J. S., and H. Riehl, 1960: On the dynamics and energy transformations in steady-state hurricanes. *Tellus*, **12**, 1-20.

Manobianco, J., V. M. Karyampudi, S. Koch, and A. J. Negri, 1991: The impact of assimilating SSM/I and GOES/IR derived precipitation rates on the numerical simulations of the ERICA IOP 4 cyclone. *Preprints, Ninth AMS Conf. on Numerical Weather Prediction*, Denver, Amer. Meteor. Soc.

Marks, F. D., 1985: Evolution of the structure of precipitation in Hurricane Allen (1980). *Mon. Wea. Rev.*, **113**, 909-930.

Mayfield, M., 1992: Preliminary report: Hurricane Bob 16-20 August 1991. National Hurricane Center, 1320 S. Dixie Hwy., Coral Gables, FL 33146-2976, 21 pp.

McBride, J. L., 1981: Observational analysis of tropical cyclone formation. Part III: budget analysis. *J. Atmos. Sci.*, **38**, 1152-1166.

--------, and R. Zehr, 1981: Observational analysis. of tropical cyclone formation. Part II: comparison of non-developing versus developing systems. *J. Atmos. Sci.*, **38**, 1132-1151.

Merrill, R. T., 1984: Structure of the tropical cyclone outflow layer. Preprints, *15th Conf. on Hurricanes and Tropical Meteorology*, Miami, Amer. Meteor. Soc., 421-426.

--------, 1988: Environmental influences on hurricane intensification. *J. Atmos. Sci.*, **45**, 1678-1687.

Miller, A. and R. A. Anthes, 1980: *Meteorology. 4th ed.* Columbus, OH: Charles E. Merrill Publishing Company.

Miller, B. I., 1958: On the maximum intensity of hurricanes. *J. Meteor.*, **15**, 185-195.

Molinari, J., and S. Skubis, 1985: Evolution of the surface wind field in an intensifying tropical cyclone. *J. Atmos. Sci.*, **42**, 2865-2879.

--------, and D. Vollaro, 1989: External influences on hurricane intensity. Part I: outflow layer eddy momentum fluxes. *J. Atmos. Sci.*, **46**, 1093-1105.

--------, and --------, 1990: External Influences on hurricane intensity. Part II: vertical structure and response of the hurricane vortex. *J. Atmos. Sci.*, **47**, 1902-1918.

Negri, A. J., R. F. Adler, and C. D. Kummerow, 1989: False-color display of Special Sensor Microwave/Imager (SSM/I) data. *Bull. Amer. Meteor. Soc.*, **70**, 146-151.

OFCM, 1992: *National Plan for Tropical Cyclone Research.* FCM-P25-1992. Washington, D.C.: G.P.O.

Palmen, E. and H. Riehl, 1957: Budget of angular momentum and kinetic energy in tropical cyclones. *J. Meteor.*, **14**, 150-159.

--------, and C. W. Newton, 1969: *Atmospheric Circulation Systems*. Academic Press, 603 pp.

Parmenter-Holt, F. C., 1992: The role of satellite remote sensing in precipitation forecasting, rainfall estimation, and water management. *International Archives of Photogrammetry and Remote Sensing*, **29**, 538-541.

Pfeffer, R. L., 1958: Concerning the mechanisms of hurricanes. *J. Meteor.*, **15**, 113-119.

--------, and M. Challa, 1981: A numerical study of the role of eddy fluxes of momentum in the development of Atlantic hurricanes. *J. Atmos. Sci.*, **38**, 2393-2398.

Ploshay, J. J., W. F. Stern, and K. Miyakoda, 1992: FGGE Reanalysis at GFDL. *Mon. Wea. Rev.*, **120**, 2083-2108.

Powell, M. D., 1985: Airborne Doppler radar observations of the hurricane boundary layer. *Preprints, 16th Conf. on Hurricanes and Tropical meteorology*, Boston, Amer. Meteor. Soc.

--------, 1989a: Boundary layer structure and dynamics in outer hurricane rainbands. Part I: mesoscale rainfall and kinematic structure. *Mon. Wea. Rev.*, **118**, 891-917.

--------, 1989b: Boundary layer structure and dynamics in outer hurricane rainbands. Part II: downdraft modification and mixed layer recovery. *Mon. Wea. Rev.*, **118**, 918-938.

Rappaport, E. N., 1991: Operational applications of SSM/I data at the National Hurricane Center. *Preprints, 19th Conf. on Hurricanes and Tropical Meteorology*, Miami, Amer. Meteor. Soc., 179-183.

Reed, R. J., A. Hollingsworth, W. A. Heckley, and F. Delsol, 1988: An evaluation of the performance of the ECMWF operating system in analyzing and forecasting easterly wave disturbances over Africa and the tropical Atlantic. *Mon. Wea. Rev.*, **116**, 824-865.

Reuter, G. W. and M. K. Yau, 1986: Numerical modelling of cloud development in a sheared environment. *Beitr. Phys. Atmosph.*, **60**, 65-80.

Rhudy, D. K., 1989: Applications of microwave radiometric measurements to infer tropical cyclone intensity and strength. M.S. Thesis, St. Louis University, St. Louis, Mo., 95 pp. Available from University Microfilms, Ann Arbor, Mi.

Rodgers, E. B., 1992: Tropical cyclone/upper-atmospheric interaction as inferred from satellite total ozone observations. Ph.D. Dissertation, Colorado State University, Ft Collins, Colorado, 250 pp.

--------, and R. F. Adler, 1981: Tropical cyclone rainfall characteristics as determined from a satellite passive microwave radiometer. *Mon. Wea. Rev.*, **109**, 506-521.

--------, J. Stout, J. Steranka and S. Chang, 1990: Tropical cyclone/upper-atmospheric interaction as inferred from satellite total ozone observations. *J. Appl. Meteor.*, **29**, 934-954.

--------, --------, --------, --------, and J-J Shi, 1991: Satellite observations of variations in tropical cyclone convection caused by upper-tropospheric troughs. *J. Appl. Meteor.*, **30**, 1163-1184.

Rosenthal, L., 1978: Numerical simulation of tropical cyclone development with latent heat release by the resolvable scales. Part I: model description and preliminary results. *J. Atmos. Sci.*, **35**, 258-271.

Sadler, J. C., 1976: Tropical cyclone initiation by the tropical upper-tropospheric trough. *Mon. Wea. Rev.*, **104**, 1266-1278.

--------, 1978: Midseason typhoon development and intensity changes and the tropical upper-tropospheric trough. *Mon. Wea. Rev.*, **106**, 1137-1152.

Samsury, C. E. and E. N. Rappaport, 1991: Predicting Atlantic hurricane intensity from research and reconnaissance aircraft data. *Preprints, 19th Conf. on Hurricanes and Tropical Meteorology*, Miami, Amer. Meteor. Soc., 516-520.

Sheets, R. C., 1992: Personal communication.

Shenk, W. E., H. Powell, V. V. Salomonson, and W. R. Bandeen, 1971: Meteorological uses of the stereographic horizon map projection. *J. Appl. Meteor.*, **110**, 582-589.

Shi, J-J., S. W. Chang, and S. Raman, 1990: A numerical study of the outflow layer of tropical cyclones. *Mon. Wea. Rev.*, **118**, 204-2055.

Simpson, R. H. and H. Riehl, 1981: *The Hurricane and Its Impact*. Louisiana State University Press, 398 pp.

Spencer, R. W., H. M. Goodman, and R. E. Hood, 1989: Precipitation retrieval over land and ocean with SSM/I: Identification and characteristics of the scattering signal. *J. Atmos. and Ocean. Tech.*, **6**, 254-273.

Stout, J. and E. B. Rodgers, 1992: Nimbus-7 total ozone observations of Western North Pacific tropical cyclones. *J. Appl. Meteor.*, **31**, 758-783.

Uccellini, L. W., P. J. Kocin, R. A. Petersen, C. H. Wash, and K. F. Brill, 1984: The President's Day cyclone of 18-19 February 1979: synoptic overview and analysis of the subtropical jet streak influencing the pre-cyclogenetic period. *Mon. Wea. Rev.*, **112**, 31-55.

U.S. Air Force, 1982: *Weather for Aircrews*. AFM 51-12, Volume 1. Washington, D.C.: G.P.O.

U.S. Fleet Weather Center/JTWC, 1987: *Annual Typhoon Report*. Guam, Mariana Island, 214 pp.

Velden, C.S., W. S. Olson, and B. A. Roth, 1989: Tropical cyclone center-fixing using DMSP SSM/I data. *Preprints, 18th Conf. on Hurricanes and Tropical Meteorology*, Boston, Amer. Meteor. Soc., J36-J39.

Weatherford, C., 1985. Typhoon structural variability. Colorado State University, Atmospheric Science Paper 391, 77 pp.

--------, and W. M. Gray, 1987a: Typhoon structure as revealed by aircraft reconnaissance. Part I: data analysis and climatology. *Mon. Wea. Rev.*, **116**, 1032-1043.

--------, and --------, 1987b: Typhoon structure as revealed by aircraft reconnaissance. Part II: structural variability. *Mon. Wea. Rev.*, **116**, 1032-1043.

Wilheit, T. T., J. L. King, E. B. Rodgers, R. A. Nieman, B. M. Krupp, A. S. Milman, J. S. Stratigos, and H. Siddalingaiah, 1982: Microwave radiometric observations near 19.35, 35, 92, and 183 GHz of precipitation in Tropical Storm Cora. *J. Appl. Meteor.*, **21**, 1137-1145.

Willoughby, H. E., 1988: The dynamics of the tropical cyclone core. *Aust. Met. Mag.*, **36**, 183-191.

--------, 1990: Temporal changes of the primary circulation in tropical cyclones. *J. Atmos. Sci.*, **47**, 242-264.

--------, J. A. Clos, and M. G. Shoreibah, 1982: Concentric eyewalls, secondary wind maxima, and the evolution of the hurricane vortex. *J. Atmos. Sci.*, **39**, 395-411.